

2014

In-Field Observations of Heavy Mining Vehicle Wheels and Analyses of Proposed Solutions to Enhance Safety

Aleksander Tonkovich
University of Windsor

Follow this and additional works at: <https://scholar.uwindsor.ca/etd>

Recommended Citation

Tonkovich, Aleksander, "In-Field Observations of Heavy Mining Vehicle Wheels and Analyses of Proposed Solutions to Enhance Safety" (2014). *Electronic Theses and Dissertations*. 5119.
<https://scholar.uwindsor.ca/etd/5119>

This online database contains the full-text of PhD dissertations and Masters' theses of University of Windsor students from 1954 forward. These documents are made available for personal study and research purposes only, in accordance with the Canadian Copyright Act and the Creative Commons license—CC BY-NC-ND (Attribution, Non-Commercial, No Derivative Works). Under this license, works must always be attributed to the copyright holder (original author), cannot be used for any commercial purposes, and may not be altered. Any other use would require the permission of the copyright holder. Students may inquire about withdrawing their dissertation and/or thesis from this database. For additional inquiries, please contact the repository administrator via email (scholarship@uwindsor.ca) or by telephone at 519-253-3000ext. 3208.

In-Field Observations of Heavy Mining Vehicle Wheels and Analyses of Proposed
Solutions to Enhance Safety

By

Aleksander Tonkovich

A Thesis
Submitted to the Faculty of Graduate Studies
through the Department of Mechanical, Automotive, and Materials Engineering
in Partial Fulfillment of the Requirements for
the Degree of Master of Applied Science
at the University of Windsor

Windsor, Ontario, Canada

2014

© 2014 Aleksander Tonkovich

In-Field Observations of Heavy Mining Vehicle Wheels and Analyses of Proposed
Solutions to Enhance Safety

by

Aleksander Tonkovich

APPROVED BY:

F. Ghrib

Department of Civil and Environmental Engineering

B. Minaker

Department of Mechanical, Automotive and Materials Engineering

W. Altenhof

Department of Mechanical, Automotive and Materials Engineering

April 22, 2014

DECLARATION OF ORIGINALITY

I hereby certify that I am the sole author of this thesis and that no part of this thesis has been published or submitted for publication.

I certify that, to the best of my knowledge, my thesis does not infringe upon anyone's copyright nor violate any proprietary rights and that any ideas, techniques, quotations, or any other material from the work of other people included in my thesis, published or otherwise, are fully acknowledged in accordance with the standard referencing practices. Furthermore, to the extent that I have included copyrighted material that surpasses the bounds of fair dealing within the meaning of the Canada Copyright Act, I certify that I have obtained a written permission from the copyright owner(s) to include such material(s) in my thesis and have included copies of such copyright clearances in Appendix 9.4.

I declare that this is a true copy of my thesis, including any final revisions, as approved by my thesis committee and the Graduate Studies office, and that this thesis has not been submitted for a higher degree to any other university or institution.

ABSTRACT

This research strives to enhance the safety of multi-piece wheel assemblies as injuries and fatalities are associated with their failure, yet information on this topic is limited.

Experiments were performed to determine mechanical performance and planar deformation characteristics of several tires to aid in numerical model development. For a 29.5-29 tire, observations included determining vertical versus lateral deflection relationships (0.310 mm/mm), and vertical (2.59 kN/mm) and lateral (6.29 kN/mm) stiffness.

A database capable of tracking wheel maintenance trends based on historical data was developed, allowing maintenance schedules to be estimated.

A safety shield system was proposed. Effectiveness of the design was examined through numerical simulation of the ISO 7141 impact test, a tire blowout, and a rotational side impact. Depending on the test condition, observations comparing shield-equipped versus standard wheels show reductions in von Mises stress between 15% and 55% and reductions in effective plastic strains between 20.3% and 92%.

DEDICATION

To my father, as I would have never strived for excellence in life without your motivating example. You are forever missed.

To my mother, for the immeasurable amount of love, support and encouragement you have always given me.

To my wife, for always standing by my side. My accomplishments are a reflection of your belief in me.

ACKNOWLEDGEMENTS

It is with the most sincere gratitude and appreciation I thank my academic advisor, Dr. William Altenhof, for his guidance and support throughout the term of my studies at the University of Windsor as his knowledge and expertise made this research possible. Furthermore, I thank fellow research group members Mr. Weldon Li and Mr. Sante DiCecco for the collaboration and knowledge we have shared.

I would additionally like to express appreciation for the contributions of Mr. Rick Banting of Workplace Safety North and all personnel at North Shore Industrial Wheel Mfg., Goodyear OTR and their dealers, Xstrata Nickel Rim mine, Xstrata Copper mine, and Musselwhite gold mine.

Finally, thank you to the Workplace Safety and Insurance Board for providing the financial support that made this research possible.

TABLE OF CONTENTS

DECLARATION OF ORIGINALITY	III
ABSTRACT	IV
DEDICATION.....	V
ACKNOWLEDGEMENTS	VI
LIST OF TABLES	XI
LIST OF FIGURES	XII
LIST OF ABBREVIATIONS	XVIII
1 INTRODUCTION AND MOTIVATION.....	1
1.1 BACKGROUND AND MOTIVATION	1
2 REVIEW OF LITERATURE.....	6
2.1 GENERAL INFORMATION ON USE OF MULTI-PIECE WHEEL ASSEMBLIES	6
2.2 SAFETY HAZARDS RELATED TO MULTI-PIECE WHEELS.....	11
2.2.1 <i>Review of Multi-Piece Wheel Incidents and Associated Difficulties</i>	<i>12</i>
2.2.2 <i>Review of Studies Related to Wheel Incidents</i>	<i>14</i>
2.2.3 <i>Summary of Recent Wheel-Related Injuries and Fatalities</i>	<i>17</i>
2.2.4 <i>Wheel Assembly Maintenance and Handling Best Practices</i>	<i>19</i>
2.3 MULTI-PIECE WHEEL AND OFF-THE-ROAD TIRE FAILURE MODES.....	20
2.3.1 <i>Tire Zipper Failures.....</i>	<i>20</i>
2.3.2 <i>Tire Explosion Failures</i>	<i>22</i>
2.3.3 <i>Wheel Failure and Tire Blowouts</i>	<i>23</i>
2.4 STANDARDS RELATED TO WHEEL TESTING	24
2.4.1 <i>ISO 7141 Road Vehicle Light Alloy Wheel Impact Test</i>	<i>25</i>
2.4.2 <i>SAE J1981 Recommended Practice Road Hazard Impact Test for Wheel and Tire Assemblies</i>	<i>27</i>
2.5 REVIEW OF MULTI-PIECE WHEEL AND TIRE RESEARCH	28
2.5.1 <i>Related Wheel Modelling Research.....</i>	<i>28</i>

2.5.2	<i>Past Multi-Piece OTR Wheel Research</i>	31
2.5.3	<i>Related Tire Modelling Research</i>	33
3	RESEARCH FOCUS	37
4	ASSOCIATED FIELD WORK AND EXPERIMENTAL TESTING	38
4.1	MINE SITE VISITS	38
4.2	MUSSELWHITE MINE TESTING INFORMATION	39
4.2.1	<i>Tire, Wheel and Vehicle Specifications</i>	40
4.2.2	<i>Testing Apparatus</i>	43
4.3	TESTING METHODOLOGY	46
4.3.1	<i>Quasi-static Deflection Testing Methodology</i>	46
4.3.2	<i>Static Deflection Scale Testing</i>	50
4.4	MUSSELWHITE OBSERVATIONS AND DISCUSSIONS	51
4.4.1	<i>Above Ground Quasi-Static Testing Observations</i>	51
4.4.2	<i>Underground Static Testing Observations</i>	60
5	HISTORICAL WHEEL TRACKING DATA ANALYSIS AND DATABASE DEVELOPMENT	64
5.1	MOTIVATION OF DATABASE DEVELOPMENT	64
5.2	DATABASE DEVELOPMENT DETAILS	66
5.3	ANALYTICAL OBSERVATIONS	70
6	SAFETY SHIELD SYSTEM	74
6.1	MOTIVATION AND DESIGN	74
6.2	FINITE ELEMENT MODEL DEVELOPMENT	80
6.2.1	<i>Validated Wheel Assembly Model</i>	80
6.2.2	<i>Model Enhancements</i>	85
6.2.3	<i>Safety Shield FE Model</i>	93
6.3	MODELLING OF SAFETY SHIELD PERFORMANCE	95
6.3.1	<i>ISO 7141 Impact Test</i>	96
6.3.2	<i>Simulated Tire Blowout Test</i>	98
6.3.3	<i>Rotational Side Impact Virtual Test</i>	101

6.4	NUMERICAL RESULTS AND QUALITATIVE OBSERVATIONS	104
6.4.1	<i>ISO 7141 Impact Testing Observations</i>	<i>104</i>
6.4.2	<i>Simulated Tire Blowout Observations</i>	<i>113</i>
6.4.3	<i>Rotational Side Impact Virtual Testing Observations</i>	<i>121</i>
7	CONCLUSIONS	129
7.1	EXPERIMENTAL TESTING SUMMARY	129
7.2	HISTORICAL WHEEL TRACKING DATA ANALYSIS EFFECTIVENESS AND FINAL SUMMARY ..	130
7.3	SAFETY SHIELD SYSTEM	131
7.3.1	<i>ISO 7141 Virtual Test:</i>	<i>132</i>
7.3.2	<i>Simulated Tire Blowout Test:</i>	<i>132</i>
7.3.3	<i>Rotational Side Impact Test:</i>	<i>133</i>
8	REFERENCES	135
9	APPENDICES	140
9.1	OBSERVATIONS OF ADDITIONAL WHEEL ASSEMBLIES DURING MUSSELWHITE TESTING	140
9.1.1	<i>Vertical and Lateral Displacement for 29.5R29 Wheel Assembly</i>	<i>140</i>
9.1.2	<i>Vertical and Lateral Displacement for 26.5-25 Wheel Assembly</i>	<i>141</i>
9.1.3	<i>Additional Wheel Assembly Vertical Displacement Comparisons</i>	<i>142</i>
9.1.4	<i>Tracked Node Deflection Responses for 29.5R29 Tire</i>	<i>143</i>
9.1.5	<i>Tracked Node Deflection Responses for 26.5-25 Tire</i>	<i>145</i>
9.1.6	<i>Load versus Deflection Data for Additional Wheel Assemblies</i>	<i>147</i>
9.2	HISTORICAL WHEEL TRACKING DATABASE MACRO CODE	148
9.2.1	<i>Statistical Analysis Data Assembly Macro Code</i>	<i>148</i>
9.2.2	<i>Scrap Code Creation Macro Code</i>	<i>158</i>
9.3	MINING WHEEL MATERIAL DATA	160
9.3.1	<i>Material Card For Numerical Model Steel</i>	<i>160</i>
9.3.2	<i>Mining Wheel Material Tensile Test and Virtual Validation Simulation Observations</i>	<i>161</i>
9.3.3	<i>Numerical Tensile Test Apparatus</i>	<i>162</i>
9.4	COPYRIGHT RELEASES	163

9.4.1	<i>Copyright Release for Figures 2.1.1 and 2.1.2.....</i>	163
9.4.2	<i>Copyright Release for Figure 2.1.3</i>	165
9.4.3	<i>Copyright Release for Figure 2.1.4</i>	166
9.4.4	<i>Copyright Release for Figure 2.4.1</i>	167
9.4.5	<i>Copyright Release for Figure 2.5.2</i>	168
10	VITA AUCTORIS	169

LIST OF TABLES

TABLE 4.2.1 – SUMMARY OF TEST VEHICLE INFORMATION	41
TABLE 4.2.2 - PHYSICAL TIRE DATA FROM GOODYEAR'S OTR ENGINEERING DATA BOOK...	42
TABLE 4.2.3 - TIRE DEFLECTION CHARACTERISTICS BASED ON GOODYEAR OTR DATA ..	43
TABLE 4.4.1 - TIRE DEFLECTION CHARACTERISTIC COMPARISON OF EXPERIMENTAL STATIC LOADING AND GOODYEAR OTR DATA.....	62
TABLE 4.4.2 - TIRE DEFLECTION OBSERVATIONS COMPARING EXPERIMENTAL STATIC LOADING TO GOODYEAR OTR ENGINEERING DATA.....	63
TABLE 5.2.1 - LIST OF MODIFIED SCRAP CODES AND DESCRIPTIONS BASED ON VALIDITY..	69
TABLE 5.3.1 - SUMMARY OF WHEEL SCRAPPING STATISTICS BY SIZE AND DESCRIPTION .	71
TABLE 6.2.1 - RIM BASE DEFLECTION AND STRAIN RESPONSES AT MAXIMUM LOAD FOR EXPERIMENTAL AND NUMERICAL OBSERVATIONS	85
TABLE 6.2.2 - TIRE MODEL MATERIAL PROPERTIES	86
TABLE 6.2.3 - ERROR ANALYSIS RESULTS FOR NEW MATERIAL AND ORIGINAL MATERIAL PROPERTY	91

LIST OF FIGURES

FIGURE 1.1.1 - ONTARIO MINING INDUSTRY FATAL INJURIES	3
FIGURE 2.1.1 – CROSS-SECTIONAL AND CUTAWAY VIEWS OF (A) RADIAL AND (B) BIAS-PLY TIRE CONSTRUCTION DESIGNS	7
FIGURE 2.1.2 - DEFINITIONS OF TERMINOLOGIES ASSOCIATED WITH TIRE GEOMETRY AS OUTLINED BY THE MANUFACTURER	8
FIGURE 2.1.3 - MULTI-PIECE WHEEL/RIM NOMENCLATURE.....	9
FIGURE 2.1.4 – (A) CATERPILLAR 797F SIZE COMPARISON, AND (B) VEHICLE INFORMATION AND CAPABILITY SPECIFICATIONS	11
FIGURE 2.2.1 - ACTUAL & POTENTIAL CONSEQUENCES OF TIRE AND RIM RELATED INCIDENTS AND ACCIDENTS	15
FIGURE 2.2.2 - FATALITIES & POTENTIAL FATALITIES – ROOT AND CONTRIBUTING CAUSES .	16
FIGURE 2.3.1 – RESULT OF TIRE ZIPPER FAILURE.....	21
FIGURE 2.3.2 - PHOTOS OF FAILED WHEELS ILLUSTRATING (A) TIRE DAMAGE DUE TO FLANGE SEPARATION, (B) RIM BASE WEAR AND FATIGUE CRACK, AND (C) A CRACKED OUTER FLANGE.....	24
FIGURE 2.4.1 - ISO 7141 TEST APPARATUS IN (A) ELEVATION AND (B) SECTION VIEW	26
FIGURE 2.5.1 - FINITE ELEMENT MODEL USED FOR IMPACT TEST SIMULATION DEVELOPED BY CERIT	30
FIGURE 4.2.1 - WHEEL ASSEMBLY DISPLACEMENT MEASUREMENT APPARATUS FOR (A) AD45B R29.5R29 TIRE, (B) R2900G 29.5-29 TIRE, AND (C) R1700G 26.5-25 TIRE..	46
FIGURE 4.3.1 - EXCITATION OF THE AD45B TEST VEHICLE USING THE CATERPILLAR 990 FRONT LOAD SCOOP.....	48
FIGURE 4.3.2 - EXCITATION OF THE A) R2900G AND B) R1700G TEST VEHICLES USING THE CATERPILLAR 990 FRONT LOAD SCOOP.	49
FIGURE 4.4.1 - RESPONSE FOR 29.5-29 TEST EVENT EXHIBITING MAXIMUM DEFLECTION IN THE A) VERTICAL AND B) LATERAL DIRECTIONS AS WELL AS A C) LATERAL DEFLECTION VERSUS VERTICAL DEFLECTION.....	53

FIGURE 4.4.2 - PLOT OF VALIDATION METRIC, V , AS DETERMINED BY EQUATION (2) AS A FUNCTION OF CONSTANT VALUES TO RELATIVE ERROR.	56
FIGURE 4.4.3 - VERTICAL DISPLACEMENT COMPARISON FOR THE 29.5-29 TIRE BETWEEN LASER DISPLACEMENT TRANSDUCER MEASUREMENTS AND HIGH-SPEED CAMERA IMAGE TRACKING USING PROANALYST.	57
FIGURE 4.4.4 - LOCATION OF POINTS TRACKED ON THE PHYSICAL TEST APPARATUS.	58
FIGURE 4.4.5 - VERTICAL DEFLECTION RESPONSES FOR TRACKED NODES DURING 29.5-29 TIRE TEST EVENT WHERE MAXIMUM DEFLECTIONS WERE OBSERVED FOR THE A) H-IN AND H-OUT POINTS, B) D-IN AND D-OUT POINTS, AND C) V-IN AND V-OUT POINTS. ..	59
FIGURE 4.4.6 - LONGITUDINAL DEFLECTION RESPONSES FOR TRACKED NODES DURING 29.5- 29 TIRE TEST EVENT WHERE MAXIMUM DEFLECTIONS WERE OBSERVED FOR THE A) H- IN AND H-OUT POINTS, B) D-IN AND D-OUT POINTS, AND C) V-IN AND V-OUT POINTS..	60
FIGURE 4.4.7 - DEFLECTION DATA FOR THE 29.5-29 TIRE SHOWING A) VERTICAL DEFLECTION VERSUS LOAD FORCE AND B) LATERAL DEFLECTION VERSUS LOAD FORCE COMPARED TO THE CORRESPONDING GOODYEAR ENGINEERING DATA POINT.	61
FIGURE 5.3.1 - FREQUENCY OF SCRAPPING DUE TO CORRESPONDING REASONS FOR A 26.5X25 WHEEL.	72
FIGURE 5.3.2 - AVERAGE WHEEL LIFE (BY SIZE) AS CALCULATED BY DATABASE.	73
FIGURE 6.1.1 - (A) EXPLODED VIEW OF SAFETY SHIELD COMPONENTS; (B) ASSEMBLED SAFETY SHIELD FRONT VIEW; (C) ASSEMBLED SAFETY SHIELD REAR VIEW.	75
FIGURE 6.2.1 - DISCRETIZED TIRE MODEL SHOWING VARIOUS REGIONS.	81
FIGURE 6.2.2 - RIM BASE (A) EXPERIMENTAL TESTING APPARATUS AND (B) STRAIN GAUGE LOCATIONS.	83
FIGURE 6.2.3 - LOCATION OF POINTS TRACKED ON THE A) PHYSICAL TEST APPARATUS AND B) NUMERICAL MODEL.	87
FIGURE 6.2.4 - VERTICAL DEFLECTION RESPONSE COMPARISON FOR EXPERIMENTAL TESTING OBSERVATIONS (EXP), THE ORIGINAL FINITE ELEMENT MODEL (FE), AND THE ENHANCED NEW MATERIAL PROPERTY MODEL (NMP), FOR TRACKED NODES DURING A 29.5-29 TIRE TEST EVENT WHERE MAXIMUM DEFLECTIONS WERE OBSERVED FOR A) V- IN, B) V-OUT, C) D-IN, D) D-OUT, E) H-IN AND F) H-OUT POINTS.	88

FIGURE 6.2.5 - LONGITUDINAL DEFLECTION RESPONSE COMPARISON FOR EXPERIMENTAL TESTING OBSERVATIONS (EXP), THE ORIGINAL FINITE ELEMENT MODEL (FE), AND THE ENHANCED NEW MATERIAL PROPERTY MODEL (NMP), FOR TRACKED NODES DURING A 29.5-29 TIRE TEST EVENT WHERE MAXIMUM DEFLECTIONS WERE OBSERVED FOR A) V-IN, B) V-OUT, C) D-IN, D) D-OUT, E) H-IN AND F) H-OUT POINTS.....	89
FIGURE 6.2.6 - FINITE ELEMENT MODEL OF SAFETY SHIELD SHOWING A) FRONT AND B) REAR VIEWS.....	94
FIGURE 6.3.1- VIRTUAL TEST APPARATUS FOR TIRE BLOWOUT SIMULATIONS ON A) SHIELD-EQUIPPED AND B) STANDARD WHEEL ASSEMBLIES.	100
FIGURE 6.3.2 - (A) SIDE, (B) FRONT AND (C) TOP PROFILE OF ROTATIONAL SIDE IMPACT VIRTUAL TEST STRIKER.	102
FIGURE 6.3.3 – A) CROSS-SECTION OF ROTATIONAL SIDE IMPACT VIRTUAL TESTING APPARATUS AND B) AN ENLARGED VIEW OF THE STRIKER TO WHEEL CONTACT AREA	104
FIGURE 6.4.1 - ISO7141 VIRTUAL TEST OBSERVATIONS FOR A) STANDARD WHEEL ASSEMBLY AND B) ASSEMBLY EQUIPPED WITH SAFETY SHIELD SYSTEM.	105
FIGURE 6.4.2 - RESULTANT CONTACT FORCE OF STRIKER DURING ISO 7141 IMPACT SIMULATION.....	106
FIGURE 6.4.3 - LOCK RING RESULTANT CONTACT FORCE DURING ISO 7141 IMPACT SIMULATION.....	108
FIGURE 6.4.4 - RESULTANT EFFECTIVE PLASTIC STRAIN (MM/MM) FOR ISO 7141 TEST FOR THE A) SHIELD-EQUIPPED WHEEL AND ITS B) OUTER FLANGE WITH THE SHIELD NOT VISUALIZED, AS WELL AS C) THE OUTER FLANGE OF THE STANDARD WHEEL.	109
FIGURE 6.4.5 - VARIOUS VIEWS SHOWING CONTOURS OF EFFECTIVE VON MISES STRESS FOR BOTH THE SAFETY SHIELD EQUIPPED (A, C) AND STANDARD (B, D) WHEEL ASSEMBLIES WHEN MAXIMUM VALUES WERE OBSERVED DURING ISO 7141 TEST (IN MPA).	110
FIGURE 6.4.6 - SHIELD-EQUIPPED ISO 7141 TEST ENERGY RESPONSES SHOWING A) KINETIC AND INTERNAL ENERGY, B) SLIDING INTERFACE ENERGY, C) HOURGLASS ENERGY, AND D) EXTERNAL WORK AND TOTAL ENERGY.....	112
FIGURE 6.4.7 – CROSS-SECTIONAL VIEW OF TIRE BLOWOUT SIMULATION DEFORMED GEOMETRY FOR A A) STANDARD WHEEL ASSEMBLY AND B) A CLOSE UP OF ITS FLANGE	

AND LOCK RING AREAS, AS WELL AS C) A SHIELD-EQUIPPED WHEEL ASSEMBLY AND D) A CLOSE UP OF ITS FLANGE AND LOCK RING AREAS.	115
FIGURE 6.4.8 - TIRE TO WHEEL RESULTANT CONTACT FORCE DURING TIRE BLOWOUT TEST PRIOR TO FAILURE OCCURRING.....	117
FIGURE 6.4.9 - LOCK RING RESULTANT CONTACT FORCE DURING TIRE BLOWOUT SIMULATION.	118
FIGURE 6.4.10 - CONTOURS OF EFFECTIVE PLASTIC STRAIN (MM/MM) IN LOCK RINGS AT FAILURE DURING TIRE BLOWOUT SIMULATION FOR A) A STANDARD WHEEL AND B) A SHIELD-EQUIPPED WHEEL ASSEMBLY.	119
FIGURE 6.4.11 – EFFECTIVE PLASTIC STRAIN CONTOURS AS OBSERVED DURING THE BLOWOUT SIMULATION FOR THE OVERALL A) SHIELD AND B) NEAR THE LOCK KEY REGION OF THE WHEEL WHERE THE MAXIMUM VALUE OBSERVED.....	120
FIGURE 6.4.12 – CROSS-SECTIONAL VIEW OF DEFORMED GEOMETRY AT FULL STRIKER IMPACT DURING ROTATIONAL SIDE IMPACT VIRTUAL TEST FOR A) STANDARD AND B) SHIELD-EQUIPPED WHEEL ASSEMBLY.	121
FIGURE 6.4.13 – CONTOURS OF VON MISES STRESS AT FULL STRIKER IMPACT DEPTH FOR A) STANDARD AND B) SHIELD-EQUIPPED WHEEL ASSEMBLY.	123
FIGURE 6.4.14 - CONTOURS OF EFFECTIVE PLASTIC STRAIN AT FULL STRIKER IMPACT DEPTH FOR A) STANDARD AND B) SHIELD-EQUIPPED WHEEL ASSEMBLY, AS WELL AS THE C) SHIELD-EQUIPPED ASSEMBLY WITH NO SHIELD OR TUBE NUTS VISUALIZED AND D) ONLY THE SHIELD AND TUBE NUTS.	124
FIGURE 6.4.15 - CONTOURS OF VON MISES STRESS IN THE OUTER FLANGES WHEN OVERALL MAXIMUM VALUES WERE OBSERVED FOR BOTH A) STANDARD AND B) SHIELD- EQUIPPED WHEEL ASSEMBLIES.	126
FIGURE 6.4.16 - CONTOURS OF EFFECTIVE PLASTIC STRAIN IN THE OUTER FLANGES WHEN OVERALL MAXIMUM VALUES WERE OBSERVED FOR BOTH A) STANDARD AND B) SHIELD-EQUIPPED WHEEL ASSEMBLIES.....	127
FIGURE 6.4.17 - STRIKER TO WHEEL CONTACT FORCE FOR ROTATIONAL SIDE IMPACT SIMULATIONS.	128
FIGURE 9.1.1 - RESPONSE FOR 29.5R29 TIRE TEST EVENT EXHIBITING MAXIMUM DEFLECTION IN THE A) VERTICAL AND B) LATERAL DIRECTIONS AS WELL AS A C)	

CROSS-PLOT SHOWING LATERAL DEFLECTION VERSUS VERTICAL DEFLECTION IS PROVIDED.....	140
FIGURE 9.1.2 - RESPONSE FOR 26.5-25 TIRE TEST EVENT EXHIBITING MAXIMUM DEFLECTION IN THE A) VERTICAL AND B) LATERAL DIRECTIONS AS WELL AS A C) CROSS-PLOT SHOWING LATERAL DEFLECTION VERSUS VERTICAL DEFLECTION IS PROVIDED.	141
FIGURE 9.1.3 - VERTICAL DISPLACEMENT COMPARISON FOR THE A) 29.5R29 AND B) 26.5-25 TIRES BETWEEN LASER DISPLACEMENT TRANSDUCER MEASUREMENTS AND HIGH-SPEED CAMERA IMAGE TRACKING USING PROANALYST FOR CORRELATION PURPOSES.	142
FIGURE 9.1.4- VERTICAL DEFLECTION RESPONSES FOR TRACKED NODES DURING 29.5R29 TIRE TEST EVENT WHERE MAXIMUM DEFLECTIONS WERE OBSERVED FOR THE A) H-IN AND H-OUT POINTS, B) D-IN AND D-OUT POINTS, AND C) V-IN AND V-OUT POINTS.	143
FIGURE 9.1.5– HORIZONTAL DEFLECTION RESPONSES FOR TRACKED NODES DURING 29.5R29 TIRE TEST EVENT WHERE MAXIMUM DEFLECTIONS WERE OBSERVED FOR THE A) H-IN AND H-OUT POINTS, B) D-IN AND D-OUT POINTS, AND C) V-IN AND V-OUT POINTS.....	144
FIGURE 9.1.6- VERTICAL DEFLECTION RESPONSES FOR TRACKED NODES DURING 26.5-25 TIRE TEST EVENT WHERE MAXIMUM DEFLECTIONS WERE OBSERVED FOR THE A) H-IN AND H-OUT POINTS, B) D-IN AND D-OUT POINTS, AND C) V-IN AND V-OUT POINTS.	145
FIGURE 9.1.7– HORIZONTAL/LONGITUDINAL DEFLECTION RESPONSES FOR TRACKED NODES DURING 29.5R29 TIRE TEST EVENT WHERE MAXIMUM DEFLECTIONS WERE OBSERVED FOR THE A) H-IN AND H-OUT POINTS, B) D-IN AND D-OUT POINTS, AND C) V-IN AND V-OUT POINTS.	146
FIGURE 9.1.8– DEFLECTION DATA FOR THE 29.5R29 TIRE SHOWING A) VERTICAL DEFLECTION VERSUS LOAD FORCE AND B) LATERAL DEFLECTION VERSUS LOAD FORCE COMPARED TO THE CORRESPONDING GOODYEAR ENGINEERING DATA POINT.....	147
FIGURE 9.1.9– DEFLECTION DATA FOR THE 26.5-25 TIRE SHOWING A) VERTICAL DEFLECTION VERSUS LOAD FORCE AND B) LATERAL DEFLECTION VERSUS LOAD FORCE COMPARED TO THE CORRESPONDING GOODYEAR ENGINEERING DATA POINT.....	147

FIGURE 9.3.1 - EFFECTIVE PLASTIC STRAIN VERSUS TRUE STRESS OF MINING WHEEL	
MATERIAL SAMPLE TENSILE TEST SHOWING VIRTUAL AND EXPERIMENTAL	
OBSERVATIONS.	161
FIGURE 9.3.2 - ENGINEERING STRAIN VERSUS ENGINEERING STRESS OF MINING WHEEL	
MATERIAL SAMPLE TENSILE TEST SHOWING VIRTUAL AND EXPERIMENTAL	
OBSERVATIONS.	161
FIGURE 9.3.3 - VIRTUAL TENSILE TEST MODEL.	162

LIST OF ABBREVIATIONS

ACARP	Australian Coal Association Research Project
BS	Bead Seat
CAE	Computer-Aided Engineering
cDAQ	Compact Data Acquisition
CPU	Central Processing Unit
DIC	Digital Image Correlation
EXP	Experimental
FE	Finite Element
GAWR	Gross Axle Weight Rating
GDP	Gross Domestic Product
ICAM	Incident Cause Analysis Method
ISO	International Organization for Standardization
LHD	Load-Haul-Dump
LS&G	Loaded Section and Growth
LTA	Less Than Adequate
MPI	Magnetic Particle Testing
MPP	Massively Parallel Processing
MT	Material Testing
NIOSH	National Institute of Occupational Safety and Health
NMP	New Material Properties
NSIW	North Shore Industrial Wheel
OD	Outer Diameter
OSHA	Occupational Safety and Health Administration
OTR	Off-The-Road
OW	Overall Width
SAE	Society of Automotive Engineers
SLR	Static Loaded Radius
TAC	Technical Advisory Committee
TPMS	Tire Pressure Monitoring System
TRA	Tire and Rim Association
WSIB	Workplace Safety and Insurance Board
WSN	Workplace Safety North

1 INTRODUCTION AND MOTIVATION

1.1 BACKGROUND AND MOTIVATION

The utilization of a country's natural resources is crucial to ensure long term economic prosperity and thus necessitates a robust mining industry, which in turn promotes the expansion of a country's fundamental infrastructure. With Canada being one of the world's largest mining nations, the mining industry contributed \$63 billion [1] to Canada's Gross Domestic Product (GDP) in 2011, with nearly 330,000 people employed in over 115 communities [2]. Furthermore, half of all Canadian rail-freight revenues are generated by the mining industry. Canada also acts as a major hub for global mining finance, with the Toronto Stock Exchange handling 83% of the world's mining equity transactions and Canada headquartering over 75% of the world's mining companies [3]. Worldwide, the mining industry is under constant expansion, driving the advancement of mining technology through the implementation of modern machinery and mining techniques, and pushing for ever-increasing mining efficiency. In Canada alone, it is predicted \$136 billion will be invested in mining projects in the next decade [3]. As technology and methodology develops, raw material extractions increase and, more importantly, previously difficult or uneconomical natural resources can now be mined.

While the economic aspects and wide breadth of influence Canadian mining has on a global scale, the most critical consideration for any industry must be the health and safety of its workers. Globally, 1.9 to 2.3 million job-related deaths occur each year and the cost to society is staggering with workplace accidents and work-related diseases attributing to 4% of the worldwide gross domestic product [4]. In the US, it is estimated

that the cost of premature workplace-related deaths was \$43 billion over a 10 year span (1992-2001), which is greater than the gross domestic product of approximately 116 different nations. Similarly tragic is that between 1996 and 2008, there were 11,959 deaths as a result of occupational accidents in Canada alone [5].

Despite comparably high standards and continual safety improvements due to Canada's status as a well-developed nation, an unacceptable number of fatalities still occur each year in the mining industry in addition to serious injuries and long-term hazardous health effects on workers. Trades, transport, and equipment operators have the highest fatality rates in Canada at 408.6 per year on average between 1996 and 2004 [6]. With the common adaptation of "zero tolerance" for workplace injuries across a variety of industries, the historically high risk environment common in the mining industry remains a concern. While improved government regulations, increases in worker training, and technological advancements are recognized to aid in the reduction of injuries and fatalities, it still remains that in Ontario mines alone 30 fatalities have occurred between 2002 and 2012. Despite no fatalities in 2010, there is no consistent trend suggesting the rate of fatalities are decreasing, as depicted in Figure 1.1.1.

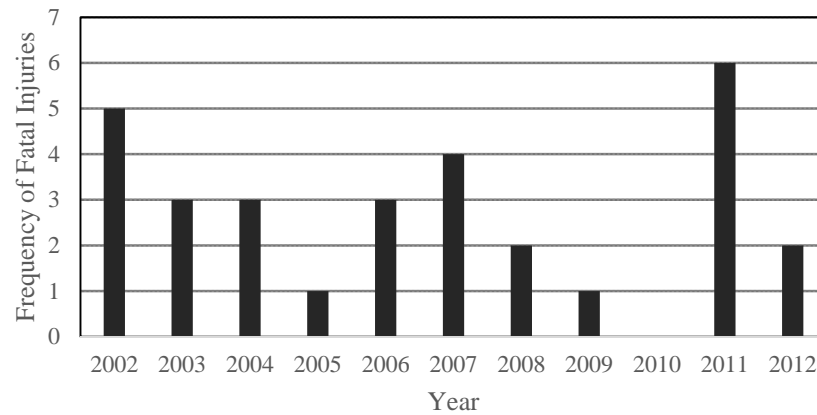


Figure 1.1.1 - Ontario mining industry fatal injuries [7]

Throughout the years, many injuries and fatalities have been associated with the use of multi-piece wheel assemblies. In recent history, fatalities related to multi-piece wheel failures occurred in the year 2000 at two different Ontario mines in addition to three accidents causing critical injuries [8]. The two most significant incidents motivating the present research occurred on July 24th, 2000 and November 22nd, 2000 at Placer Dome Limited's Detour Lake Mine in Timmins, Ontario, and Goldcorp's Musselwhite Mine in Musselwhite, Ontario, respectively. When the first incident occurred, two workers were inflating tires on a Kubota M5030 utility tractor using three-piece rims when the wheel assembly suddenly and unexpectedly failed, resulting in the death of one worker and critical injury of the other [9].

The second incident occurred during scheduled maintenance on an underground haul vehicle. During maintenance, one of the multi-piece wheels catastrophically failed, resulting in two mechanics being thrown three meters as a result of the force released from the wheel. Tragically, the incident claimed the life of Mr. Jerome Burns, while a second mechanic suffered severe facial injuries and a compound fracture of the left arm [10]. Through the course of an investigation into the incident, and the related court

proceedings, official recommendations were specifically suggested in relation to the use of multi-piece wheels by the Ontario Ministry of Labour [10]:

- a) The Ministry of Labor and all industries using multi-piece wheel rim assemblies should require further research to be conducted by engineers to construct a tire cage or a holding device to contain these large multi-split rims and tires during inflation.*
- b) The Ministry of Labour and all industries using multi-piece wheel rim assemblies should require further research to be conducted by engineers to manufacture a better quality, (eg. thicker and stronger) safer rim for heavy equipment.*

In specific reference to the second suggestion, (b), an initial study was conducted under the support of the Workplace Safety and Insurance Board (WSIB) of Ontario led by Dr. William Altenhof, of the University of Windsor. Under the guidance of Dr. Altenhof, M.A.Sc. student Vivek Vijayan performed a structural analysis of multi-piece heavy mining vehicle wheels through the use of innovative engineering techniques and the development of a numerical wheel model to evaluate the fatigue life of wheels. Based on an exhaustive review of research available in open literature and not proprietary in nature, it is believed that the work and journal publications by Vijayan et al. [11] [12] is the only research that specifically addresses the desire to improve multi-piece wheel assemblies for the purposes of increasing safety and quality from a design perspective. Though work has been conducted to develop best practices and safety regulations related to the use, assembly, and maintenance of multi-piece wheels, studies focused on design considerations are either extremely limited or proprietary to wheel and tire manufacturers and suppliers.

Counter to Off-The-Road (OTR) tire technology and designs that have advanced in recent decades, wheel designs have remained relatively unchanged in the last 50 years. The work of Vijayan et al. [11] [12] is discussed in detail in succeeding sections; however, the most pertinent conclusions of their study is that further work was required to address the discrepancy between virtual analysis results and in-field observations since an infinite fatigue life was predicted for the three-piece wheel that was considered. Additional conclusions recommended a better understanding of the effect of worker negligence that results in damage to rim components during maintenance and assembly as well as the effect of environmental conditions and impact during use. A potentially critical limitation of Vijayan's work was that the tire was not included in fatigue analyses nor was the interaction between the wheel and tire during in-field loading conditions considered.

In its simplest form, the motivation behind the research efforts presented in this thesis is to reduce injuries and fatalities associated with the operation and maintenance of vehicles equipped with multi-piece wheel assemblies, which carries with it significant social and economic benefits. This is achieved by gaining a better understanding of the inherent hazards of these wheels and assessing their mechanical performance to a degree greater than ever previously completed, based on the review of open literature. Proposed methodologies and mechanical devices, developed using various engineering techniques and the finite element analysis approach, are designed as the initial steps to reduce and mitigate risks associated with multi-piece wheels.

2 REVIEW OF LITERATURE

2.1 GENERAL INFORMATION ON USE OF MULTI-PIECE WHEEL ASSEMBLIES

More than ever, mining operations employ a vast portfolio of heavy machinery to attain the highest levels of operational efficiency possible, which necessitates proper equipment operation and maintenance and in turn requires maintaining the highest standards of safety. In the case of mineral extraction and transport, mining vehicles are often pushed to their limits to carry larger, heavier loads faster and quite often over unfavourable terrain conditions, in an effort to maintain high productivity. Off-The-Road tires, like the mining vehicles they are used on, are often exposed to very harsh operating and environmental conditions, consisting of severe loading, uneven terrain, and even side-impact due to narrow mine pathways. These demanding performance characteristics call for complex structural tire designs with large tread, sidewall, and bead thicknesses along with stiff, durable materials for abrasion and cut resistance. As a result, it is typically impossible to mount/dismount an OTR tire onto a traditional single piece wheel, such as the designs found on passenger vehicles, without resulting in irreversible damage to the tire or wheel. This aspect necessitates the use of multi-piece wheels, typically consisting of multiple components assembled together with the tire.

Similar to passenger vehicle tires, OTR tires are broadly categorized based on their construction and design, with the main types being bias-ply and radial tires, and each having different compositions and performance characteristics. The major differences between these two styles are the direction of the cord plies built into the tire. Radial tires typically have cords perpendicular to the bead of the tire, along with one steel body ply or

multiple alternative material plies, and then multiple crossed plies or belts made of steel cords used to stabilize the tread area. In contrast, bias-ply tires have fabric plies typically made of nylon or polyester that are angled from bead to bead in a criss-cross pattern, resulting in stiffer sidewalls. Each have their advantages and disadvantages; however, radial tires are a more modern design and used almost exclusively for on-road vehicles. Figure 2.1.1 helps highlight these differences.

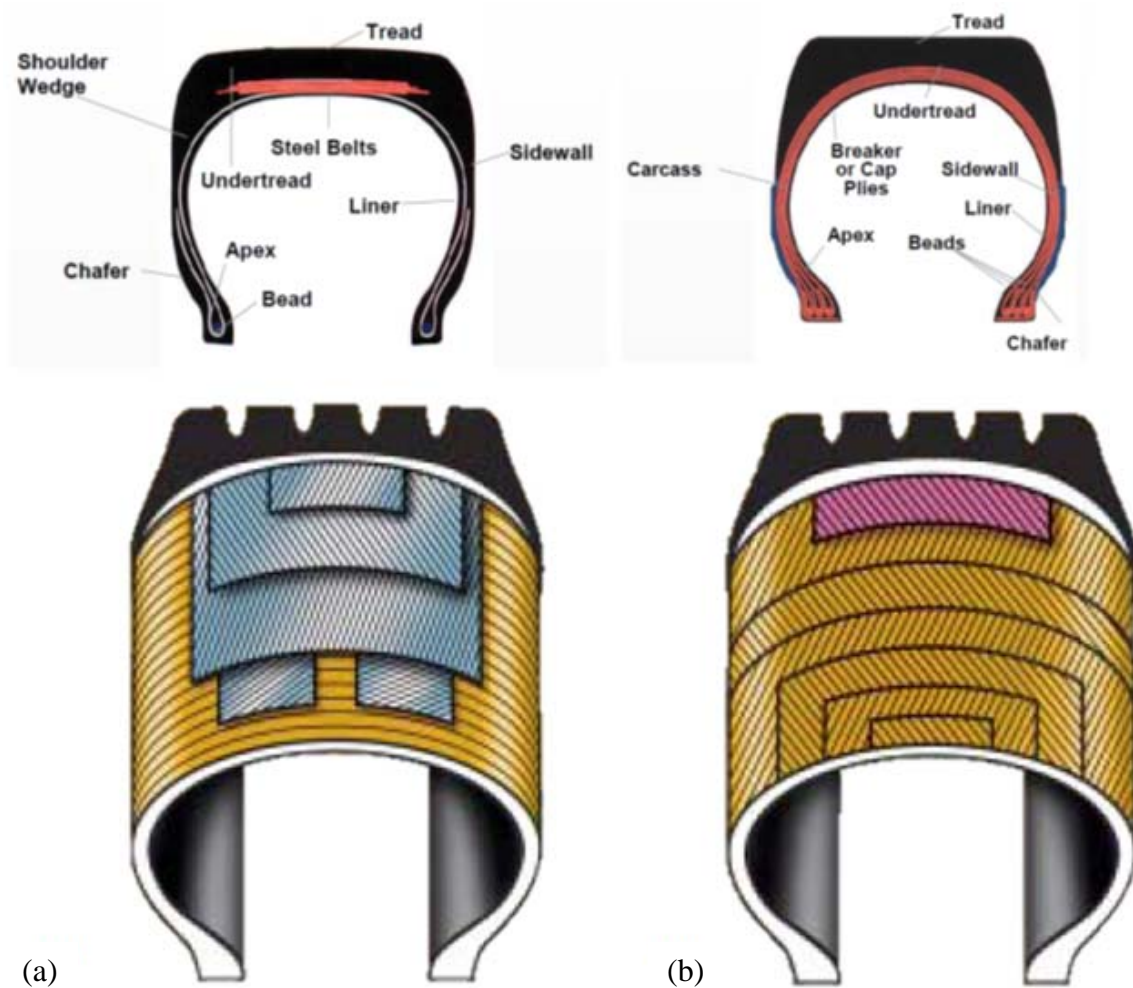


Figure 2.1.1 – Cross-sectional and cutaway views of (a) radial and (b) bias-ply tire construction designs [13].

For reference, Figure 2.1.2 describes terminologies associated with tire geometry and construction pertinent to the referenced engineering data discussed in future sections. Wheel and rim geometry is standardized by the Tire and Rim Association, Inc., located in Copley, Ohio, USA, and these standards are generally followed by manufacturers globally. Where applicable, the U.S. Imperial system of measurements was used, as it is the base standard for tire and wheel sizes. For example, a 29.5R29 tire has a section width of 29.5 inches, a standard aspect ratio of 1, and a wheel diameter of 29 inches, and a 59/80R63 tire would be a radial tire with a section width of approximately 59 inches and an aspect ratio of 80, yielding a section height of 47.2 inches and a wheel diameter of 63 inches.

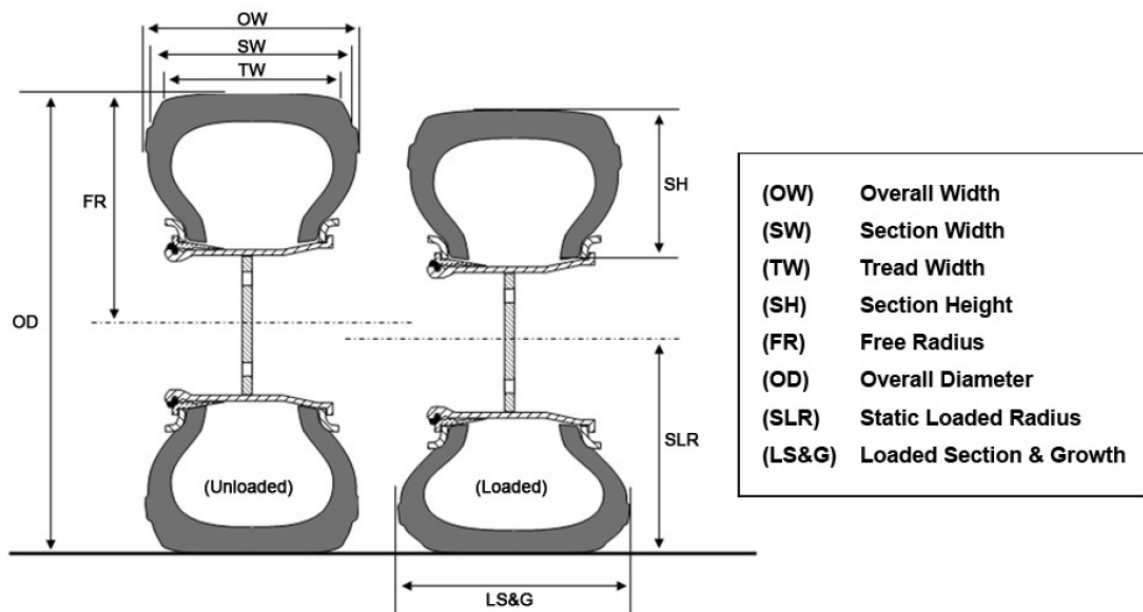


Figure 2.1.2 - Definitions of terminologies associated with tire geometry as outlined by the manufacturer [14].

Conventional multi-piece wheels, such as those used on heavy mining vehicles, are typically constructed of structural steel and contain a variety of features and components,

including: (1) a rim base, (2) mounting disc, (3) front flange, (4) rear flange, (5) lock ring, (6) O-ring(s)/Seal ring(s), (7) bead seat (BS) band, and (8) support disc, as illustrated in Figure 2.1.3 for a five-piece wheel. Depending on the style and complexity of the wheel, certain components may be combined into one forged or machined component (e.g. the rear flange is part of the rim base in a three-piece wheel design compared to a five-piece wheel).

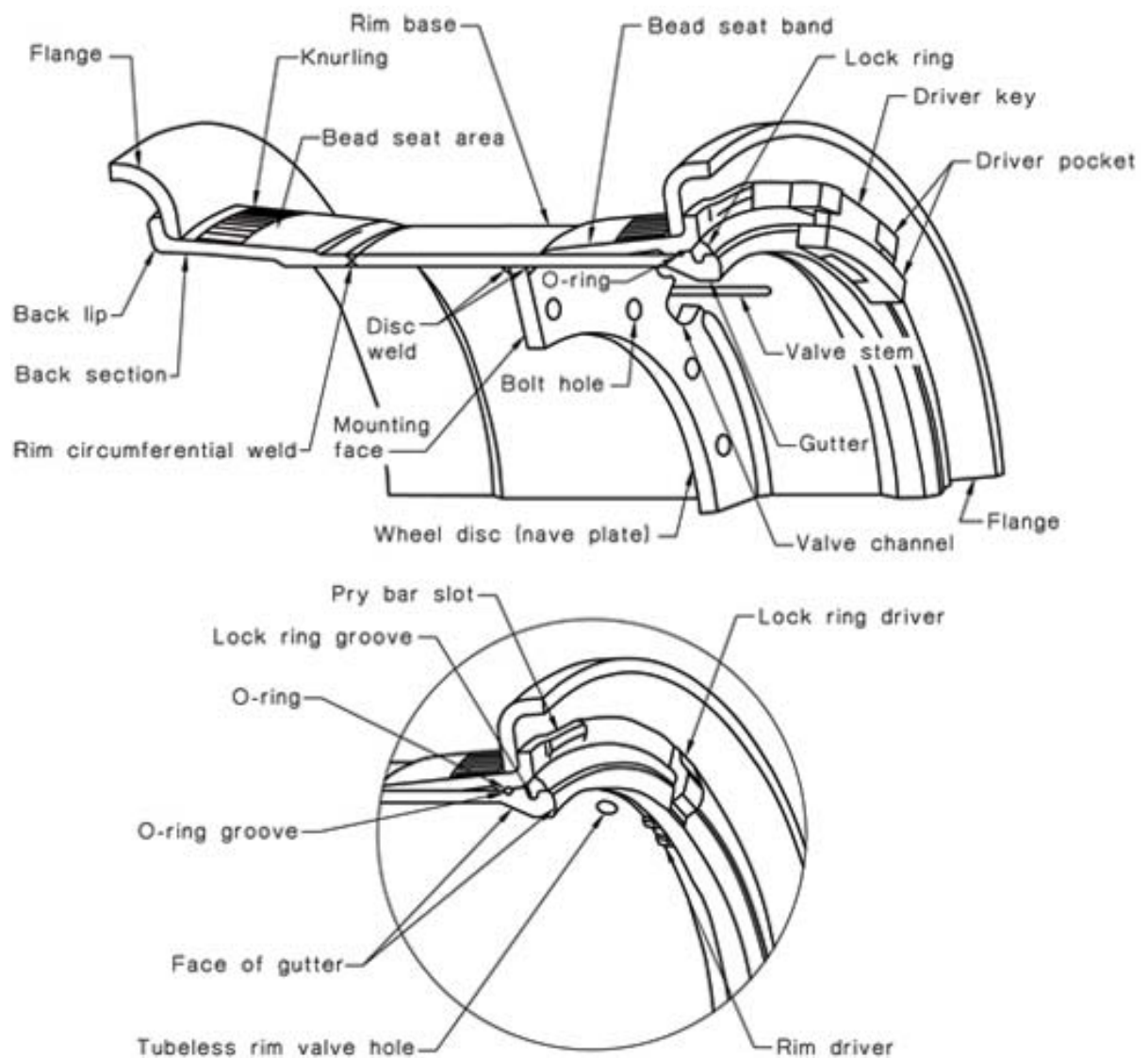


Figure 2.1.3 - Multi-piece wheel/rim nomenclature (Figure reproduced with permission from SAI Global Ltd under Licence 1312-c007) [15].

An important note regarding multi-piece wheel nomenclature would be the usage of the terms “wheel” and “rim”, which may vary from the common usage in relation to passenger vehicle wheels. Though the terms “rims” and “wheels” are often interchanged when referencing passenger vehicles that typically utilize single-piece wheels, this distinction is unique for multi-piece wheels. The main difference would be that a rim does not include a mounting flange that allows it to be secured to a vehicle, in contrast to a wheel, though a rim could possibly consist of multiple pieces itself such as a removable flange or lock ring. Furthermore, the term “wheel assembly” would include all components of the rim/wheel and a mounted tire.

Regardless of wheel assembly style, typical assembly procedures consist of first mounting the rear flange onto the rim base, followed by the tire. Subsequently, the front flange is placed against the tire and a lubricated rubber O-ring is installed in its groove on the rim base. The O-ring is responsible for ensuring that an airtight seal is maintained when the tire is pressurized. The BS band is then put in place, often requiring careful effort to slide between the tire and rim base while ensuring the O-ring remains seated and undamaged. Next, the most critical component is installed, the split lock-ring, which ensures the proper engagement of wheel components. Lastly, tire pressurization is initiated, providing the engagement force between the lock ring and adjacent components to safely secure the components for operation.

Wheel assemblies used off the road have a broad range of sizes based on application, but to get an appreciation of their overwhelming size, one could consider one of the world’s largest tires. The 59/80R63, manufactured by Bridgestone and Michelin, is used on the Caterpillar 797 series haul trucks, as shown in Figure 2.1.4 below. At a cost of

approximately \$5 million, the Caterpillar 797 has a gross vehicle weight of 623,700 kg and is equipped with six multi-piece wheel assemblies, valued at \$42,500 each [16]. With a payload capacity of approximately 363 tons and a loaded top speed of 68 kph, each wheel assembly consists of enough steel to produce two small automobiles, enough rubber for 600 passenger vehicle tires, and is pressurized to over 690 kPa [17].

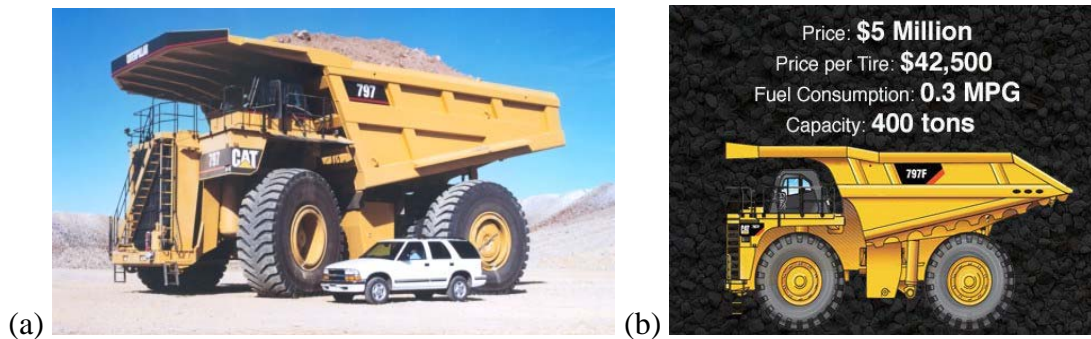


Figure 2.1.4 – (a) Caterpillar 797F size comparison, and (b) vehicle information and capability specifications [16].

2.2 SAFETY HAZARDS RELATED TO MULTI-PIECE WHEELS

Though they are the only viable solution to mounting OTR tires, multi-piece wheels present potential safety hazards inherent to their design, due to the working mechanism that maintains engagement of wheel components, the high operating pressures of tires, and their typically severe environmental and loading conditions. Emphasized by the work of Vijayan et al. [11], the corrosive operating environments and high cyclic and sudden impact loadings were reported to result in premature wheel failures, with often tragic consequences.

Any pneumatic wheel and tire assembly is hazardous by its very nature, in that they are pressure vessels designed to contain large volumes of highly compressed gas while supporting payloads of varying magnitudes. In circumstances where an uncontrolled loss

of pressure occurs due to a tire or wheel failure, an explosive force can be released where failed wheel and tire components become dangerous projectiles. A standard medium-duty truck tire, 0.5m (20 inches) in diameter and pressurized to 690 kPa, contains a potential explosive force of approximately 180 kN [18]. In one case of where a haul truck tire exploded, fragments of the wheels were thrown up to 200 m away from the vehicle [19].

2.2.1 Review of Multi-Piece Wheel Incidents and Associated Difficulties

With the primary goal of this research being to improve the safety of multi-piece wheel assemblies, the incidents discussed in the following section provide the most significant motivation possible to any noble research effort: that any improvement which reduces the frequency or severity of wheel assembly failures will reduce injuries and save lives.

The review of incidents related to multi-piece wheels is a critical first step in researching methods to enhance the safety of wheel assemblies. Without an appropriate level of understanding regarding the failure modes of wheels, it would be impossible to have confidence that any proposed solutions to mitigating risks associated with wheels would be effective. Secondly, incident reviews provide insight into the human aspect related to wheel and tire use, assembly, and maintenance, which similarly aids in the development of feasible safety-enhancing devices.

Important to note is the difficulty associated with reviewing and compiling information regarding incidents accurately. Firstly, the majority of reports found related to multi-piece wheels are situations involving injuries and fatalities. The issue with this is two-fold: (1) this typically results in investigations and legal proceedings that may

either delay the release of information or reduce details that are provided out of respect for the injured or guilty; and (2) often incident reports do not encompass scenarios where wheels or tires have failed in a “near-miss” situation. An example of the latter would be when a failure occurs, but does not result in catastrophic failure or associated injuries, though could have, given a worker’s closer proximity to the wheel assembly. In the latter case, it is then important not to simply assume that since such information is not available, the frequency of “near-misses” is low.

Furthermore, an additional challenge to assembling statistics regarding incidents is the avenue by which such information is shared. The majority of incidents are reported through government organizations and research foundations such as Workplace Safety North (Ontario, Canada), the Workplace Safety and Insurance Board (Ontario, Canada), the Occupational Safety and Health Administration (U.S. Dept. of Labor), National Institute of Occupational Safety & Health (U.S. Dept. of Health and Human Services), the Safety Institute of Australia (Australia), and the Australian Coal Association Research Project (ACARP, Australia). The issue with this is that many regions that have prevalent mining, construction, and other industries using heavy vehicles equipped with multi-piece wheels are in developing nations that suffer from a lack of safety standards and governing safety organizations, and as a result have less than satisfactory reporting systems. Additionally, though wheel designs have been relatively unchanged since the 1950s, historical tracking of incidents is difficult since reporting has only been more prevalent in recent years. The frequency of incidents is believed to have been higher in the past given poorer maintenance, assembly, and safety procedures as well as the lack of standardization of construction and geometry.

2.2.2 Review of Studies Related to Wheel Incidents

For the purposes of reviewing incidents, two of the most comprehensive incident review summaries are referenced. This includes the literature review of Vivek Vijayan [20] and the Australian Coal Association Research Project (ACARP) study to review and analyze tire related accident and incidents by T. Rasche and T. Klinge [21].

As part of his M.A.Sc. thesis work, entitled *Numerical model development of a heavy mining vehicle multi-piece rim and wheel assembly for structural analysis* [12], Vijayan included a comprehensive review of a variety of articles regarding best practices related to the servicing of multi-piece wheels as well as articles associated with fatalities, injuries, and other wheel failures spanning between 1989 and 2005 from around the world. All articles found were available in the public domain and in total 32 were included; eight were related to servicing wheels, 15 were incident reports related to fatalities, five were incident reports resulting in injuries, and four were incidents involving neither injuries nor fatalities yet the potential to inflict either. For the purposes of brevity, the review can be referenced directly for details of the incidents, as the second study to be discussed provided information on more incidents and in greater detail.

In 2006, an even more detailed review of incidents by Tilman Rasche and Thomas Klinge, two Australian industry leaders in mining risk management and wheel assembly safety, was commissioned through an ACARP study grant and conducted by Klinge & Co. Pty Ltd.. This study, entitled *Review and Analysis of Tyre Related Accidents and Incidents – an ACARP Study to Improve Tyre & Rim Maintenance and Operational Safety of Rubber Tyred Earthmover Equipment* [21], incorporated a total of 82 incident and accident reports available in the public domain. It was determined that 33% of

incidents resulted in the death of a tire servicemen or other personnel; however, an additional 50% were related to similar modes of failure and classified as “potential fatalities.” The actual and potential consequences related to incidents and accidents were classified into the subsequent categories shown in Figure 2.2.1.

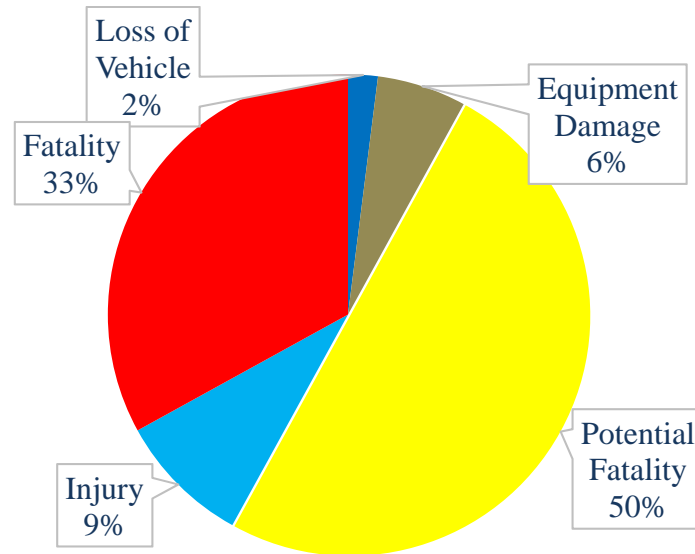


Figure 2.2.1 - Actual & Potential Consequences of Tire and Rim Related Incidents and Accidents [21].

Even more important was the detailed analyses of incidents using the Incident Cause Analysis Method (ICAM) to categorize failure modes. Analysis showed that “Less Than Adequate” (LTA) material testing/fatigue non-destructive testing was the leading root cause of failures, followed closely by heating of the wheel assembly or studs, LTA matching of assembly components, LTA rim integrity, and LTA deflation practice. A summary of all root and contributing causes of fatalities and potential fatalities is shown in Figure 2.2.2.

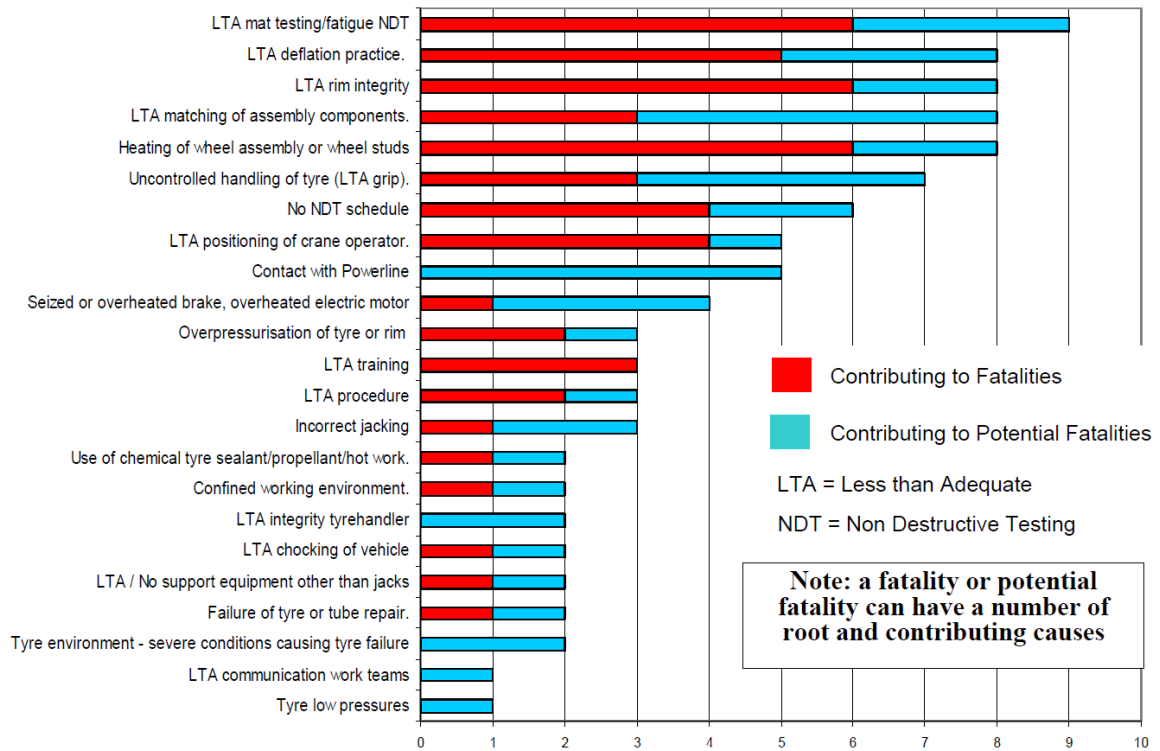


Figure 2.2.2 - Fatalities & Potential Fatalities – Root and Contributing Causes [21].

2.2.3 Summary of Recent Wheel-Related Injuries and Fatalities

Since both of the previously mentioned studies were completed by 2007, wheel-related injuries and fatalities that occurred more recently were not included. Listed below are several incidents with an associated brief summary of the occurrence showing that wheel assembly issues continue to be hazardous risks:

- a) February, 25th, 2012; Edmonton, Alberta, Canada [22]: Two workers were welding a wheel to repair a flat tire when the tire exploded. Due to an ongoing investigation, further details are limited. The incident resulted in one fatality (53 year old male) and an additional serious injury (54 year old male).
- b) September 27th, 2011; Queensland, Australia [23]: While being prepared for vehicle frame servicing, two maintenance workers noticed a small bulge in the sidewall of the 24.00R35 tire. The tire failed catastrophically but fortunately proper safety procedures were followed; only minor injuries were experienced by three workers due to the air blast and resultant cloud of dust and loose gravel.
- c) January 17th, 2011; Newport News, Virginia, USA [24]: During inflation of a 24 inch multi-piece wheel, the wheel failed and a serviceman was thrown against the floor from the force. Despite using a 22 inch long extension on the inflation tool, the worker sustained severe head trauma and died in hospital.
- d) October 14th, 2010; Clyde, Ohio, USA [25]: During the cleaning of a commercial truck equipped with a multi-piece rim, the failure occurred and resulted in the fatality of an auto detailer (58 year old male). The failure was described as explosive and resulted in metal fragments and other wheel material being projected at the worker's forehead and left arm.
- e) January 18th, 2010; Norco, California, January 18, 2010 [26]: A split rim equipped with a pneumatic tire was being replaced on a fork lift by two maintenance workers. The assembled wheel was installed on the vehicle; however, it was observed by one of the workers that the tube of the tire was

pinched by the two halves of the rim during inflation. While the tire remained partially inflated, one worker started to remove the wheel using an impact wrench and the other left to get a device to deflate the tire; however, the tube of the tire failed in a blowout fashion, resulting in rim separation. A failed rim component became a projectile and struck the worker in the forehead, resulting in fatal wounds.

- f) August 28th, 2009; Elk Grove Village, Illinois, USA [27]: A truck tire technician was replacing four tires and followed proper procedure by assembling and inflating using a safety cage; however, failure occurred while the wheel was being reinstalled on a trailer chassis, resulting in fatal head injuries.
- g) August 28th, 2009; Fort McMurray, Alberta, Canada [28]: A maintenance worker assigned to service tires on multiple heavy haul trucks was struck and killed by wheel components when a wheel being inflated in a tire manipulator failed. The worker had difficulty installing the lock ring during reassembly of the wheel. Analysis from a related investigation concluded that the lock ring was most likely never correctly seated and the lack of lubricant used during assembly may have contributed. Investigation of the incident showed that components of the wheel landed as far as approximately 47 meters away from the tire while inflation pressures were between 365 kPa and 900 kPa.
- h) January 23rd, 2009; Hazard, Kentucky, USA [29]: During inflation on a 12.00R20 Goodyear tire mounted to a multi-piece wheel, the wheel separated with explosive force and components struck the tire serviceman in the head, resulting in fatal injuries. Despite the presence of multiple restraining devices designed for the inflation of wheel assemblies, they were not used.
- i) December, 2007; New York, USA [30]: After noticing a three-piece wheel assembly equipped with an underinflated 17.5-25 tire, a worker began re-inflating the tire and it blew out. The lock ring was propelled outwards and struck the worker in the head, causing fatal injuries.
- j) December 31st, 2007; Massachusetts, USA [31]: While a mechanic (59 year old male) attempted to replace a dual-wheeled container handler vehicle's front inner tire mounted on a five-piece rim, the outer wheel failed during removal in a

blowout condition. The resulting force pushed the mechanic into a nearby forklift's mast, causing fatal injuries. An investigation found a crack that had propagated in the lock ring groove area, as well as severe wear and rust.

It is important to note that although the majority of the fatalities discussed in the previous incident reports are attributable to the lack of conformance to proper safety procedures as will be discussed in Section 2.2.4, one has to recognize that all incidents were either the direct or indirect result of the mechanical performance of the wheel components. This suggests that the hazards of multi-piece wheels are inherent to their design, an issue that can only be resolved by the combination of better usage practices related to wheels and tires, a greater understanding of the underlying failure mechanisms of the wheels and tires, and consideration for how failures may be mitigated through design modifications and safety devices.

2.2.4 Wheel Assembly Maintenance and Handling Best Practices

Organizations such as the Occupational Safety and Health Administration (OSHA) of the United States Department of Labor, National Institute of Occupational Safety & Health (NIOSH) of the United States Department of Health and Human Services, and Workplace Safety North (WSN) of Ontario, Canada, have made safety regulations or best practice suggestions associated with multi-piece wheels. Most mining companies also maintain strict operation and maintenance procedures regarding multi-piece wheel assemblies. Though commonalities are present in many of the procedures, it is believed the most comprehensive document is the Australian Standard AS4457-1997, *Earth-moving machinery – Off-highway rims and wheels – Maintenance and repair* Part 1 and 2

[15]. The procedures are very detailed; however, some general recommendations are listed below [15]:

- a) Only trained personnel are allowed to service multi-piece wheels, using the correct tools and following specific procedures.
- b) Always remove the valve core and exhaust all air from a single tire and from both tires of a dual assembly prior to demounting a tire.
- c) Stay out of the trajectory paths of the wheel components and use a safety cage or other restraining device when inflating a tire.
- d) Never re-inflate a tire of multi-piece wheel when the pressure is below 80% of recommended pressure while the wheel is on the vehicle. Demount the tire and disassemble the wheel assembly.
- e) Enforce scheduled preventive inspection and maintenance. Multi-piece wheels should be viewed as consumable items requiring proper maintenance.

2.3 MULTI-PIECE WHEEL AND OFF-THE-ROAD TIRE FAILURE MODES

As a first step to mitigating safety risks of any hazard, it is critical to understand exactly what the risks are and their root cause. This imperative process is the basis of the wheel tracking database development discussed Section 5. In the case of OTR tires, their failure modes can be classified into two broad categories: tire zipper ruptures and tire explosions. Failure of the wheel or wheel component(s) constitute the remaining type of wheel assembly failure mode and result in tire blowouts.

2.3.1 Tire Zipper Failures

Tire zipper ruptures occur along the circumference of the upper sidewall of a tire and result in instantaneous air loss in a severe manner. They are a fatigue-based failure that initiate from a single point and instantly open in both directions due to the transfer of load

to adjacent body plies until all pressure is evacuated. The origin for the name of this type of failure is due to the post-failure appearance of the ruptured area where typically an even line of broken steel cords are exposed. This is shown in Figure 2.3.1 below.



Figure 2.3.1 – Result of tire zipper failure [21].

The cause of zipper ruptures are most commonly attributed to operating a tire severely underinflated or for a prolonged duration while below nominal tire pressures [32]; however, damage induced through other avenues can result in similar effects, such as over-inflation. Given proper inflation, a tire's steel cords are meant to be kept in constant tension through the course of wheel rotation even as they pass through the tire foot print. Underinflating a tire allows for excessive sidewall flexing and compression of the cords, resulting in heat buildup, and severe bending and fatigue of the cords. As a result of this cyclic loading and bending, cords can become fatigued and fail internally even prior to a rupture. Once the tire is re-inflated to proper pressure, the weakened sidewall can no longer support the load and pressure, and failure ensues. Prior to failure, damage can be indicated by bulging or wrinkling of the sidewall as well as crunching or popping sounds, but is often overlooked in a working environment. Once rupture occurs,

the rapid loss of air through the puncture in the tire brings about the release of a lethal force and can result in serious injuries and fatalities. For example, due to the dislodgement of wheel components, the blast of air hurling a serviceperson against a wall or other equipment, or simply permanent hearing damage due to the loud blasting sound. The larger the wheel assembly and the higher the pressures involved are, the greater the hazard.

2.3.2 Tire Explosion Failures

Tire explosions are typically the most severe failure modes as they not only involve the rapid release of air, similar to a blowout or zipper failure, but would normally involve a chemical reaction and/or fire. The most basic explosive failure would be due to a tire's direct contact to extreme heat or fire; however, unexpected and thus more dangerous causes of explosions are pyrolysis or the presence of flammable gases in tires, as their presence would not be obvious.

Pyrolysis is the chemical decomposition of a tire resulting in the buildup of flammable gases within a tire [33]. This often occurs after exposure to heat such as an overheated vehicle braking system or the use of a torch to remove wheel studs, but contact with a high voltage power line has also been known cause pyrolysis [33]. The use of ether during tire mounting, bead sealant or puncture repair compounds have also resulted in similar failures.

Regardless of the source of the explosion, these types of failures are most often catastrophic in nature. In addition to the increased force from an explosive release, components of both the wheel and tire commonly break down, becoming dangerous projectiles endangering surrounding workers and equipment; this is in contrast to a zipper

failure where components typically remain more contained. A review of 82 publicly available cases of tire and wheel accidents by Tilman Rasche states 20% of failures are a result of pyrolysis, 6% are due to a tire fire, and 2% and 1% are the result of equipment fires or flammable propellants in the tire, respectively, with the remaining 71% associated with non-fire related incidents/accidents [21].

2.3.3 Wheel Failure and Tire Blowouts

Tire blowouts due to wheel or wheel component failure essentially encompass all other causes of tire and wheel failures due to the wheel assembly's inability to: maintain internal pressure, maintain proper engagement of locking wheel components, support vehicle load, or a combination of these. Such failures are not limited to multi-piece wheels and though precise causes may be difficult to identify without investigation, tire blowouts are the most common type of failure. Wheel integrity can be jeopardized due to a variety of causes including: impact damage, fatigue, corrosion, wear due to improper assembly or maintenance, and tire over or under inflation. Figure 2.3.2 below highlights some of these common causes.

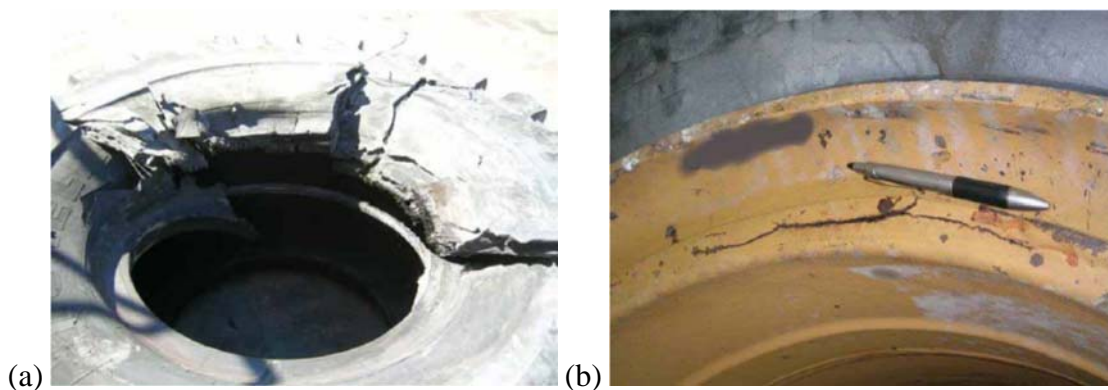




Figure 2.3.2 - Photos of failed wheels illustrating (a) tire damage due to flange separation, (b) rim base wear and fatigue crack, and (c) a cracked outer flange [21].

The blowout of multi-piece wheels in OTR applications can be particularly hazardous due to the higher tire pressures used and very large size of wheel assemblies. End results may be similar in a tire blowout as they would be in a zipper rupture or a tire explosion, but the propelling of failed rim components with great force and distance is more common. Incidents often occur during vehicle or wheel maintenance when the wheel/tire equilibrium is disturbed. Specific types of injuries and fatalities vary, but several details are provided in the incident reports section, Section 2.2.2, and tire blowout failure is a main focus of research efforts in an attempt to mitigate risk and enhance the safety of wheels.

2.4 STANDARDS RELATED TO WHEEL TESTING

Literature related to multi-piece wheel assembly design and testing is both very limited and typically specific details are unavailable due to their proprietary nature belonging to manufacturers. Similarly, manufacturing standards and design validation techniques appear to be non-existent, other than geometrical designs outlined by the Tire and Rim Association (TRA) [34] and handling and maintenance standards [15]. For

these reasons, throughout the research work presented here, reference to existing standards applicable to passenger car and light trucks is made, including the Society of Automotive Engineers (SAE) Surface Vehicle Recommended Practice and the International Organization for Standardization (ISO) International Standards.

2.4.1 ISO 7141 Road Vehicle Light Alloy Wheel Impact Test

While equivalent to the SAE J175 test, the ISO 7141 standard specifies a test procedure for evaluating the lateral curb impact collision properties in a laboratory setting. Though intended for passenger car or special vehicle applications using wheels manufactured either wholly or partially from light alloys, the test is meant for quality control purposes of a new, unused wheel. As shown in Figure 2.4.1, the test apparatus is designed to vertically strike a wheel and tire assembly that is mounted on a 13 degree angle with a steel striker with an impacting face with minimum dimensions of 375 mm and 125 mm. The support stand also integrates two natural rubber isolators in the wheel support structure.

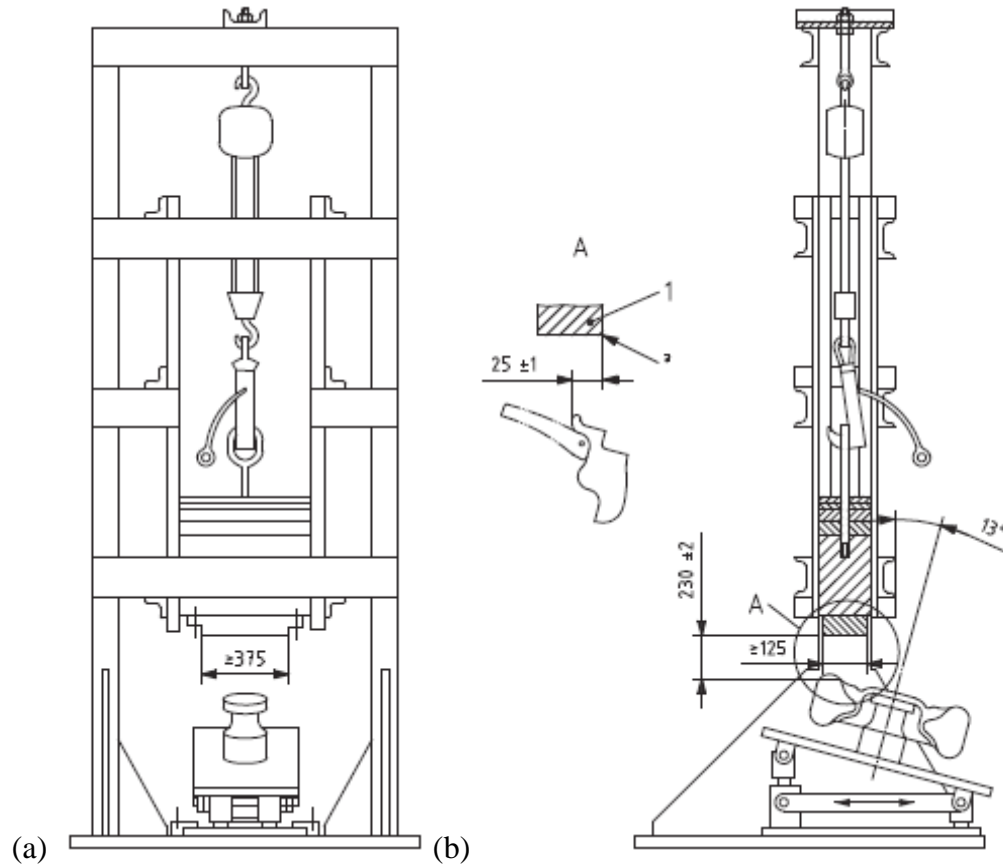


Figure 2.4.1 - ISO 7141 test apparatus in (a) elevation and (b) section view [35]

The striker mass is to total 60% of the maximum static wheel loading as specified by the wheel or vehicle manufacturer plus 180 kg, within a tolerance of 2%. Furthermore, the wheel is to be pressurized to the inflation pressure specified by the vehicle manufacturer, or inflated to 200 kPa if such information is unavailable, and mounted to have its highest point presented to the striker with an overlap of rim flange set to 25 mm and a tolerance of 1 mm. The striker is then dropped from a height of 230 mm above the rim flange and allowed to freefall. Failure criteria for the test as set by the standard is as follows:

- a) Visible fracture(s) penetrate through a section of the centre member of the wheel assembly;
- b) The centre member separates from the rim;
- c) The tire loses all air pressure within 1 minute, and is not considered to have failed due to deformation of the wheel or fractures in the area of the rim struck by the striker face plate.

2.4.2 SAE J1981 Recommended Practice Road Hazard Impact Test for Wheel and Tire Assemblies

The purpose of the J1981 standard is to evaluate the frontal impact performance of new wheel and tire assemblies by simulating a road hazard impact and establishes performance criteria to measure the functional degradation of the wheel. The standard is specific to passenger cars, light trucks, and multi-purpose vehicles and it is meant to be equivalent to vehicle pothole tests commonly performed by vehicle manufacturers, indicating that many test criteria are vehicle specific. The standard outlines specifications for the striker geometry, drop height, drop angle, striker mass centre, wheel holding fixture, pendulum, bed plate, frame and catcher. For the interest of brevity, further details can be referenced from the standard itself [36], which highlights the testing apparatus and further details that specify test parameters along with rationale for the standard.

Test acceptance criteria for the wheels are such that: (1) no visible fracture or fractures can penetrate through a section of the wheel; (2) there can be no separation of the centre member from the rim; (3) the local radial indentation on the outermost portion of the rim flange area directly impacted must be less than 10 mm; and (4) there cannot be a total loss of air pressure within one minute due to the rim indentation. For the purposes of validating large OTR wheel assemblies, it would be difficult to practically perform the

J1981 test given the much larger size and mass of such wheels; however, consideration of the failure criteria can aid evaluation when other test evaluations are performed.

2.5 REVIEW OF MULTI-PIECE WHEEL AND TIRE RESEARCH

Extensive efforts yielded very limited information regarding multi-piece wheel research in published journals. Typically, any pertinent information on design or safety aspects of wheel assemblies are related to the manufacturing of wheels, tires, or associated products and specific engineering data was proprietary and unavailable. The majority of available literature associated with multi-piece wheels is related to observed failures and specific incident reports, or best practices and regulations related to the handling and maintenance of wheels, such as the examples discussed in Section 2.2.4. As a result broadening of the literature review to include traditional automotive wheel and tire applications is necessary.

2.5.1 Related Wheel Modelling Research

In an effort to demonstrate the ability of finite element (FE) simulations to reduce test time and cost associated with the development and validation of a wheel and tire, the work of Chang and Yang [37] accurately predicts results of a wheel impact test following the SAE J175/ISO 7141 test standard for the purpose of validating that a wheel design will meet safety requirements. In their model, an aluminum wheel is modelled with tetrahedral elements and a mesh convergence study is performed with satisfactory results. The support structure is included in the model using hexahedral elements along with integrated rubber mounts and a hexahedral rigid striker is dropped from the ISO-standard height of 230 mm above the highest point of the tire-wheel assembly. Given the nature

of the test, symmetry is utilized with appropriate constraints implemented in the simulation and final results are validated using an actual test stand and instrumented wheel measuring strain response using two rosette gauges.

Adequate correlation is shown between the simulation results and real world observations with approximately 10% error; however, the wheel failure prediction is based on the assumption that fracture occurs if the maximum strain energy density exceeds the total plastic work of the wheel material during a tensile test. Crack initiation does not occur in the simulation nor in physical tests and the researchers believe there is merit to induce rupture at impact through the use of a heavier impact load. Furthermore, an additional shortcoming is that the tire is not modelled or present during testing.

The work of Cerit [38] similarly demonstrates the ability to implement numerical impact testing techniques and does so on a cast aluminum alloy wheel using three dimensional finite element methods. The methodology followed allows for a higher fidelity analysis of results when compared to the work of Chang and Yang [37] as this study includes modelling the wheel, striker and tire while taking into account nonlinear material properties, large deformation, and detailed contact parameters. The purpose of the investigation is to study stress and displacement distributions in the wheel and not simply evaluate based on a pass/fail criterion. The simulation is performed using commercial finite element explicit code ABAQUS and uses symmetry with respect to geometry, loading and boundary conditions; results are evaluated by using the von Mises yield criterion. Uniformity of shape and form for elements is followed as much as possible, and though the tire model accurately represents the geometry appropriately, it is described as being simplified to reduce simulation effort requirements by altering details

not essential in cornering behaviour. The model is shown in Figure 2.5.1 to illustrate mesh distribution and the symmetry of the test apparatus.

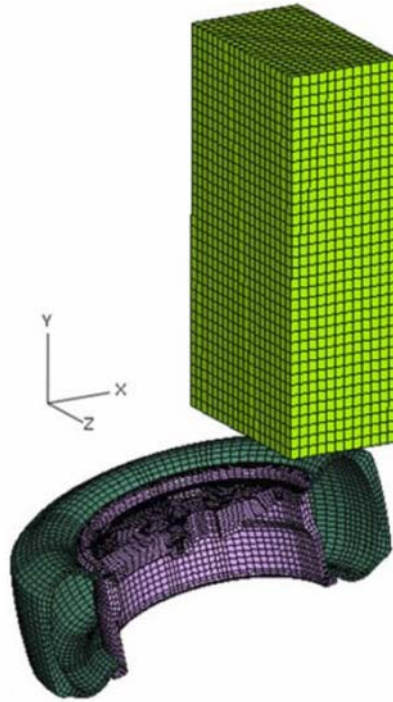


Figure 2.5.1 - Finite element model used for impact test simulation developed by Cerit [38].

Numerical results are analyzed and suggest severe plastic deformation would occur as a result of predicted levels of von Mises stress that exceed the yield strength of the material. Maximum stresses were predicted to occur in the lug region of the wheel which corresponds to real world observations in the passenger vehicle application under study. Overall, the work presented demonstrates the effectiveness of finite element methods to reliably estimate the dynamic response of an impact test and the benefits of using such methods for the optimization of wheel designs.

2.5.2 Past Multi-Piece OTR Wheel Research

The most applicable published research work is found in the International Journal of Heavy Vehicle Systems, entitled '*A finite element approach for prediction of fatigue life for a three-piece mining vehicle wheel*' by Vijayan et al. [11]. The past work was specifically related to three-piece mining wheels and involved the numerical estimation of their mechanical performance under fatigue loading. Currently no test standards exist that are specifically applicable to the multi-piece wheels used for OTR applications and as such this presents a challenge for adequately understanding the mechanical performance of a wheel and its fatigue life. As an initial step to understand the performance of current wheel designs, the SAE J1992 wheel cornering fatigue test standard, which is typically used for military application multi-piece bolted wheels, was applied. Based on a FE model developed and validated through experimentally observed strains, the numerical analysis of the SAE J1992 fatigue loading conditions was used to predict element-based fatigue factors of safety.

Using the load rating of the wheel obtained from its manufacturer and the gross vehicle weight of the mining vehicle, an approximate value of the test load to be applied to the wheel during experimental testing was calculated as 22 kN. According to the SAE J1992 testing protocol, the wheel assembly should be able to withstand a minimum of 20,000 cycles of the applied rotary fatigue load in order to pass the test in which it is clamped at the outer flange on a test stand and has a rigid shaft installed at the wheel mounting surface through which load is applied.

A quasi-static bending load was applied in a direction perpendicular to the centreline of the wheel and shaft assembly at the far end tip of the shaft. Strain gauges were

mounted at critical areas on the wheel to measure strains under the load. A finite element model of the three-piece wheel was created and modelled with representative the same boundary and loading conditions similar to the experimental test. The numerical model was able to predict the strain/load behaviour for approximately 80% of all strain gauge positions within 15% error. Validation of the model, for the loading conditions considered, was indicated and the model was further used to assess the fatigue performance of the multi-piece wheel assembly under a fluctuating (rotating) bending load consistent to the protocol outlined in the testing standard SAE J1992.

Numerical simulation of the fatigue test was implemented and an in-house fatigue analysis software package that incorporated three multi-axial fatigue theories was developed. These theories were based upon: (1) Goodman fatigue life predictions, incorporating Sines and von Mises definitions for the alternating and mean stress components, (2) Lemaitre's simplified approach for high cycle fully reversed fatigue loading, and (3) a critical plane approach. All fatigue theories indicated an infinite life should be expected for the three-piece wheel. However, in this analysis no consideration for component degradation (for example, corrosion or severe localized deformation due to material impact) was implemented, and it is suggested component damage and corrosion are two critical issues that are responsible for the discrepancy between predicted results and in-field observations. The efforts by Vijayan et al. [11] clearly illustrate that appropriate engineering tools can accurately and precisely predict mining wheel structural behaviour when subjected to mechanical loads; however, additional research is warranted to study the effect on wheel life as a result of environmental and localised damage endured during vehicle operation.

Unfortunately, based on present search efforts, literature specifically related to design improvements or innovation efforts to address safety problems of multi-piece wheels was unavailable in public domains.

2.5.3 Related Tire Modelling Research

A pneumatic tire is a highly complex structure designed to accommodate varying payloads and road imperfections by means of elastic deformation, and often operated under demanding conditions. As discussed, the foundation of a tire consists of a number of layers of flexible cords with a high modulus of elasticity [39]. These cords are spatially oriented in a matrix of low modulus rubber and together act to form the carcass of a tire. All other components interact with the tire carcass to give desired performance characteristics, further complicating tire analysis. For these reasons and more, tires in general pose a significant challenge when conducting virtual simulation and modelling.

Given the complex nature and physical dimensions of OTR tire structures, great challenges arise in accurately modelling and predicting their dynamic performance under load and in-use, when applying computer-aided engineering (CAE) methods. Additionally, a significant challenge in OTR tire modelling is simply the lack of experimental data pertinent for model validation. An in-depth literature review on the topic of OTR tires reveals that there is no extensive information available regarding the load-deflection behaviour of OTR tires in open literature and typically tire modelling and experimentation is restricted to manufacturers and considered proprietary in nature. Tire manufacturer Goodyear OTR does provide limited load-deflection tire data [14]; however, the data is specified for only a single loading condition and gives no indication regarding the linearity of the load-deflection behaviour of the tire. For validation

purposes, full scale vehicle testing is required to obtain high fidelity in-field data encompassing the general and localized vertical and side-wall deformation of the OTR tire as a function of load, as discussed in Section 4.3. Fortunately, to assist in modelling efforts, research from the automobile industry related to passenger vehicle tire testing and modelling is an applicable reference to develop OTR simulation techniques and testing methodology.

To create a detailed tire model for crash applications, Reid et al. [40] conducted two types of tire tests: single-sided compression and double-sided compression. The first test was achieved virtually by placing a rigid, flat, ground surface below the tire and subsequently prescribing a displacement to the centre of the wheel. Results were validated using data obtained from the tire manufacturer Goodyear; however, these results were very limited and based on only 35 mm of compression. The second test follows similar methodology to the first, except the prescribed motion was made in reference to a solid plate placed on top of the tire, thus resulting in double-sided compression. In both tests, load deflection curves were obtained and were used to improve the accuracy of the tire model. The researchers took a unique approach to the model development, which avoided the discretization of all structures of the tire and wheel; however, the majority of the components that influenced the response of the tire and wheel assembly were carefully modelled such that good predictive capabilities of the model existed under a number of testing conditions.

Orengo et al. [41] simulated the tire blowout on a passenger vehicle, using the commercial software LS-DYNA. In the numerical tire model, the modelling of different tire components was simplified to shell, beam and solid elements. The model was

subsequently verified against experimental observations and found to correlate well, thus validating the model simplifications for their purposes.

In the study of Burke and Olatunbosun [42], a model of a 195/65R15 tire was created using Nastran for the purposes of static tire to road interaction investigations. In their work, a gap formulation was implemented to model the interaction, so that the contact patch area, shape, and deflection were automatically accounted for under a given load and inflation pressure. To validate their model, a downward force was applied to the wheel centre and tire displacement, as a function of load, was recorded and compared against model behaviour. This simplistic approach was used to assess the predictive capabilities of the numerical model.

The work of Neves et al. [43] created a model of a 175/65R14-82T tire used on passenger vehicles. The purpose of the model was to investigate tire performance under sudden impact loadings and model validation was performed using full wheel and tire impact test experimentation. A laser Doppler Polytec OFV-323 was used to measure the velocity of the indenter, which was subsequently time differentiated to obtain acceleration and impact force data. Other instrumentation included the OFV-3020 laser-capturing system, and a high-speed camera that recorded the impact events at a rate of 10,000 frames per second. Indenter mass and tire inflation pressure were varied throughout experiment for a greater range of testing conditions. This work demonstrates appropriate methodology for both experimentation and validation techniques that correspond to model development.

Nguyen et al. [44] studied the load-indentation behaviour of aircraft tires due to runway debris. In-field observations were studied using advanced digital image

correlation (DIC) techniques on Goodyear Flight Custom 6.50-10 tires obtained for a C-130 Hercules aircraft nose wheel. The wheel assemblies were mounted in an Instron TT-DM testing machine fitted with a 5 kN load cell to measure applied indentation loads. In parallel, an Aramis DIC system using two 1.3 megapixel cameras was used for acquiring strain measurements. Each tire was coloured with a stochastic pattern of white dots for DIC calibration and tracking. Cameras were maintained at a safe operating distance away from the testing apparatus, preventing data acquisition within the immediate proximity of the indenter, in the tire grooves or close to the tire shoulders. Testing was performed for a series of tire pressures with results demonstrating a good correlation between tire inflation pressure and released indentation energy.

As mentioned in Section 2.5.2, the focus of the research by Vijayan et al. [11] dealt with the predictive capabilities of the finite element (FE) method in modelling the stress-strain behaviour of a multi-piece wheel assembly, for which they used LS-DYNA. No consideration was given to the influence a pneumatic tire might have on the load distribution seen by the multi-piece wheel. Given the discrepancy between the infinite fatigue life predicted in their research and failures observed in industry, this suggests that both the development of a high fidelity tire model capable of accurately representing the tire-wheel boundary constraints and loading due to vehicle operation is fundamental in assessing failure mechanisms of the assembly.

3 RESEARCH FOCUS

The research detailed in this thesis will focus on understanding the hazards of multi-piece wheels commonly used on heavy mining vehicles as a critical first step to enhance their safety. A systematic approach will be followed to mitigate safety risks as highlighted by the following steps:

- a) Wheel, tire, and heavy vehicle equipment suppliers and manufacturers, as well as multiple mine sites will be visited to conduct onsite surveys to aid in familiarization of wheel assemblies. Furthermore, instrumented real-world testing at mine sites to collect both quantitative and qualitative data will be conducted and used as the basis for the development of finite element wheel assembly models.
- b) An analysis of historical wheel tracking data and development of a database capable of actively analysing the state of wheels will be completed. In an effort to improve efficiency and safety, advanced statistical methods will be used to make a database that is a simple yet effective tool to provide unique insight into the common issues, failure modes, and average lifespan of wheel assemblies.
- c) Based on the observed needs of multi-piece wheel assembly users, a mechanical device capable of enhancing the safety of wheel assemblies will be conceptualized as a solution. Such a device would encompass fail-safe design methodology and be validated using advanced FE methods. While intended to mitigate some of the risks associated with wheel assembly handling and operation, it would subsequently also increase the durability of wheels.

4 ASSOCIATED FIELD WORK AND EXPERIMENTAL TESTING

4.1 MINE SITE VISITS

With only limited information available from manufacturers, information on vehicle loading and dynamic responses, along with detailed mechanical characteristics of OTR tires used on heavy mining vehicles, are unavailable in open literature. As a result, initial research efforts focused on familiarization with vehicle performance requirements, operating environments, and wheel assembly characteristics through mine site and equipment supplier visits. In-field visits allowed exposure to the mining industry in general and vehicle testing was performed with the main purpose of collecting critical data for computer modelling and simulation. Locations throughout northern regions of Ontario, Canada were visited and include:

- a) **McDowell-Driftech** of Sudbury, Ontario; a heavy equipment dealer with repair and refurbishment services. The researchers conducted a facility tour and performed vehicle testing with limited data acquisition to familiarize themselves with a range of typical mining equipment.
- b) **Royal Tire OTR Dealership** of Sudbury, Ontario; an OTR tire and service centre specializing in Goodyear products. The researchers conducted a facility tour and reviewed used and scrap tire and wheel inventory for the purpose of examining the condition of wheels. Additionally, a wheel and tire assembly process was demonstrated.
- c) **North Shore Industrial Wheel (NSIW) Mfg.**, in Sudbury and Sault Ste. Marie, Ontario; a wheel sales, manufacturing, and repair facility, and a major contributor to research efforts. The researchers conducted a review of their facilities, and particularly their wheel inventory, that included a wide range of wheel styles based on different applications. Also reviewed were their multi-piece wheel

manufacturing and repair processes, as well as inspection capabilities and in-house wheel tracking and recertification processes.

- d) **Goodyear Canada Inc. Retread Facility** of North Bay, Ontario; a specialized tire retreading facility capable of OTR tire retreading. The researchers conducted a facility tour and reviewed their damaged tire inventory for analysis purposes, tire repair techniques, and the retread manufacturing process.
- e) **Xstrata Nickel Rim South Mine** of Sudbury, Ontario; an underground nickel mining facility. The researchers received underground safety training, a mine tour, and performed minor vehicle instrumentation and data acquisition during in-field operation.
- f) **Xstrata Copper Kidd Mine**, located in Timmins, Ontario; the world's deepest copper and zinc mine with both open pit and underground mining. The researchers conducted data acquisition on an instrumented Sandvik-Toro 1400 LHD while performing a vehicle validation, ramp braking test procedure.
- g) **Fountain Tire** of Thunder Bay, Ontario; an OTR tire and service centre specializing in Goodyear products. The researchers conducted a facility tour and review of their used and scrap tire inventory.
- h) **Goldcorp Musselwhite Mine**, in the Opapamiskan Lake Area of northern Ontario; the site of a remote underground gold mine and processing mill. The researchers received underground mine procedure training, a detailed tour of facilities, and conducted extensive aboveground and underground instrumented vehicle testing.

4.2 MUSSELWHITE MINE TESTING INFORMATION

The most extensive and pertinent experimental testing performed was completed at Musselwhite Mine in July of 2011 and was critical for the development of high-fidelity wheel and tire models. The research group focused on mining wheel safety from the University of Windsor travelled to Musselwhite mine, located approximately 700 km north of Thunder Bay, Ontario, Canada.

Accompanied by the principle investigator, Dr. William Altenhof and PhD candidate, Mr. Zhanbiao (Weldon) Li, numerous vehicles were reviewed, instrumented, and tested both aboveground and underground. Additionally, a variety of tire styles were tested, including: radial or bias, new or retreaded, and smooth or aggressive, high-traction tread. To gain a better understanding of tire behaviour and characteristics, a variety of measurements were taken using different approaches to excite the test vehicles. Testing on underground heavy vehicle scales as well as more severe active excitation testing above ground was conducted to provide static and quasi-static vehicle excitation, as described in the following detailed sections.

4.2.1 Tire, Wheel and Vehicle Specifications

For the purposes of brevity, discussion is limited to three vehicles tested at the mine site and analysis limited to specific maximum excitation test events performed on each vehicle of interest. All test vehicles were Caterpillar brand equipment and were either load-haul-dump (LHD) scoop vehicles or an underground articulated truck. Only one wheel assembly was measured during the course of each vehicle test, with the specific machine, tire, and wheel information of interest summarized in Table 4.2.1.

Table 4.2.1 – Summary of test vehicle information

Machine	Tire Specification	Tire Design	Wheel Specification
Caterpillar AD45B Truck (equipped with push box)	Goodyear 29.5R29 RL-5K; L-5 Type 6S Cold Tire Pressure: 660 kPa	Radial	NSIW Model HT2000 5-piece wheel
Caterpillar R2900G LHD Scoop	Goodyear 29.5-29 SMO; D/L-5D Type 6S Cold Tire Pressure: 591 kPa	Bias	5-piece wheel; Unknown manufacturer
Caterpillar R1700G LHD Scoop	Goodyear 26.5-25 SMO; D/L-5D Type 6S Cold Tire Pressure: 646 kPa	Bias	Rim #719 5-piece wheel; Unknown Manufacturer

All tires of interest were manufactured by Goodyear and as such the Goodyear *Off-The-Road Tire Engineering Data* [14] book is referenced for comparison and validation purposes, as shown in Table 4.2.2 for each specific tire. The U.S. Imperial system of measurements was used as it is the base standard for tire and wheel sizes; however, where possible, data is based on the SI system of units or presented in both. All observations are based on SI unit measurements.

Table 4.2.2 - Physical Tire Data From Goodyear's OTR Engineering Data Book [14]

Tire Model	29.5R29 RL-5K; L-5 Type 6S	29.5-29 SMO; D/L-5D Type 6S	26.5-25 SMO; D/L-5D Type 6S
Inflated Overall Diameter	79.7" (2024 mm)	78.9" (2004 mm)	71.0" (1803 mm)
Inflated Overall Width	30.1" (764 mm)	30.1" (765 mm)	27.4" (696 mm)
Loaded Section and Growth	34.2" (869 mm)	33.0" (838 mm)	29.9" (759 mm)
Static Loaded Radius	35.0" (890 mm)	36.3" (922 mm)	33.0" (838 mm)
Mass	2112 lbs (958 kg)	2875 lbs (1304 kg)	1737 lbs (788 kg)
Volume	1230 L	1016.7	664.5
Rim Width - Flange Height (inch/mm)	25.00" - 3.5" 635 mm - 88.9 mm	25.00" - 3.5" 635 mm - 88.9 mm	22.00" - 3.0" 559 mm - 76.2 mm
Tread depth	3.75" (95 mm)	4.3" (108 mm)	4.0" (102 mm)
Rated Load at Rated Tire Pressure**	231 kN at 648 kPa	230 kN at 627 kPa	167 kN at 552 kPa

** Note: Approximate load does not include wheel assembly static weight

Using the Goodyear OTR data, it is possible to calculate basic deflection characteristics. Given the above information and the 29.5R29 for example, it is known that the unloaded Overall Diameter (OD) is 2024 mm or an approximate radius of 1012 mm, and the Static Loaded Radius (SLR) is given as 890 mm at a rated tire pressure of 800 kPa and 267 kN load; meaning a loaded tire should decrease in radius by 122 mm. Furthermore, change in section width can be calculated as the difference between the Loaded Section and Growth (LS&G) and the unloaded, inflated Overall Width (OW) which yields an increase of approximately 105 mm, or a one side “bulge” of 57.5 mm. Similar results for all tires are summarized in Table 4.2.3 below.

Table 4.2.3 - Tire Deflection Characteristics Based on Goodyear OTR Data [14]

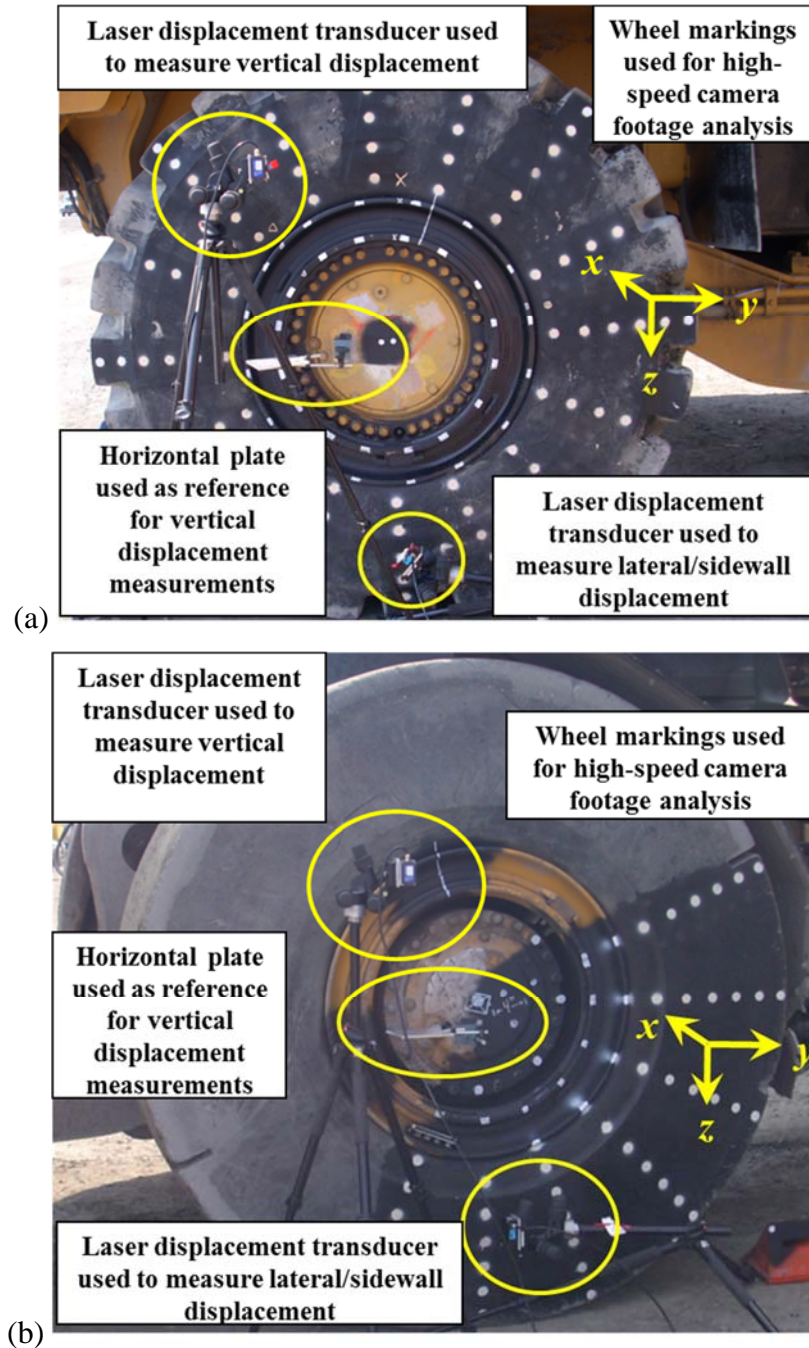
Tire Model	29.5R29 RL-5K; L-5 Type 6S	29.5-29 SMO; D/L-5D Type 6S	26.5-25 SMO; D/L-5D Type 6S
Inflated, Unloaded Radius (mm)	1012	1002	901.5
Static Loaded Radius (mm)	890	922	838
Decrease of Radius (mm)	122	80	63.5
Unloaded Overall Width (mm)	764	765	696
Loaded Section and Growth (mm)	869	838	759
Increase in Section Width (mm)	105	73	63
Approximate Load/Vertical Deflection (kN/mm)	1.89	2.89	2.63
Approximate Load/Lateral Deflection (kN/mm)	4.4	6.3	5.3

4.2.2 Testing Apparatus

A testing methodology was developed and replicated for each vehicle to minimize measurement error. The three test vehicles represent a wide range of vehicle and wheel assembly styles, with significantly different payloads. The wheel of interest was selected based on the researchers' capacity to best capture maximum excitation, such as the rear wheels of the AD45B truck, for example, since load input could be more easily and safely completed through the bucket of the truck versus anywhere on the front of the vehicle. In the case of the LHD vehicles, the vehicles' own scoops were used to create a controlled simulated loading condition with maximum excitation exerted on the front wheel assemblies. Additionally, the testing methodology accurately reflected how load would be input during vehicle operation.

All vehicles were initially prepared by setting up the required instrumentation. To prepare for aboveground quasi-static excitation testing, a National Instrumentation NI-9188 CompactDAQ (cDAQ) 8-slot ethernet chassis data acquisition system was utilized to obtain transducer data connected wirelessly to a control laptop using a D-Link DIR-655 XTREME N Gigabit router. Due to the large tire size, desire to use non-invasive measurement techniques, and limited testing time available at the mine site, observations were acquired using optical methods. Acuity AR700 series laser displacement transducers with measurement ranges of 300mm and 100mm were used to take vertical deflection and sidewall lateral deflection measurements, respectively. The vertical measurements were obtained through use of a magnetically mounted horizontal plate, which acted as a reference point for the vertical displacement measurement. The horizontally mounted plate was attached to the hub of the wheel assembly. The sidewall lateral deflection measurements were taken as close to the centreline of the tire as possible on the lower “bulge” of the tire sidewall; where maximum deflection was anticipated, and measured directly on the surface of the tire. These transducers were connected to the NI-9188 cDAQ chassis with an NI-9215 module capable of measuring the voltage output from the transducers. Acquisition of the displacement transducer measurements occurred at 5 kHz. Additionally, high-speed camera images were recorded to capture greater aspects of the tire deformation field. A Fastec Imaging Troubleshooter HR camera was utilized and time synchronized with the NI-9188 cDAQ data using a NI-9401 digital I/O module. Digital images having a resolution of 640 by 480 pixels were acquired at 125 Hz and with a shutter speed of the camera specified as 4 milliseconds. The use of industrial-grade Arri 1000W spot lights was necessary at times

to ensure optimal lighting for video capture. To track tire displacements with the high speed images, careful marking of the tire using white paint was necessary to provide reference points during image post-processing. The tire preparation, as well as equipment setup, is shown in Figure 4.2.1(a)-(c) for each test vehicle of interest.



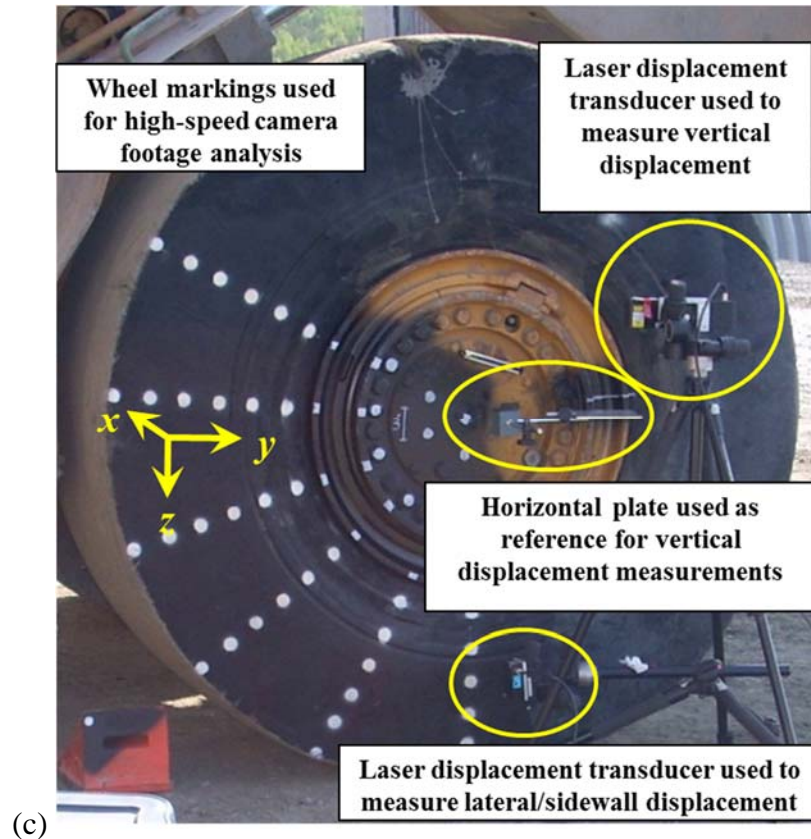


Figure 4.2.1 - Wheel assembly displacement measurement apparatus for (a) AD45B R29.5R29 tire, (b) R2900G 29.5-29 tire, and (c) R1700G 26.5-25 tire.

****Note:** Positive vertical displacement is downwards in the z -axis direction, positive lateral/sidewall displacement is inwards in the x -axis direction, and positive longitudinal displacement is towards the front of the vehicle in the y -axis direction.

4.3 TESTING METHODOLOGY

4.3.1 *Quasi-static Deflection Testing Methodology*

Quasi-static testing was performed aboveground near the mine site's maintenance building, where initial instrumentation took place. To induce the desired severe loading conditions in a safe, controlled manner a significantly higher capacity front load aboveground scoop, a Caterpillar 990, was employed. Excitation for each test vehicle was unique based on their designs and how load could be safely transferred with minimum risk of operator, researcher, and equipment damage.

For the Caterpillar AD45B truck, the Caterpillar 990 was aligned with the rear of the AD45B and its bucket was used to evenly apply downward load to the test vehicle's box as close to the axle line as possible. For the test event where maximum deflection was observed, excitation consisted of a series of two step function-type inputs where the load was first applied, held for approximately 3 seconds and then additional downward force was input and held for an additional 3 seconds, and then all load was removed. The test setup is shown in Figure 4.3.1.

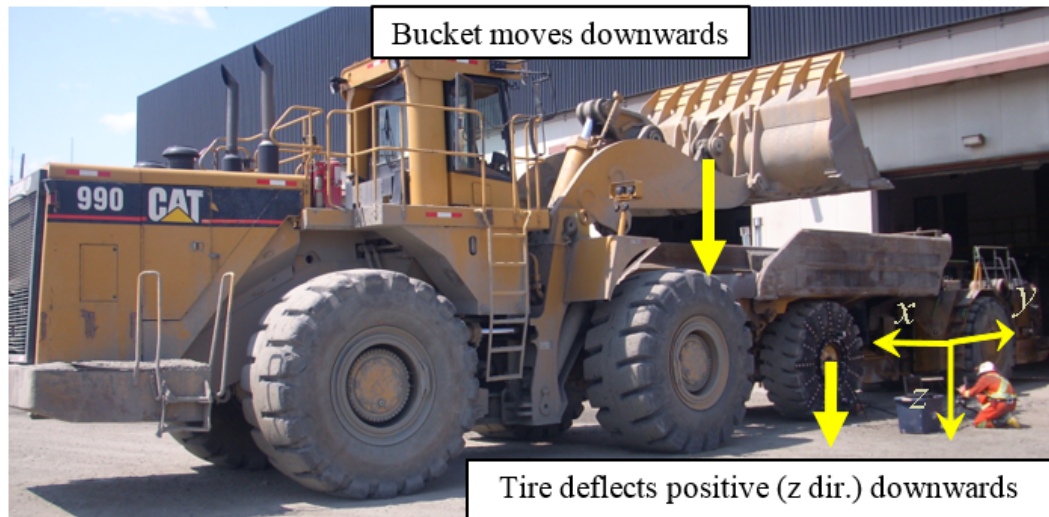


Figure 4.3.1 - Excitation of the AD45B test vehicle using the Caterpillar 990 front load scoop.

Excitation of the R2900G and R1700G were identical. In both cases, the test vehicles' scoops were actuated by their operator against the rear structural protective metal of the Caterpillar 990 front load scoop. The relative size and weight differences between the vehicles allowed the Caterpillar 990 to act as an anchor of sorts for the test vehicles and when the scoops were activated, significant tire deformation was observed. Load input during the test events where maximum excitation occurred was similar to a singular step function where load was applied, held for approximately 3 seconds and completely removed. The experimental setup for both test vehicles is shown in Figure 4.3.2.

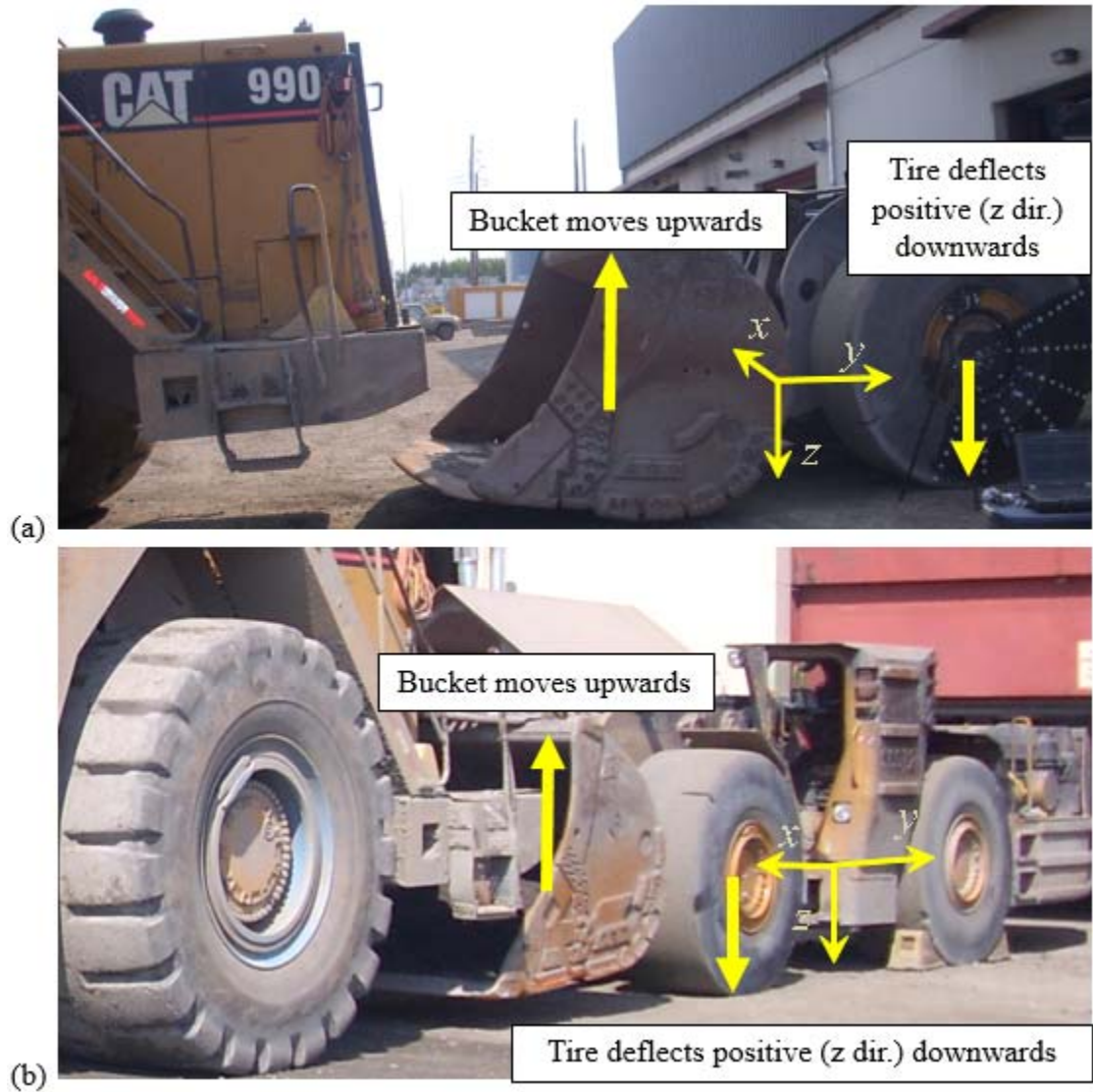


Figure 4.3.2 - Excitation of the a) R2900G and b) R1700G test vehicles using the Caterpillar 990 front load scoop.

During the course of testing, significant test vehicle tire deflections were observed with no substantial movement of the Caterpillar 990. At least six tests were performed which appeared to provide suitable observations for each vehicle/testing configuration based upon a brief review of data at the mine site.

4.3.2 Static Deflection Scale Testing

Static deflection testing occurred at the mine site's underground Mettler Toledo Model 7566 Extreme Duty heavy vehicle weigh scale. Testing involved loading the test vehicles to varying payloads of ore and obtaining the static load-deflection behaviour of each respective tire of interest.

Initial intentions were to collect additional quasi-static or possibly even dynamic load responses using some or all of the instrumentation utilized during aboveground testing; however, this was not possible due to a hardware malfunction with the scale's analog output controller. Ideally, optical measurement methods, such as those used aboveground, would also be duplicated during the underground testing; however, given the harsh surroundings, low lighting, and limited time available with the vehicles at the scales, these measurement techniques proved impractical. Measurements were instead taken by manually measuring vertical tire deflection as a function of load using the vehicle's axle centre point to the ground as a reference measurement and the visual output of the scale. Maximum lateral tire sidewall position, or "tire bulge," was also recorded by measuring along the centreline of the wheel assembly from the face of the axle to the maximum lateral point. To ensure accuracy and confidence, measurements were recorded five times per payload with the tires rotated slightly between readings, while having only the axle with the wheel assembly of interest on the scale, to have reference weights recorded as well. Since payloads were always loaded as evenly as possible, it was approximated that the recorded weight was evenly split between both wheels on the scale.

4.4 MUSSELWHITE OBSERVATIONS AND DISCUSSIONS

4.4.1 Above Ground Quasi-Static Testing Observations

Aboveground testing constituted all quasi-static excitation testing that was performed. Since both laser displacement transducers and high-speed camera footage was recorded, a comparison between both observations techniques was completed to ensure correct and consistent measurements. Laser displacement measurements considering only the planar motion of the wheel (i.e. the vertical displacement of the wheel hub) could be compared with the high speed images as only in plane observations from the post-processing of the images could be completed.

Post-test examination of the observations revealed that varying results were observed for the six tests completed on a given vehicle. This was a result of the lack of consistent vehicle excitation applied by the operator and not, to the best of the researchers' knowledge, significantly associated with any variation in testing apparatus. Analysis of the observations indicated that when considering deformation behaviour, exclusive of loading/excitation, that consistent findings were obtained. For example, regardless of the degree of vehicle excitation, relationships between vertical wheel displacement and sidewall tire bulge were practically identical for a given wheel/tire configuration. Thus, it was evident that consistent tire deformation characteristics were observed amongst the six tests completed for a given vehicle. This was the case for all three vehicles tested. For clarity and brevity, results from only the most significant loading/excitation condition, which resulted in the greatest degree of tire deformation and wheel displacement, are presented within this thesis.

For the 29.5-29 tire, Figure 4.4.1 (a) and (b) present the vertical wheel displacement and tire lateral displacement as functions of time. Cross-plotting such information results in Figure 4.4.1 (c) which illustrates the lateral tire displacement as a function of wheel vertical displacement. As can be observed in these figures, maximum values of vertical deflection and sidewall lateral deflection were observed to be 74.9 mm and 27.1 mm, respectively. Maximum values of vertical deflection and sidewall lateral deflection for the 29.5R29 tire were observed to be 72.2 mm and 23.3 mm, respectively. Maximum values for the 26.5-25 tire were observed to be 78.9 mm and 25.6 mm for vertical and sidewall lateral deflection, respectively. Vertical and lateral displacement information for the 29.5R29 and 26.5-25 tires are presented in Appendices 9.1.1 and 9.1.2.

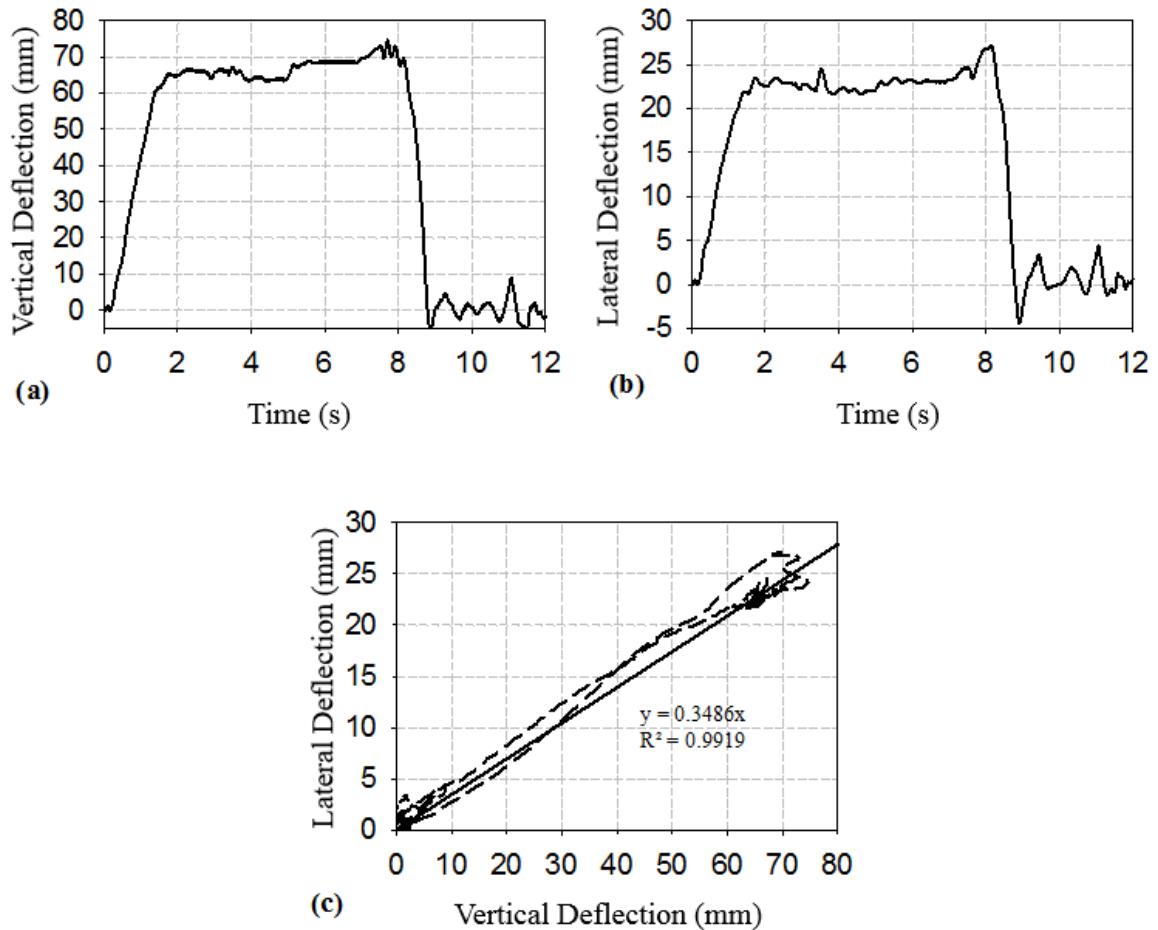


Figure 4.4.1 - Response for 29.5-29 test event exhibiting maximum deflection in the a) vertical and b) lateral directions as well as a c) lateral deflection versus vertical deflection.

A minor degree of hysteresis was observed in the lateral tire displacement presented as a function of vertical wheel displacement. This observation may be attributed to the dissipative nature of the tire materials and construction, a result of measurement error, or slipping occurring between any contacting interfaces. The last two reasons presented are believed to have only a very minor contribution to the observed hysteresis. In general a direct relationship between lateral tire displacement and vertical wheel displacement were observed for all tires tested. Linear regression of lateral/vertical deflection observations was performed for each tire tested and the following proportionality constants were

determined for each tire: 0.310 mm/mm (29.5R29), 0.346 mm/mm (29.5-29), and 0.332 mm/mm (26.5-25). Coefficients of determination (R^2) for each proportionality constant were determined to be near unity having values of 0.9931, 0.9922, and 0.9815, respectively.

A minor shortfall was noted when considering the sidewall lateral displacement measurements. The laser displacement transducer was supported by a fixed height tripod levelled on solid ground that was isolated from the test vehicle and directed to measure near the anticipated point of maximum sidewall deflection on the tire. Given that input excitation was essentially vertical and the wheel assembly was deflecting similarly, the sidewall deflection measured was not a fixed point on the tire, but rather a continuous vertical line proportional to the vertical range of motion and amount of lateral deflection.

To investigate local tire deformation behaviour, post-processing of the digital images acquired with the high speed camera was completed using the digital image analysis software, ProAnalyst. To ensure suitable calibration within the digital image analysis as well as consistent measurements between both the laser displacement transducer and the image analysis, an examination of the error between the two measurement techniques was completed, for the vertical displacement of the wheel hub only. A rigorous error analysis that involved comparisons between the two measurement techniques within the complete time domain of data acquisition was completed. Additionally, a validation metric 'V', as proposed by Oberkampff and Trucano [45] was computed. The error between the two measurement techniques was quantified using equation (1) and the validation metric was determined using equation (2). Equation (1) uses the principle of a simple, standard error calculation; however, the absolute error between a finite range of

experimental and corresponding FE data points are taken and averaged. This provides the average absolute error between numerical and experimental data for a span of the independent variable, which in this case is time measured in seconds.

$$\text{Accumulated Relative Error} = \frac{1}{t_2 - t_1} \cdot \int_{t_1}^{t_2} \left| \frac{O_{Tracked}(t) - O_{Laser}(t)}{O_{Laser}(t)} \right| dt \quad (1)$$

$$\text{Validation Metric} = 1 - \frac{1}{t_2 - t_1} \cdot \int_{t_1}^{t_2} \tanh \left(\left| \frac{O_{Tracked}(t) - O_{Laser}(t)}{O_{Laser}(t)} \right| \right) dt \quad (2)$$

The above validation metric has the four advantages. First, it normalizes the difference between the transducer (laser) results and the tracked (ProAnalyst) data by computing a relative error norm. Second, the absolute value of the relative error only permits the difference between the transducer results and the tracked data to accumulate. Third, when the difference between the transducer results and the tracked data is zero at all measurement times, then the validation metric is unity. And fourth, when the summation of the relative error becomes large, the validation metric approaches zero. Figure 4.4.2 shows how the validation metric given in equation (2) varies as a function of constant values of the relative error throughout the specified domain. If the summation of the relative error is 100% of the experimental measurement, the validation metric would yield a value of 23.9%. Numerical error occurs when attempting to evaluate the relative error if the laser transducer measurement is near or equal to zero. Correspondingly, in the assessment of the relative error, only relative errors were considered if the transducer measurement was greater than 10% of its maximum value.

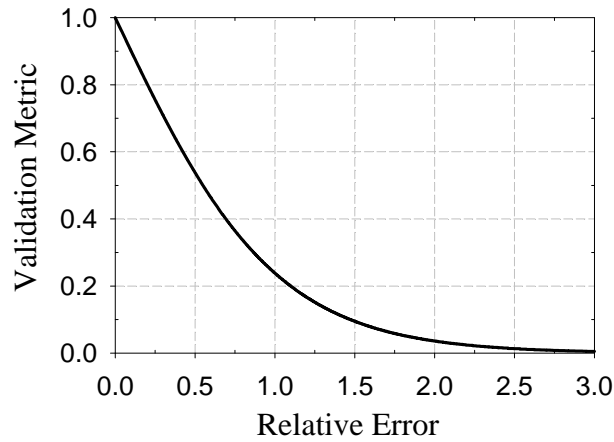


Figure 4.4.2 - Plot of validation metric, V , as determined by equation (2) as a function of constant values to relative error.

Figure 4.4.3 illustrates the vertical displacement comparison for the 29.5-29 tire between laser displacement transducer measurements and digital image analysis tracking. It is obvious that an extremely good correlation between the two measurement techniques exists. The error and validation metrics for the R29.5R29, 29.5-29, and 26.5-25 wheel assemblies were determined to be 1.24% and 0.988, 1.12% and 0.989, and finally, 4.05% and 0.959, respectively. It is worth noting that the extreme loading on the 26.5-25 tire as well as the applied “step” excitation, resulted in notable rotation of the wheel/tire assembly during excitation, which influenced the vertical displacements measured from the laser displacement transducer. Figures illustrating the comparisons for the 29.5R29 and 26.5-25 wheel assemblies are found in Appendix 9.1.3. This resulted in a slightly higher error, however, the magnitude of the error is low. This analysis ensured confidence with regards to the optical measurement techniques applied within this research.

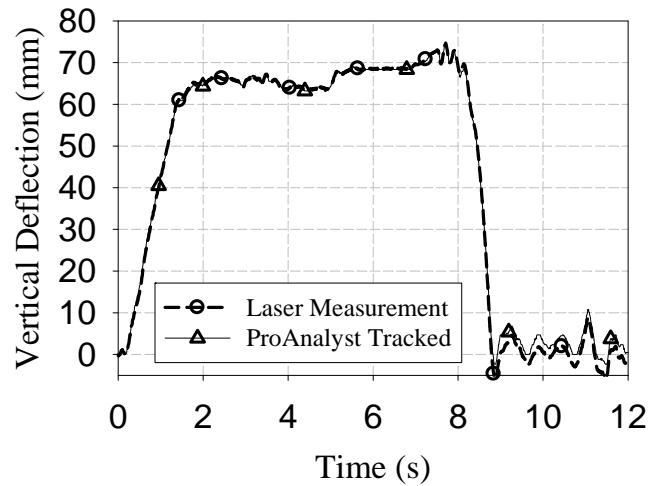


Figure 4.4.3 - Vertical displacement comparison for the 29.5-29 tire between laser displacement transducer measurements and high-speed camera image tracking using ProAnalyst.

Determination of local tire deformation behaviour occurred after the error analysis was completed. Six locations amongst all markings applied to the tire were considered for tracking. Figure 4.4.4 illustrates the locations of these points for the 29.5-29 tire and similar locations were used for the remaining two tires. The selection of these points was based upon the desire to eliminate any excessive analyses, yet provide a thorough understanding of the local tire deformation. As a result, points H-in, H-out, D-in, D-out, V-in, and V-out, were selected for planar tracking (y/z plane of motion).

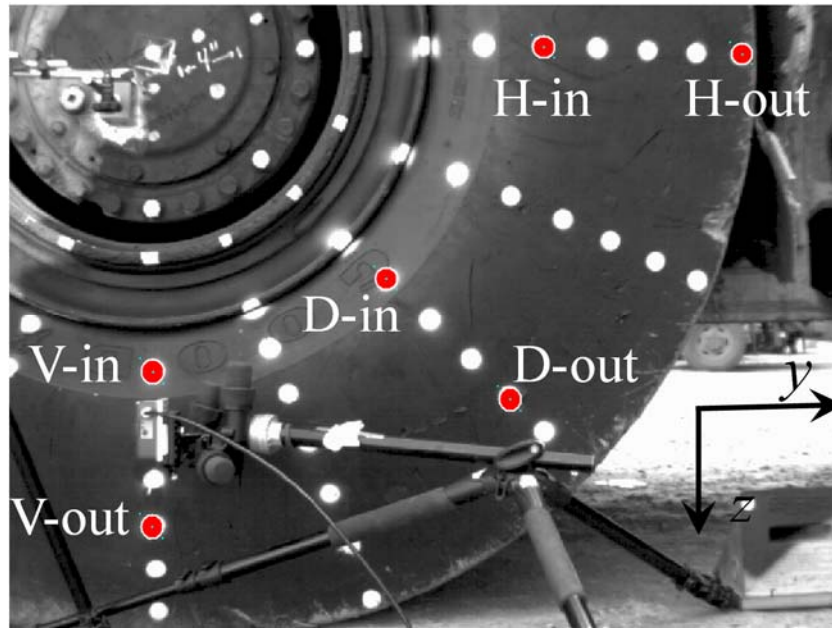


Figure 4.4.4 - Location of points tracked on the physical test apparatus (29.5-29 tire shown).

Figure 4.4.5 (a)-(c) and Figure 4.4.6 (a)-(c) illustrates the vertical (z -axis) and horizontal (y -axis) deflections associated with the tracked locations for the 29.5-29 tire. From the observations, one can conclude the effectiveness of the results given certain expected obvious outcomes. For example, the V-out point experiences approximately 50% of the vertical displacement of the V-in point since it is at the mid-span of the tire's radius. Conversely, the respective D and H points experience very similar vertical displacement since the effect of tire squat at these locations are minimal.

It is important to note that the vertical deflection of all points, more notably H-in, H-out, D-in, D-out, and V-in do not return to a value of zero after excitation is removed. This is a result of the minor degree of angular rotation which the tire/wheel assembly experienced during testing. Displacements for tracked locations on the other two tires are presented in Appendices 9.1.3 and 9.1.4.

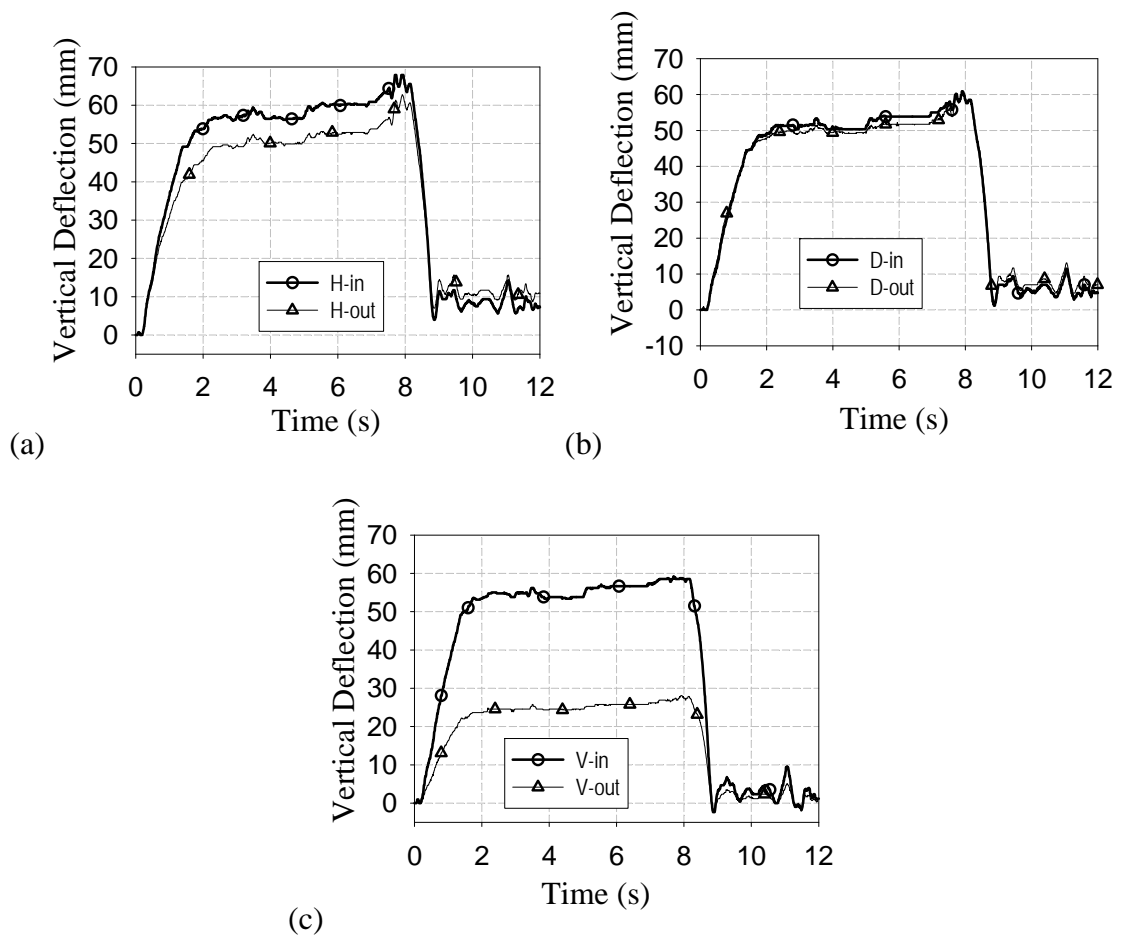


Figure 4.4.5 - Vertical deflection responses for tracked nodes during 29.5-29 tire test event where maximum deflections were observed for the a) H-in and H-out points, b) D-in and D-out points, and c) V-in and V-out points.

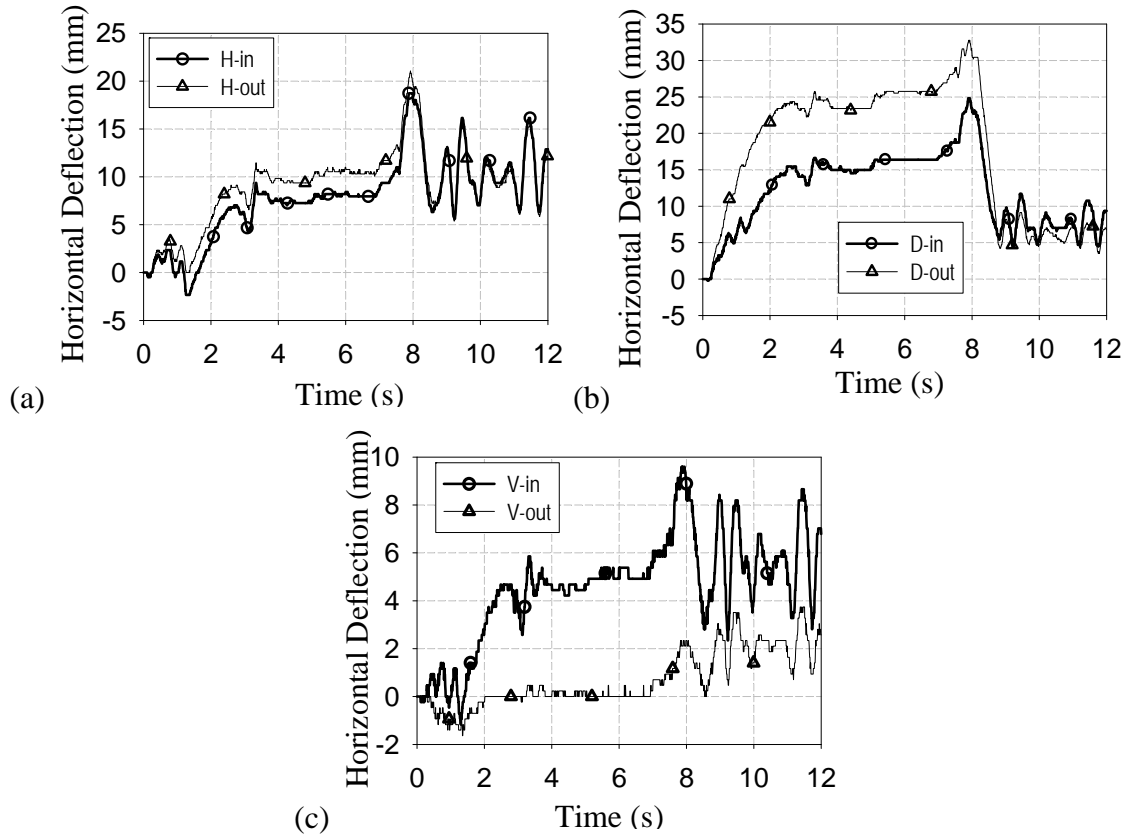


Figure 4.4.6 - Longitudinal deflection responses for tracked nodes during 29.5-29 tire test event where maximum deflections were observed for the a) H-in and H-out points, b) D-in and D-out points, and c) V-in and V-out points.

4.4.2 Underground Static Testing Observations

The underground testing consisted of numerous vertical and sidewall lateral deflection measurements at corresponding payloads, for each vehicle, on the mine site's heavy vehicle weigh scale. Linear measurements were taken manually and weight readings were based on the scale's visual output, with the purpose being to correlate load-deflection characteristics of the tires. As validation of the testing methodology, observations are summarized in Figure 4.4.7 where experimental measurements are compared to established manufacturer engineering data, as discussed in Section 4.2.1, for the 29.5-29 tire. Additional plots for the 29.5R29 and 26.5-25 tires may be found in

Appendices 9.1.6. The observed loads are based on recorded weight measurements and divided in half under the assumption both wheels are equally loaded. Furthermore, the observations are corrected to remove approximate static wheel and tire weights to equally compare to the engineering data points.

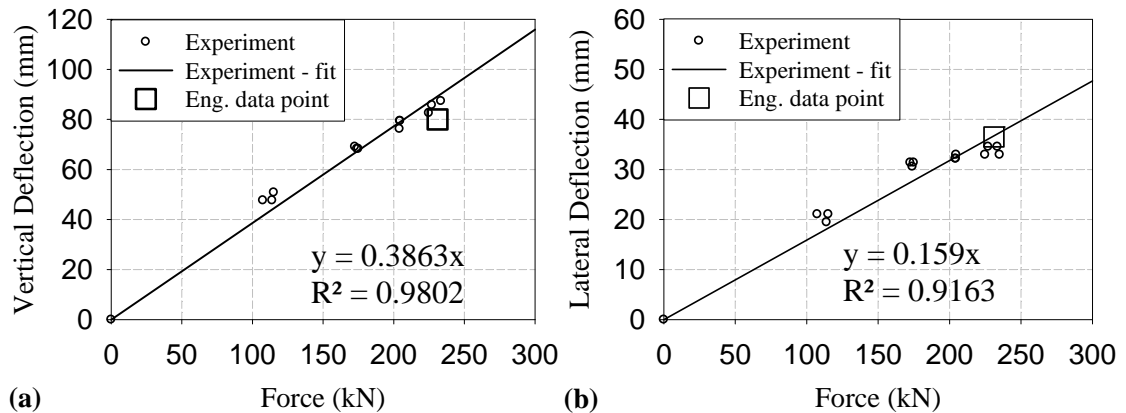


Figure 4.4.7 - Deflection data for the 29.5-29 tire showing a) vertical deflection versus load force and b) lateral deflection versus load force compared to the corresponding Goodyear engineering data point [14].

Regression analysis, to determine a linear relationship between force/displacement, was completed for each vertical and lateral set of deflection observations. Based on the equations of these lines, approximations of the load/deflection (stiffness) behaviour were quantified. Furthermore, these relationships were used as an additional method to validate the experimental methodology through comparison with manufacturer data.

First, load versus vertical and lateral deflection values were determined and compared to manufacturer values based on underground static loading. This was achieved by using the values of linear regression, for example 0.3863 mm/kN and 0.159 mm/kN for the 29.5-29 tire, and solving the inverse to determine kN/mm values. These are summarized in Table 4.4.1 and include reference manufacturer data for comparison.

Table 4.4.1 - Tire Deflection Characteristic Comparison of Experimental Static Loading and Goodyear OTR Data

Tire Model	Experimental Observations		Goodyear OTR Data [5]	
	Approximate Load/Vertical Deflection (kN/mm)	Approximate Load/Lateral Deflection (kN/mm)	Approximate Load/Vertical Deflection (kN/mm)	Approximate Load/Lateral Deflection (kN/mm)
29.5R29 RL-5K; L-5 Type 6S	2.41 at 660 kPa	5.57 at 660 kPa	1.89 at 648 kPa	4.4 at 648 kPa
29.5-29 SMO; D/L-5D Type 6S	2.59 at 591 kPa	6.29 at 591 kPa	2.89 at 627 kPa	6.3 at 627 kPa
26.5-25 SMO; D/L-5D Type 6S	2.68 at 646 kPa	5.38 at 646 kPa	2.63 at 552 kPa	5.3 at 552 kPa

Subsequently, an additional critical comparison was made by evaluating the ability of the experimentally observed load-deflection behaviour in predicting deflection relative to the Goodyear engineering data values. This is achieved by determining a given deflection corresponding to the reference load provided in the Goodyear OTR engineering data book and comparing the calculated deflection to the expected deflection values. The corresponding error was determined to vary between 0.2% and 21.5% as described by equation 3, with a total overall average of 9.6%. These findings are summarized in Table 4.4.2 below.

$$Error = 1 - \left| \frac{(Experimental\ Deflection\ Value)}{(Engineering\ Deflection\ Value)} \right| \quad (3)$$

It is important to note error is introduced in this comparison due to varying tire pressures, since Goodyear engineering data is provided as deflection for a given load at a specified tire pressure and were different than the test vehicles' tire pressures, which are shown in Table 4.4.2. Furthermore, all tires under investigation have been used for some undetermined amount of time in the field and showed signs of wear and general

deterioration. The degree of deterioration is impossible to quantify. This is another source of error as manufacturer specifications are based on a new tire, and tread wear, sidewall damage and deterioration, and overall manufacturing variances affect tire performance and deflection characteristics. Additionally, no information is provided by the manufacturer that states multi-piece wheel information or the general testing apparatus used to determine deflection data; it is appropriate to assume testing methodologies may have varied between the manufacturer and experimental observations.

Table 4.4.2 - Tire Deflection Observations Comparing Experimental Static Loading to Goodyear OTR Engineering Data [14].

Tire Model	Experimental Observations		Goodyear OTR Data [5]		Percent Error of Experimental Observations To Goodyear Data	
	V.D.* (mm)	S.D.** (mm)	V.D. (mm)	S.D. (mm)	V.D.	S.D.
29.5R29 RL-5K; L-5 Type 6S	94.0 at 660 kPa	40.6 at 660 kPa	122 at 648 kPa	52.5 at 648 kPa	21.5%	21.1%
29.5-29 SMO; D/L-5D Type 6S	87.5 at 591 kPa	36.1 at 591 kPa	80 at 627 kPa	36.5 at 627 kPa	11.1%	0.2%
26.5-25 SMO; D/L-5D Type 6S	61.5 at 646 kPa	30.7 at 646 kPa	63.5 at 552 kPa	31.5 at 552 kPa	2.0%	1.6%

*V.D. refers to vertical deflection; **S.D. refers to sidewall deflection.

5 HISTORICAL WHEEL TRACKING DATA ANALYSIS AND DATABASE DEVELOPMENT

5.1 MOTIVATION OF DATABASE DEVELOPMENT

Historically, wheel and tire maintenance was less than adequate, as industry often had the mentality that they are a low maintenance and highly durable asset that requires little attention. This has simply not been the case and is particularly true in the last few decades, as the demands on wheel assemblies have grown, as technological advancements have been made. As heavy machinery technology has improved, vehicles now have more power and load carrying capability, yet the size of wheels have often remained the same [21]. To compound the issue, in recent years, there has been a global shortage of tires available, meaning extensive efforts have been exerted to extend tire life and sharing between vehicles and mines, resulting in pushing the limits of wheel assemblies.

The hazards of multi-piece wheels are clear by the incident reports reviewed in Section 2.2.2; however, studying this information only provides insight into the state of the wheel assembly after failure has occurred. At this point it is obviously too late for preventative measures, and in certain cases, difficult to identify causes leading to a failure. For this reason, and since the most effective way to mitigate risk is through design improvements and devices or processes that manage risk at the source, the development of a historical wheel tracking analysis database was conducted. The main purposes of the database is to provide insight into the causes requiring wheel maintenance and/or removal from service, and to determine the most common methods in which wheels are damaged. The benefits of this are two-fold; through understanding how

wheels are getting damaged, this can be taken into account to develop more robust designs that consequently improve safety and reduce losses through the reduction of downtime. Secondly, having a better understanding about the durability and life span of wheels allows for better maintenance practices. For example, perhaps specific wheels are reviewed annually; however, statistics show it would be more effective to service every ten months. The historical wheel tracking analysis database is to be used as a tool that provides a novel method to actively analyze the state of wheels and reason for scrapping, in an effort to both improve efficiency and safety through the use of advanced statistical methods.

The consensus of industry specialists engaged through the course of this research is that proper wheel assembly maintenance and awareness is essential to ensuring safety and minimizing downtime when it comes to wheels, tires, and vehicle operation in general. Additionally, it was noted that a detailed wheel assembly management and tracking system is required. An industrial partner to the current research, NSIW Mfg., were engaged primarily based on the wheel maintenance and recertification services they provide to mining operations. A relatively new addition to their services is the *North Shore Rim Tracking System*: a tracking system that maintains historical records of a customer's wheels and rims. Though not used by all customers to date, usage is increasing with additional mines being added to the system. It provides detailed information on any maintenance or repair history of wheels, and is typically used in combination with their recertification program to determine when annual inspections and service are required, as well as historical tracking of wheel scrapping. After receiving

permission of NSIW's Ontarian customers, the electronic database was shared with the research group.

A thorough review of literature available in the public domain yielded limited information highlighting common wheel and rim repairs and reasons for removal from service, and even less specifically related to the frequency of such damage outside of the scope of incident reports. Based on literature review and industry engagement, it is believed that such information is typically proprietary to a customer, supplier, and/or maintenance service, or may not be effectively organized for the purpose of review, particularly in the case of smaller mining operations. They may be familiar with causes for wheel repair or replacement and follow proper handling and maintenance procedures, but do not keep extensive records of such information.

5.2 DATABASE DEVELOPMENT DETAILS

The first step to develop the database is a thorough review of the existing data and how it is stored. Created by a contracted third party, and based on the Microsoft Access platform, the rim tracking system user interface is simple, yet effective for tracking purposes.

The present state of the system allows for adequate recording of wheel information, preparation and tracking of work orders, summarizing inventory by customer, and limited automated reporting capability. Organized by customer, the system can prepare complete history reports for a specific wheel/rim or more comprehensive reports showing the current status of all rims or broken down by categories organized by manufacturer, tire size, rim type, repair status, the type of work being completed, or date ranges. However, the system has its limitations and is unable to effectively allow compilation of data for

statistical review or comparison between customers for review of issues on a broader scale.

For this reason, the development of the new historical wheel tracking analysis database was undertaken. Furthermore, the long-term goal of the database is for it to act as a tool that would continue to be used to actively track trends in wheel usage, repair and scrapping. As such, simplicity, robustness, and ease of use were high priorities for the database. It is the belief that any changes to wheel assembly usage, maintenance procedures, modification or design innovations, or the implementation of safety devices cannot be adequately evaluated if effective tracking and analysis is not performed. Without first evaluating the current state of affairs, it would be impossible to accurately compare changes in the future under real-world operating conditions.

To ensure simplicity and ease of use, the new database was created using the popular and widely-used Microsoft Excel platform with heavy use of macro programming using the software's built-in functionality of Microsoft Visual Basic for Applications coding. After first exporting raw data from NSIW's tracking system during the development phase, the database was then setup to automatically read in source data based on NSIW's formatting and storage parameters for seamless integration of the two systems. Though the current state of the database is specific to analyzing NSIW's data, it is a proof of concept to demonstrate the ease of developing such a system and the added benefits the capability provides for analysis and tracking purposes.

Initial efforts focused upon assembling data from all mine sites referenced by the reasons their wheels were removed from service and scrapped, for the purposes of statistical review of different characteristics. With the main focus of this research being

to enhance the safety of multi-piece wheels used on mining vehicles, a matter of interest was determining the most commonly used style of wheels and the greatest factors resulting in their damage and scrapping. The mentality behind this was the thought that by studying the most common wheels and then focusing research efforts on addressing the most common reasons they are damaged and scrapped, the greatest improvement to safety and highest reduction due to scrapping would be yielded.

The greatest challenge to data analysis and developing the database tools was maintaining the integrity of the data and preventing a “garbage-in/garbage-out” scenario. To prevent misleading observations, it was ensured proper, valid data was being compared and two significant challenges had to be overcome: 1) lack of information and 2) validity of scrap codes/reasons. Related to the first issue, all wheels and rims stored in the database had accurate scrap dates input as well as a related reason; however, an accurate in service date was not always available. It was determined the main reasons for this was because many customers joined the tracking system with many wheels already in service, some wheels were bought used and then put into service, and similarly some wheels were purchased with used vehicles. For these reasons, original service dates are unknown and subsequently, of the total number of wheels tracked by the system that were scrapped (3021 individual wheels), only 2010 are included in the assembled data and completed through an automated process.

The second issue required a thorough review of all data and in particular, scrap codes and descriptions. It was discovered that within the NSIW tracking system certain mines had different numerical scrap code referenced to a different corresponding description. Furthermore, certain reasons for scrapping were ignored because they were not pertinent

to the analysis. For example, “rim sold/returned with scoop/truck” or “machine no longer in service” are more a matter of circumstance than an issue related to wheel damage that would be of interest. As a result, 47 different scrap codes are reduced to a total of 13 valid combined codes referenced by the database and are shown in Table 5.2.1. This further reduces available wheel data from 2010 wheels to only 1441. Macros created for use in the database are provided for reference in Appendix 9.2.

Table 5.2.1 - List of Modified Scrap Codes and Descriptions Based on Validity

Scrap Code Number	Description of Modified Scrap Codes
3	MPI Failure (Var. Locations)
5	MT Failure (Var. Locations)
13	Fails Gutter Gauge Test
14	Fatigue Cracks (Visual)
15	Excessive Wear (Var. Locations)
19	Rim Gouged
20	Rim Bent / Damaged
22	Rim Torched
23	Excessive Corrosion
28	Due to notch in Lock Ring Groove
30	Rim Base Split Adjacent to Centre Plate
32	Rim Base Weld Failure
34	Centre Plate Weld Failure
38	U.I. Failure
40	Requires Centre Plate (Max limit attained)
45	Requires Back Section - Limit of 1 Attained

The current state of the database was evaluated by NSIW Mfg. and industry experts representing mines that released wheel information for the analysis. Overall, extremely positive feedback was received regarding the database; as well some new avenues of

improvement were suggested. Future development could include revisions to the database's real-time statistical tracking of wheel repair issues and the improved ability to further breakdown statistics by mine site as well as by vehicle application for a given wheel size, though the latter is not possible for most wheels due to the current limited information that is recorded in the NSIW tracking system.

5.3 ANALYTICAL OBSERVATIONS

Success has been observed through the development of the database as it provides insight into major causes of wheel failure and scrapping. The most commonly used multi-piece wheels have been identified to be 26.50 x 25, 29.5 x 25, and 29.5 x 29, in descending order. Furthermore, the top reasons for wheels and rims to be removed from service is due to being bent or similarly damaged, failing a magnetic particle inspection (MPI) indicating the presence of a crack, or excessive wear in a critical region of the wheel. Table 5.3.1 below shows the frequency of wheel/rim scrapping referenced by scrap description of all represented wheel sizes.

Table 5.3.1 - Summary of Wheel Scrapping Statistics by Size and Description

Scrap Description	10.00 X 20	12.00 X 20	12.00 X 24	12.80 X 18	14.00 X 24	15.50 X 25	16.90 X 24	17.50 X 25	18.00 X 25	21.00 X 25	23.90 X 25	26.50 X 25	29.50 X 25	29.50 X 29	29.50 X 35	33.25 X 29	80.65 X 29	87.65 X 29	Total # of Scrapped Wheels
MPI Failure (Var. Locations)	1	3	18		2			4	19	12		175	53	56	7	11	2	3	366
MT Failure (Var. Locations)		4	4		1			1	8	11		112	3	9		12	1	1	167
Fails gutter gauge test												6							6
Fatigue Cracks (Visual)			8						2			20	1	1		1			33
Excessive Wear (Var. Locations)	1	3	31		1	1	1	1	11	5	2	159	10	7		4			237
Rim Gouged					1				1		1	12						1	16
Rim Bent / Damaged		2	56	1	7	2	1	1	5	4		260	61	2	1				403
Rim Torched			6						2	3		15							26
Excessive Corrosion			7			5		1	4			14	1	2					34
Due to notch in Lock Ring Groove										1		13							14
Rim Base Split Adjacent to Centre Plate												8							8
Requires Centre Plate (Max limit attained)			11		1	1		3	33	22		51	2	4		1		1	130
Requires Back Section (Limit of 1 Attained)														1					1
Total Number by Tire Size	2	12	141	1	13	9	2	11	85	58	3	845	131	82	8	29	3	6	1441

The database also has built-in plotting functions setup to allow for easier in-depth data comparison. For example, a simple to use drop-down list allows the user to select a wheel size of interest and then a plot is generated showing the frequency of all applicable scrap reasons, as seen for a 26.5x25 wheel for reference in Figure 5.3.1.

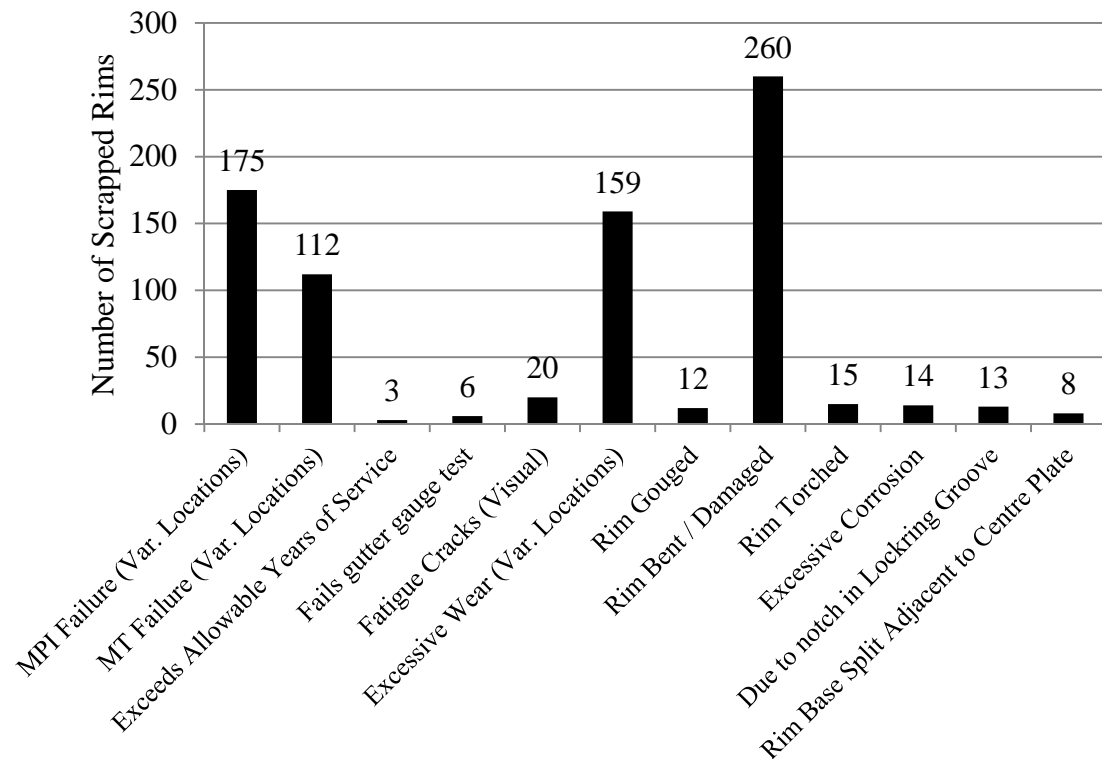


Figure 5.3.1 - Frequency of scrapping due to corresponding reasons for a 26.5x25 wheel.

Additionally, a study to determine average wheel life was performed and is a similarly automated tool in the database that only considers wheels with appropriate scrap reasons related to actual fatigue or damage. However, it is important to understand the limitations of these statistics and it should be considered a very broad analysis. The average life is determined by calculating the duration of time, in days, between the wheel's in-service date and being scrapped. Other than similarly being limited to wheels

with applicable date information available, admittedly there is the inability to take into account time that the wheels may have been out-of-service for maintenance or time that the vehicle was not being used, for example. However, for wheel sizes with a large enough sample, it could be assumed that the effect of outliers would be negligible.

Overall, the information is still valuable as it provides novel insight into wheel life and similar studies or information have not been found in open literature. The data has a wide range of uses including aiding in the development of scheduled maintenance routines, as well as budgetary planning to take into account wheel replacement and vehicle operating costs. Additionally, it is the hope that continued use of the database will provide insight into the effectiveness of any safety improvement devices, such as the safety shield system discussed in Section 6, or allow comparison between alternative or new wheel designs. A summary of average wheel lives is found in Figure 5.3.2 below.

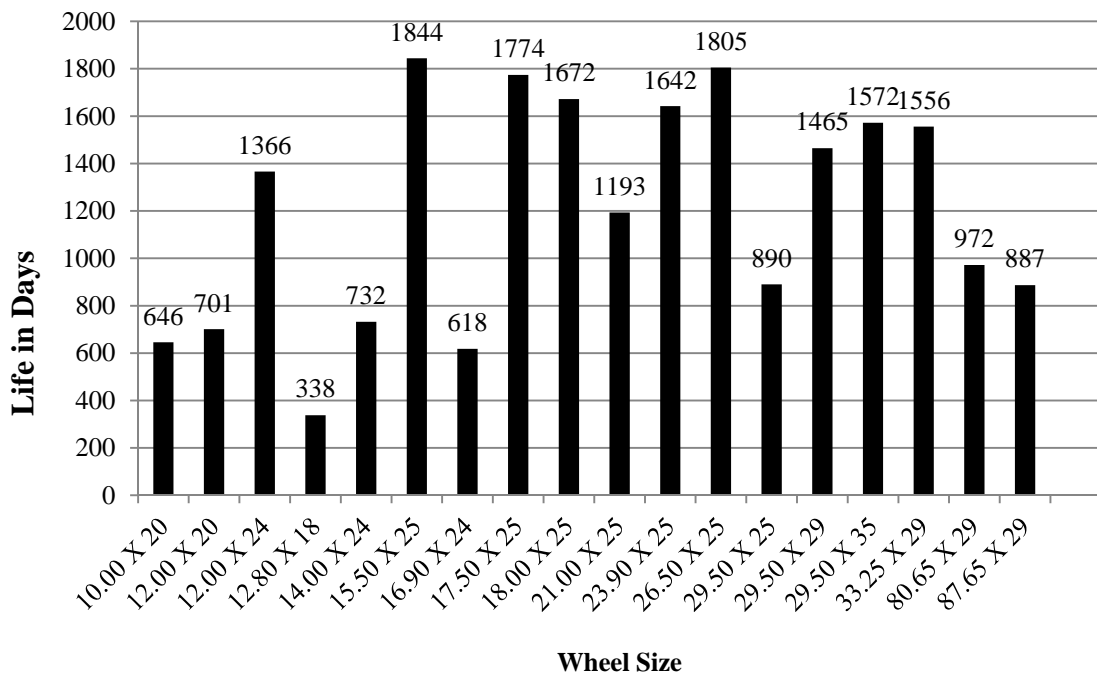


Figure 5.3.2 - Average wheel life (by size) as calculated by database.

6 SAFETY SHIELD SYSTEM

6.1 MOTIVATION AND DESIGN

As demonstrated in previous sections, the inherent hazards of present multi-piece wheel assembly designs and their common failure modes are evident. By reviewing the analyses of historical wheel tracking data and particularly the frequency of damage beyond repair resulting in a wheel's removal from service, it is evident that the durability, reliability, and overall safety of multi-piece wheels is not optimized. For these reasons, the feasibility of a failsafe wheel protection device was explored with consideration given for integrated features to mitigate common mishandling practices, to better control hazards should failure occur, and improvement on the longevity of wheels and wheel components.

In an attempt to encompass as many features as possible that would protect those exposed to wheels - in a variety of situations and environments - from common failures, an initial design was created using the Dassault Systèmes' CATIA software package and based on literature and incident reviews as well as personal contact with industry. The safety shield system is presented in Figure 6.1.1 below and highlights its main components, including an outer shield/barrier and "tube nuts" that allows the assembly to be secured to the vehicle.

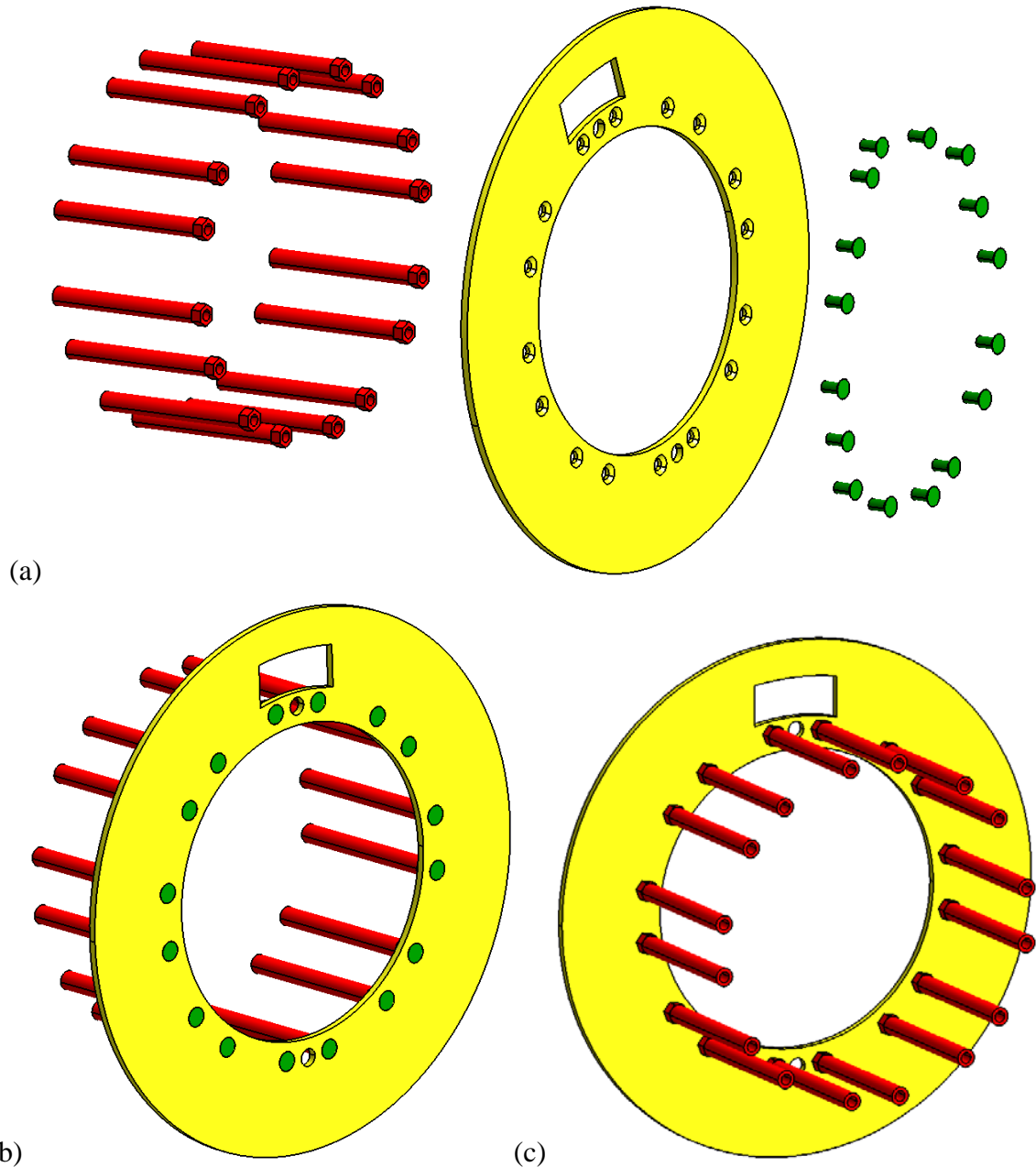


Figure 6.1.1 - (a) Exploded view of safety shield components; (b) assembled safety shield front view; (c) assembled safety shield rear view.

Designed to be as simple and cost effective as possible, the shield was constructed of common mild steel that was readily available and similar to what was used for construction of the wheel assembly. The “tube nut” is a round tube with a threaded base to allow for it to be secured to the wheel mounting stud with a heavy hex nut welded to

the top, allowing the shield to be secured to it using standard tapered Allen head fasteners. The material may vary depending on strength requirements of the particular application, but for the purposes of validation and design efforts detailed in future sections using a 29.5-25 wheel, they were sized as though they are 1020 DOM structural round steel tube. This tube has a 1.25" outer diameter, 0.25" wall thickness, and 0.75" inner diameter to allow for tapping of a 13/16" thread as used for the mounting fasteners that secure the wheel to the vehicle, and a large-sized, high-grade 3/4" hex nut welded to them. Welding a high-grade nut to mild steel would result in a weak point at the weld and for the purposes of long-term, mass production it would be recommended to machine one-piece, special purpose fasteners out of a high-strength material. These would require appropriate dimensions specific to the desired application.

The basic premise of the safety shield system was to incorporate the following features using a fail-safe design methodology:

- a) Act as a consumable resource that protects and limits the exposure of the wheel flange and other critical wheel components.
- b) Incorporate a valve removal device that ensures zero pressure during disassembly or wheel dismounting from the vehicle.
- c) Integrate a tire pressure monitoring system (TPMS) for enhanced tracking of tire pressures and to ensure the vehicle is not being overloaded.
- d) Include an over-pressurization blow-off valve should tire pressures rise to dangerous levels throughout operation.
- e) Add a visual pressure go/no-go site glass for operator ease to provide a method to determine if tire pressure falls within acceptable operating range without requiring maintenance personnel to approach the wheel at close range.

Developed using wheel geometrical data provided by NSIW Mfg., the safety shield is intended to mitigate the hazards of wheel and tire failures by creating a physical barrier between the equipment and operators or maintenance personnel. Additionally, it is designed to improve wheel life by reducing the amount of impact and abrasion the wheels are exposed to during operation. It was established that many critical failures related to wheels are frequently due to fatigue and damage resulting in the failure of flanges, lock rings, and bead seat bands that are essentially all the outer components most susceptible to damage while in use. For these reasons, the shield completely separates the outer wheel surface from its operating environment. An additional qualitative benefit of the shield is that it is fully accessible from the perspective of an outside observer or maintenance personnel. For example, should the shield itself experience impact or fatigue damage then it is more easily inspected and identified than wheel components with unexposed surfaces.

Incident reviews suggest that improper wheel handling and assembly practices are a substantial cause of concern. The safety shield design incorporates numerous key features that ensure proper wheel handling procedures that must be followed by users or the wheel simply cannot be removed or disassembled; such as requiring a zero pressure condition. This is achieved through a ratcheting valve removal device/over-sized valve cap. The premise is that the valve cap is sized such that it must be removed prior to removal of the shield, which similarly must be removed before the wheel fasteners are accessible. The cap is to incorporate a ratcheting feature that allows it to be threaded onto the valve stem; however, it automatically removes the core as one complete unit if it is unfastened, and subsequently results in the release of all air pressure.

Proper tire pressure promotes wheel safety and ensures adequate load carrying capability, which thereby prevents damage to tires and extends life. Tire pressure monitoring systems (TPMS) have become standard requirements on new passenger vehicles manufactured or sold in North America [46]. This stems from the recall of 6.5 million Firestone tires in 2000 due to premature failures and studies that revealed under-inflation is the leading cause of failures for passenger vehicle tires. Unfortunately, this legislation did not extend to OTR tire applications, yet the literature review presented here demonstrated it is similarly a cause for concern with both pressure too high and too low. To combat this issue, three proposed solutions are: an internal tire pressure monitor accompanied by a visual operator display, an over-pressure blow-off valve, and a “Go/No-Go” site glass.

Commercially available systems that are designed for OTR tire applications are capable to fulfill the required purposes; however, through the course of the author’s interaction with industry, it was determined they are not widely embraced. The system would allow operators to monitor pressures during operation since tire pressure is expected to fluctuate; however, minimum and maximum limits must be observed to maintain safety. It can also aid in determining if too high of a payload is being carried as temperature and pressure would subsequently rise.

The blow-off valve would be individually calibrated to ensure a controlled release of pressure if it is too high for the specific tire/wheel application. This is a simple solution to aid in the prevention of catastrophic failures, possibly as a result of excessively high pressures due to overloading, pyrolysis, or if contact is made with electrical wires or a heat source. Though it may be difficult to mitigate a rapidly increasing pressure through

a single blow-off valve, a gradual overpressure could be controlled and at a minimum, venting of air pressure is a clear and audible indicator for maintenance personnel, for example.

The purpose of the “Go/No-Go” site glass is to provide a simple visual aid directly on the wheel assembly that indicates if the tire pressure is within an acceptable range. The mentality behind this is for indication if the assembly is safe to approach without having to take a physical measurement or be inside the vehicle and use the TPMS monitor. This would be helpful for situations where someone may be working in close proximity to the vehicle attempting to perform maintenance, or if the wheel is in storage. Ideally, this could be integrated with the blow-off valve for simplicity in packaging and installation onto the wheel assembly.

An additional proposed design trait is that it would ideally have zero pressure within the tire during assembly and handling until it is securely installed on the vehicle with the shield in place. However, a minimal tire pressure after assembling the wheel is required to ensure all components remain correctly seated, though many mine sites that have been engaged have wheel handling procedures that call for full operating pressures. Though this is not an issue for a correctly assembled wheel in proper condition, in situations where damage or fatigue is an issue unknown to maintenance personnel, for example, serious safety concerns may arise while handling or storing the wheel assembly. A potential solution for this is to incorporate an internal bead locking system, such as Staun Internal Beadlocks [47] that would maintain minimal pressure to provide engagement force directly applied to the tire bead and wheel assembly locking components in an

encapsulated pressure vessel inside the tire. It is suggested that the feasibility of implementing such a device be explored through future research.

6.2 FINITE ELEMENT MODEL DEVELOPMENT

6.2.1 Validated Wheel Assembly Model

During initial numerical simulations, a wheel assembly model developed by fellow researcher, PhD candidate Mr. Zhanbiao (Weldon) Li, was used and previously validated using the experimental data collected at Goldcorp Inc.'s Musselwhite Mine. The model is based on a five-piece NSIW wheel and a bias-ply Goodyear 29.5-29 SMO D/L-5D Type 6S tire, as equipped on a Caterpillar R2900G with specific experimental data provided in Section 4. The primary reason for its selection over other wheel assemblies was for its more common usage and scrapping as determined by the historical tracking database and because the R2900G had the highest gross axle weight rating.

For the purposes of brevity, reference can be made to the peer-reviewed, co-authored journal article “Development and validation of a FE model of a mining vehicle tyre” [48] published in the *International Journal of Vehicle Design*, for specific model development information and validation techniques. The virtual model exhibited good correlation between published engineering data and experimental findings with respect to the force/vertical wheel displacement relationship and lateral deflection. Furthermore, simulation predictions were rigorously compared to the experimentally determined displacement fields of various tire locations with maximum percentage error estimates no greater than approximately 30%, with the majority of locations having error less than approximately 5%.

The model was developed using commercial CAE software Hypermesh for the purposes of simulation using LSTC's LS-DYNA nonlinear dynamic solver. The tire was discretized into several regions, each with their own material properties, and based on the tire's physical construction and geometry, as shown in Figure 6.2.1.

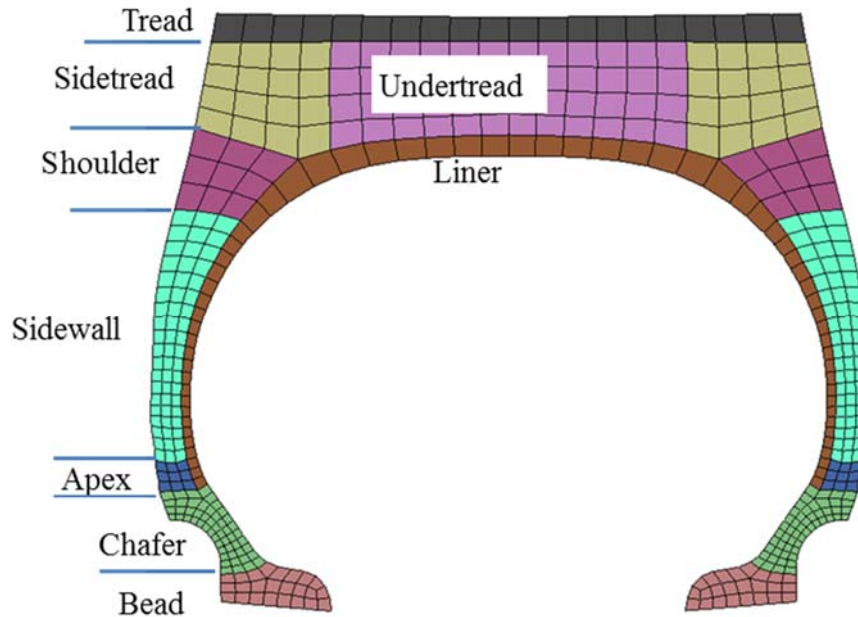


Figure 6.2.1 - Discretized tire model showing various regions.

The wheel model was generated based on geometry from the wheel manufacturer and in-field measurements, and discretized using Hypermesh. For the purposes of tire validation, all wheel components were given an elastic material model representative of mild steel; except the wheel mounting ring which was treated as a rigid component for purposes of applying load. Specific properties given to the steel include a density of $7.8 \times 10^{-9} \text{ kg/mm}^3$, an elastic modulus of 2.1×10^5 , and Poisson's ratio of 0.28. Though adequate for tire validation, an elastic material would not be suitable for shield design validation efforts where plastic deformation is expected.

Validation of the rim base was performed through experimental testing of a 29.5-25/3.5 (Dia.-width/flange height) sized wheel, commonly used for 29.5-29 or 29.5R29 OTR tires. The rim base was instrumented with five model KFG-5-350-C1-11L3M3R Omega Engineering brand strain gauges in various locations and was positioned within a specially designed fixture to support the structure and maintain stability through the test. The fixture consisted of two 50.8 mm thick steel support blocks at the base which were machined to conform to the contour of the rim base at the designated supporting locations. An external load was applied in the z-axis direction (as indicated in the Figure 6.2.2) using a hydraulic actuator and measured using a PCB model 1204 strain gauge-based load cell with a 222 kN capacity. An aluminum block with a contact area of 80 mm x 103 mm was placed onto the rim base and under the piston head to ensure the stability of the wheel was not disturbed due to possible non-symmetric loading conditions and to reduce stress concentration levels. Two AR700 laser displacement transducers were used: an AR700-1 (model AP7010010) with a measurement range of 25 mm for vertical deflections and an AR700-0500 (model AP7010005) with a measurement range of 13 mm to measure lateral deflections. Data acquisition was controlled by a Dell laptop and using a National Instruments compact DAQ USB system (model cDAQ-9174) measuring at a frequency of 2 kHz. Figure 6.2.2 illustrates the experimental test apparatus and strain gauge locations 1 through 5.

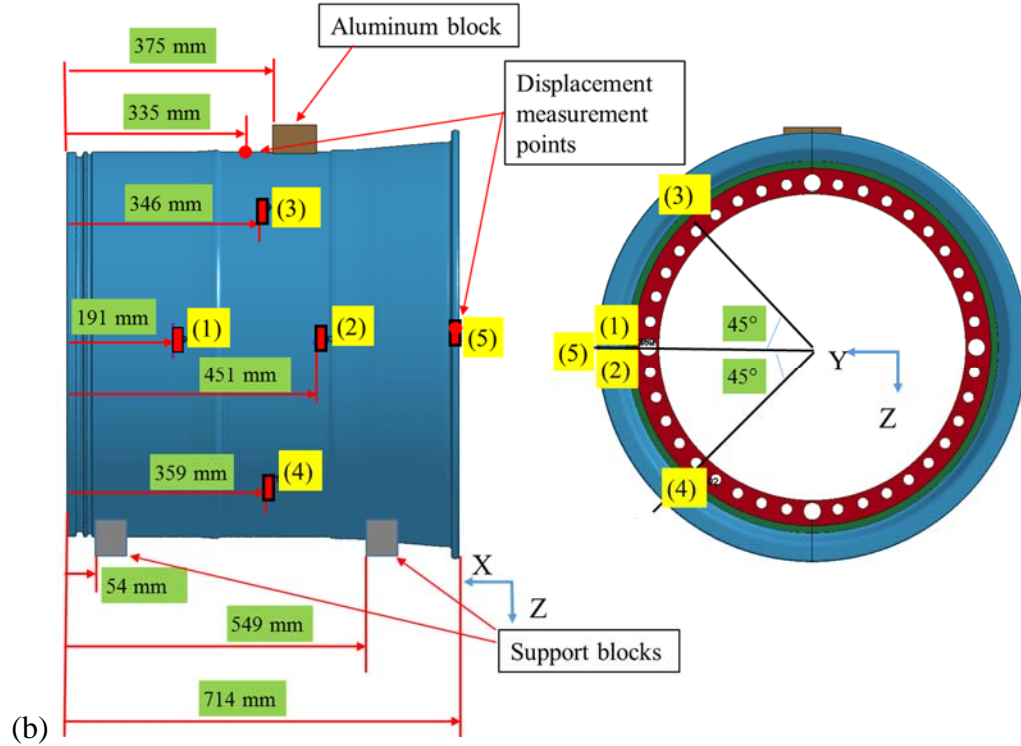
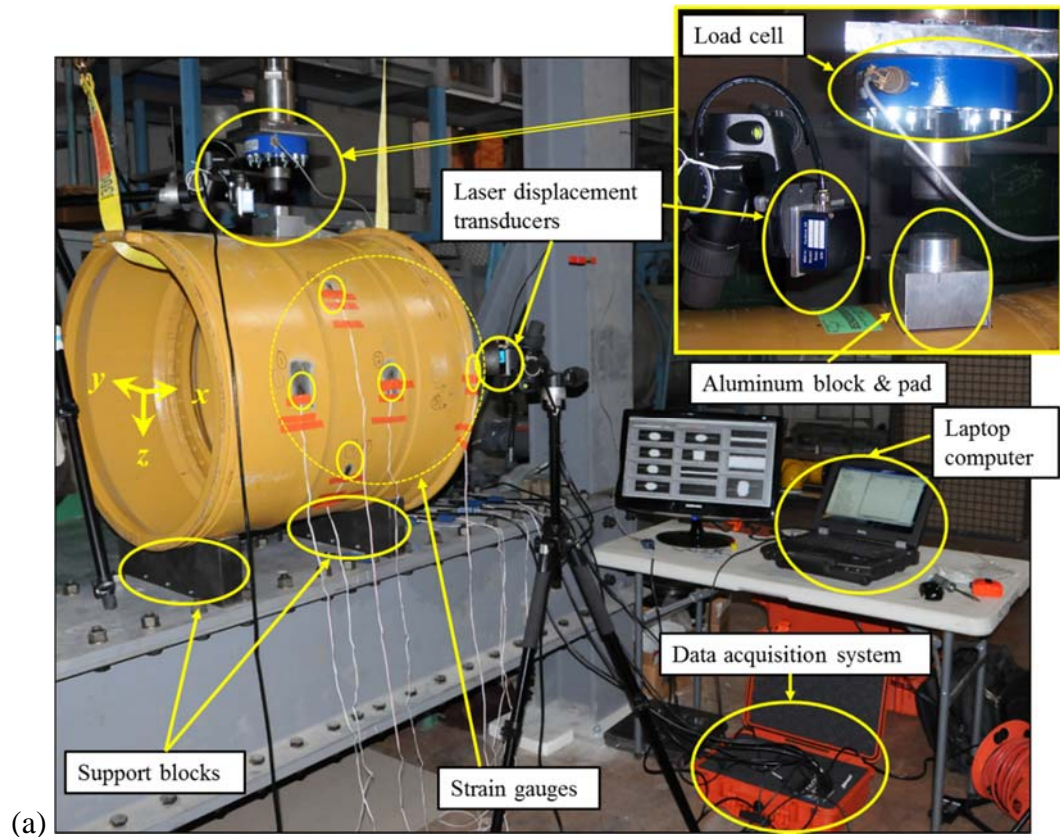


Figure 6.2.2 - Rim base (a) experimental testing apparatus and (b) strain gauge locations.

Primarily through the efforts of fellow researchers, PhD. candidate Zhanbiao (Weldon) Li and MASc. candidate Sante DiCecco, observations made showed approximately identical results for seven tests in total, while under identical boundary and testing conditions, thus demonstrating consistency and repeatability. As anticipated, analysis of data collected showed linear relationships for the deflection/load and strain/load responses of the rim base for all regions monitored during the testing. Maximum applied load was 160 kN to ensure loading was maintained below the 220 kN capacity of the load cell and below all elastic deformation limits of the wheel; this loading corresponded to deflections of approximately 3 mm and 2 mm in the vertical and lateral directions, respectively.

Since the purpose of the experimental test was to validate the wheel model, numerical simulation of the experimental test under representative loading and boundary conditions was completed using LS-DYNA. Given the symmetries of loading, boundary conditions, and geometries, only half of the rim base was modelled. In order to measure the surface strain of the rim base, 0.01 mm thick shell elements were extracted from the outer surface. This is a common practice in FE modelling for durability analysis of solid structures in order to accurately capture surface stresses and strains, which are most critical in fatigue and engineering analyses involving crack formation at exterior surfaces. The effect on the rim stiffness by adding the thin layer of shell elements was assumed to be negligible. The Belytschko-Tsay shell element formulation was used for the shell elements with three integration points through the thickness. The strains output from the midpoint of the shell elements were used for comparison to the experimental test

observations for all five strain gauge locations. Acceptable correlation was observed and results are summarized in Table 6.2.1.

Table 6.2.1 - Rim Base Deflection and Strain Responses at Maximum Load For Experimental and Numerical Observations

	Top Deflection (mm)	Side Deflection (mm)	Strain Response (ue) by Gauge Location				
			1	2	3	4	5
Experimental	3.00	2.10	292.19	197.26	127.62	102.86	901.90
Numerical	3.32	2.20	316.21	232.64	130.14	62.42	872.31
Percent Error	10.5%	4.8%	8.2%	17.9%	2.0%	39.3%	3.3%

6.2.2 Model Enhancements

During initial virtual shield impact tests, issues were observed with the contact between a rigid striker and the tire sidewall. Despite extensive efforts to overcome issues and improve contact behaviour, it was determined the most effective course of action would be the reevaluation of the material properties of the tire. As discussed in the previous section, the tire model was validated with experimental data; however, it was limited to the purposes of studying highly localized deformations and broader overall performance, which it accomplishes effectively. Conversely, for the requirements of safety shield testing, inadequate stiffness properties were given to critical areas of contact causing numerical instabilities.

To combat these instabilities, adjustments were made to the material properties of each section of the tire based on literature references, engineering judgment, and numerical validation using an iterative approach. The work of Reid et al. [40] demonstrates the process of creating a tire model appropriate for crash and durability

simulation applications, using laboratory testing observations for validation. Despite differences in the structure and material of passenger and OTR tires, reference is made to the limited material properties they discuss and is used as a basis to develop a modified tire model, altering specific regions based on experience and design properties of OTR tires. Table 6.2.2 below compares the original material properties of the tire model and the new. Note that all sections of the tire are modelled using an isotropic elastic material constitutive relationship, with the exception of the beam elements representing the steel belts/cords of the tire. These were modelled as discrete elastic beams with initial tension applied. During validation efforts, the wheel components were modelled as elastic steel. The density of the tire was kept uniform and the mass of the virtual model corresponds to published manufacturer specifications.

Table 6.2.2 - Tire Model Material Properties

Description	Density (10^{-9} kg/mm ³)		Young's Modulus (MPa)		Poisson's Ratio	
	Original	Altered	Original	Altered	Original	Altered
Sidewall	1.43	1.43	0.8	20	0.33	0.45
Liner	1.43	1.43	40	40	0.33	0.495
Bead	1.43	1.43	5000	500	0.33	0.495
Sidetread	1.43	1.43	5	15	0.33	0.45
Tread	1.43	1.43	50	50	0.33	0.495
Wheel Steel	7.80	7.80	2.10×10^5	2.10×10^5	0.28	0.28
Shoulder	1.43	1.43	1	15	0.33	0.45
Apex	1.43	1.43	4	20	0.33	0.45
Chafer	1.43	1.43	500	500	0.33	0.45
Undertread	1.43	1.43	60	60	0.33	0.45
					Initial Tensile Force (N)	
Belts	7.83	7.83	1.00×10^4	5000	50	20

It is important to note that caution must be used with values of Poisson's ratio approaching 0.5. This is due to the fact a perfectly incompressible material has a value of exactly 0.5 and a greater value would predict a negative volume at a specific strain value, based the classical solution for Poisson's ratio. The selected values for the altered model range from 0.45 to 0.495, since this is an accepted range for many rubber materials [49] and similar values were used with success in the work of Reid et al [40].

Similar efforts to validate the tire model, as was performed originally using quasi-static testing observations and documented in the paper by Li et al. [48], was repeated with acceptable results as discussed in the following sections. As highlighted in Section 6.2.1, tire motion observations were collected with a high speed camera and this was used to correlate localized deflection behaviour, as shown below in Figure 6.2.3.

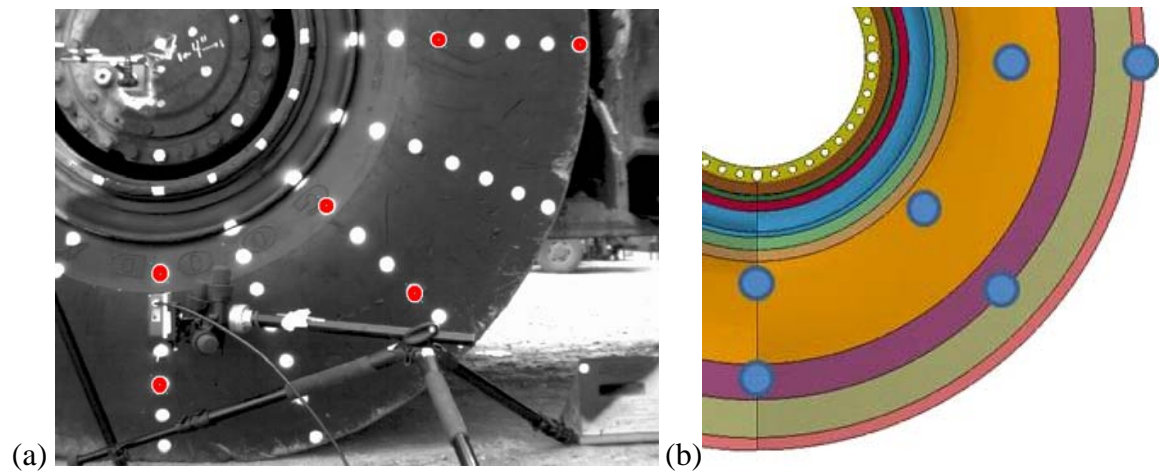


Figure 6.2.3 - Location of points tracked on the a) physical test apparatus and b) numerical model.

Comparison was made between the experimental observations, original FE model, and the enhanced model with new material properties (NMP). In the following figures, vertical deflection is compared for all the points under consideration. For the purposes of

brevity, only one of the events collected during testing exhibiting the most severe loading conditions is shown below in Figure 6.2.4.

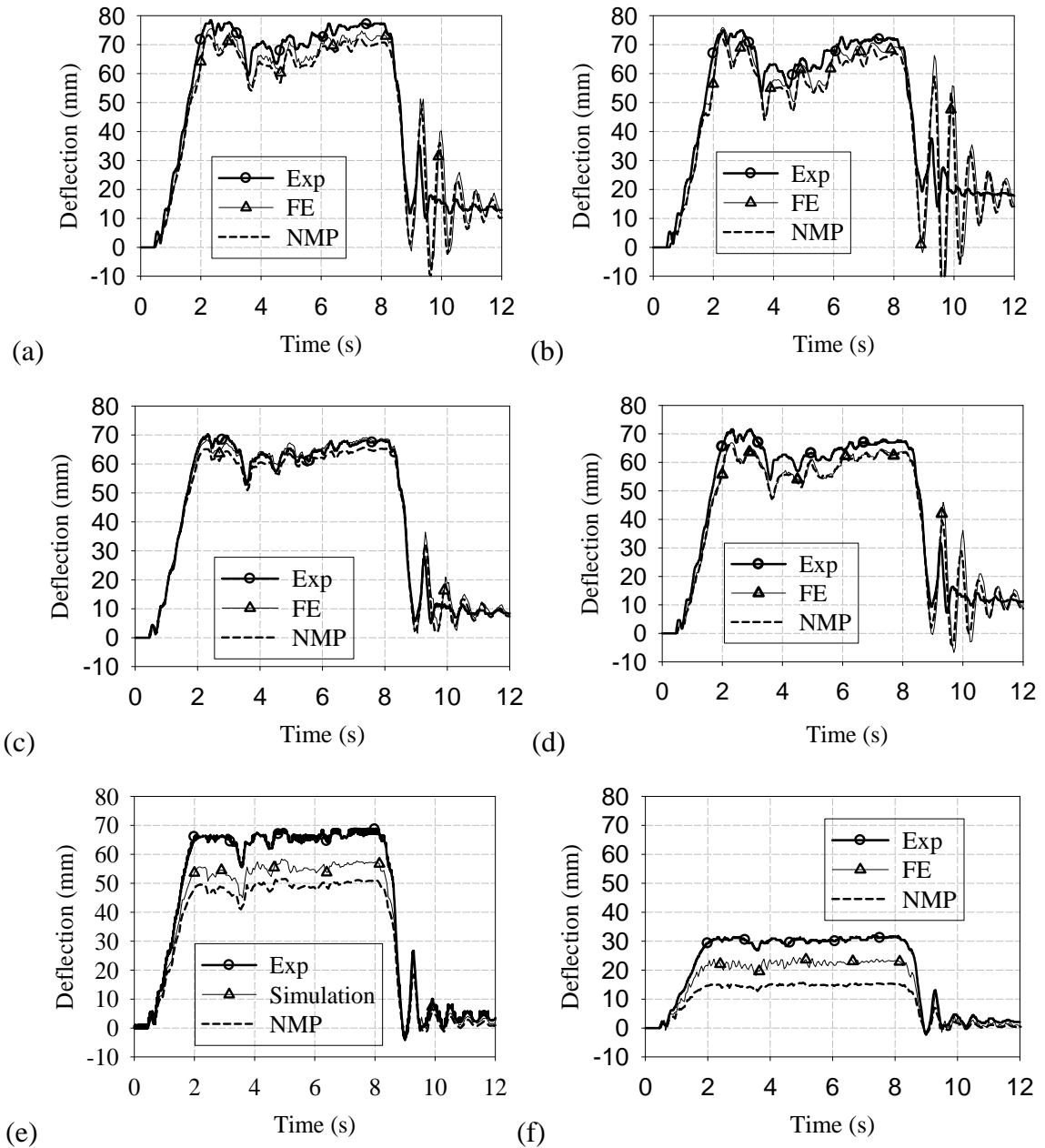


Figure 6.2.4 - Vertical deflection response comparison for experimental testing observations (Exp), the original finite element model (FE), and the enhanced new material property model (NMP), for tracked nodes during a 29.5-29 tire test event where maximum deflections were observed for a) V-in, b) V-out, c) D-in, d) D-out, e) H-in and f) H-out points.

Similarly, comparisons are made for all points in the longitudinal direction and are presented in Figure 6.2.5.

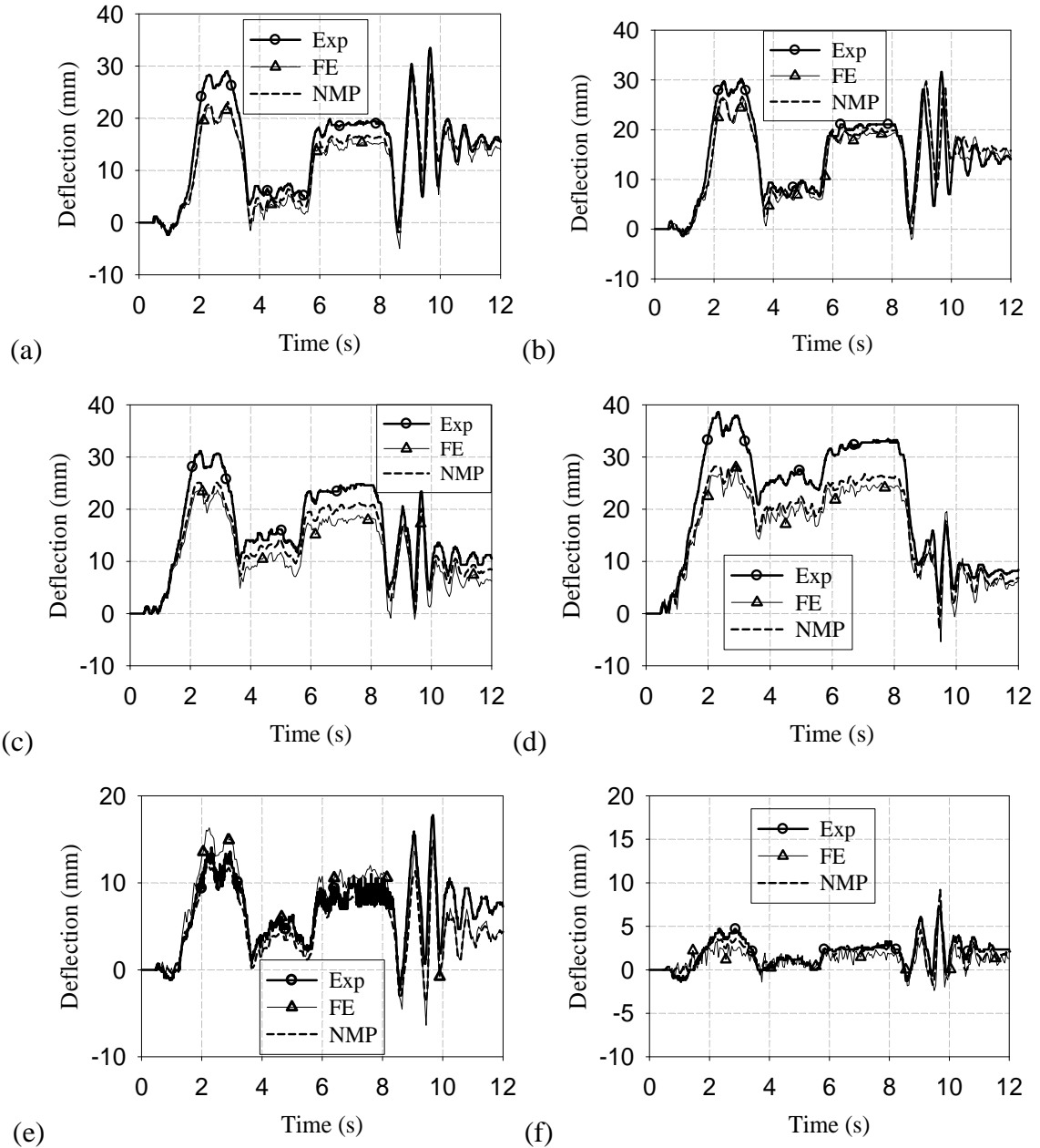


Figure 6.2.5 - Longitudinal deflection response comparison for experimental testing observations (Exp), the original finite element model (FE), and the enhanced new material property model (NMP), for tracked nodes during a 29.5-29 tire test event where maximum deflections were observed for a) V-in, b) V-out, c) D-in, d) D-out, e) H-in and f) H-out points.

A rigorous error analysis was performed to better quantitatively compare both material models to the experimental data for each tire location of interest using the same principles and approach as those presented in Section 4.4.1; however, now comparing the FE results to experimental observations. This was accomplished using equations (1) and (2), where the validation metric is unity when the difference between the FE results and the tested data is zero throughout the independent variable domain, and similarly approaches zero when the accumulated relative error becomes large. The results of error analysis efforts are summarized below in Table 6.2.3, where both the new material property and original material property models are compared to experimental observations, as well as a percent difference between the two to illustrate the effect of the material property changes.

Table 6.2.3 - Error Analysis Results for New Material and Original Material Property

		New Material Property Model		Original Material Property Model		
Direction	Point	Accumulated Relative Error	Validation Metric	Accumulated Relative Error	Validation Metric	Validation Metric Percent Difference
Vertical Displacement	H-in	4.6	95.7%	6.8	93.4%	-2%
	H-out	11.8	88.9%	9.1	91.3%	2%
	D-in	4.8	95.3%	2.6	97.5%	2%
	D-out	10.3	89.9%	9.7	90.4%	1%
	V-in	10.3	89.9%	14.9	85.3%	-5%
	V-out	50.3	53.6%	26.4	74.3%	21%
Longitudinal Displacement	H-in	84.1	75.0%	26.4	74.3%	-1%
	H-out	4061.9	82.3%	105.9	67.7%	-15%
	D-in	431.8	81.3%	354.4	71.6%	-10%
	D-out	22.9	78.2%	27.9	73.0%	-5%
	V-in	3728.5	76.3%	3484.5	76.6%	0%
	V-out	2.2 x10 ⁹	68.5%	1.2 x10 ⁸	53.4%	-15%

In addition to providing great advances in contact and impact deformation behaviour, the new material properties improve numerical results for the majority of points or have a negligible difference, with the exception of the vertical displacement of the V-out point. Selecting a different FE point for the V-out location may aid in error analysis results; however, given the improvement in longitudinal displacement and acceptable results for all other locations, it is not a major concern.

Furthermore, for future simulations where plastic deformation may be expected, an elastic material property for metal components would not be suitable. For this reason, an elasto-plastic material model was implemented. Experimental tensile testing was performed by fellow researcher, Mr. Sante DiCecco, using a specimen retrieved from a 29.5-25 mining wheel rim base. Testing was performed at ambient temperature, using a

50 kN universal testing machine equipped with a computer data acquisition system and extensometer. This was used to determine the true stress and the effective plastic strain of the material, then input for use in the material model. In addition to a nominal density value of $7,850 \text{ kg/mm}^3$ and Poisson's ratio of 0.303 [49], a stress-effective plastic strain relationship was obtained to determine values for Young's modulus and a 0.2% offset yield strength of 215.4 GPa and 369.9 MPa, respectively. Based on engineering stress and strain value, an ultimate tensile strength of 471.5 MPa was observed. The material property card used is presented in Appendix 9.3.1 and a curve was generated for input into the material model and is provided for review in Appendix 9.3.2.

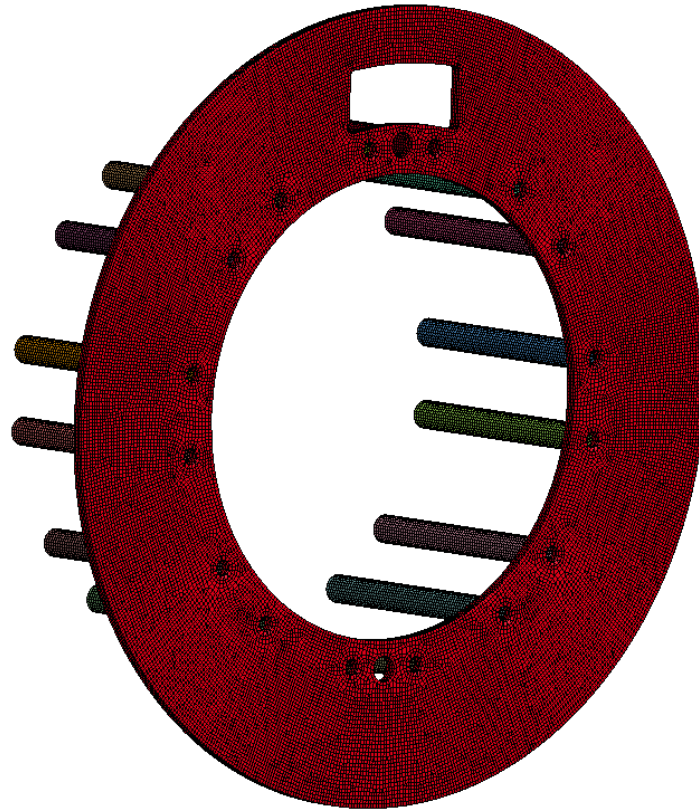
A check of the material model's robustness was performed using a simulation replicating the experimental tensile test. An axisymmetric meshed model was created based on the geometry of the experimental specimen with the base series of nodes restrained and a prescribed motion applied to the top series of nodes. Quadrilateral shell elements with side lengths of approximately 0.45 to 0.67 mm were created for the symmetric profile used to generate the axisymmetric solid.

Numerical results were processed to create a true-stress versus effective plastic strain curve. This was accomplished by tracking the displacement of two nodes approximately 25.4 mm apart near the midpoint of the test specimen, which is representative of the measurements observed by the extensometer during experimental testing. Similarly, nodal force was tracked for the series of nodes to which motion was prescribed and a resultant force calculated based on geometry and symmetry, which represents the experimental load measurement observed. Overall, these results were used to perform a quantitative error analysis using equations (1) and (2), and an accumulated relative error

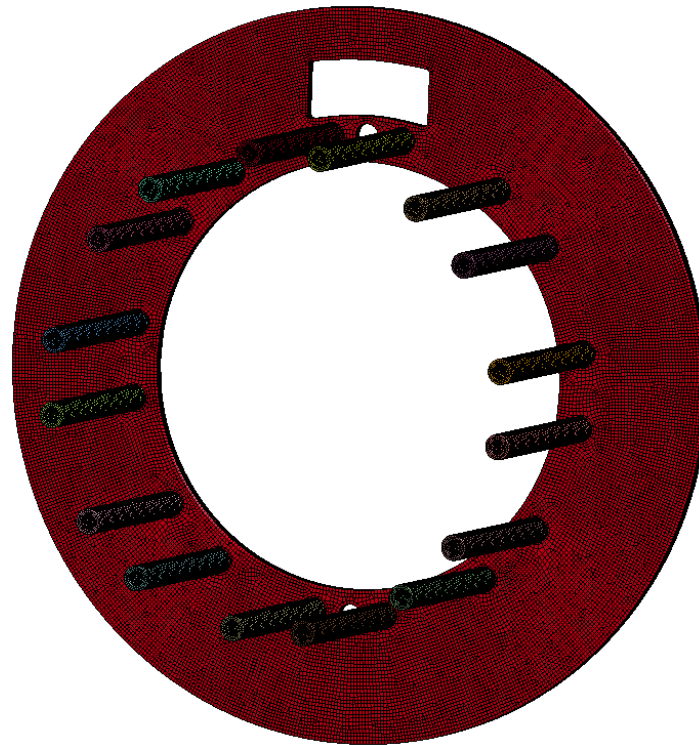
and a validation metric were determined to be 0.08 and 0.999, respectively. An illustration of the numerical test apparatus is presented in Appendix 9.3.3.

6.2.3 Safety Shield FE Model

The safety shield design was developed using computer modelling and finite element analysis techniques following similar methodology as the multi-piece wheel and tire models. Using LSTC's LS-PrePost and Hyperwork's Hypermesh, a finite element model was created using three dimensional elements for both the shield and tube nuts, as is shown in Figure 6.2.6. Complex geometry, such as minor radii, the hexagonal sides of the tube nut, and other finer details not critical to analysis were removed. The full shield consists of 12,581 solid elements and each tube nut consists of 783 elements, for a total of 12,528 for all 16 tube nuts. A constant stress solid element was used for all elements within this model for its computational efficiency, though this element type is susceptible to hourglassing: a nonphysical mode of deformation that can occur in under-integrated elements yet produce no stress. To combat this, a stiffness-based hourglass control, as well as hourglass energy tracking, was invoked for all simulations which involves applying artificial internal forces to resist hourglass mode deformation. A Flanagan-Belytschko stiffness form with exact volume integration for solid elements was implemented with an hourglass coefficient of 0.15.



(a)



(b)

Figure 6.2.6 - Finite element model of safety shield showing a) front and b) rear views.

The purpose of the model is to test the shield and associated mounting hardware under various conditions using virtual modelling, given the expense and complexity of fabricating physical prototypes. Additionally, great expense and difficulty would be associated with testing the shield when mounted on wheel assemblies or during in-field use, as well as the associated potential safety concerns. However, this can be easily performed virtually by combining the safety shield system with the validated tire and wheel model.

6.3 MODELLING OF SAFETY SHIELD PERFORMANCE

The virtual testing methodology is discussed in the subsequent sections, followed by quantitative and qualitative observations. All simulations were performed on a Dell Precision T7600 workstations equipped with dual Intel Xeon ES-2680 central processing units (CPUs) operating at 2.7 GHz with 8 cores each (16 total, 32 threads) and 64 gigabytes of ram. LS-DYNA revision 7, single precision, was used as the solver and operated in MPP (massively parallel processing) mode. Solutions do not employ mass scaling.

Prior to the construction of initial tire and wheel FE models, a mesh sensitivity study was successfully completed to determine a suitable level of mesh discretization as well as element size for multi-piece mining wheel assemblies [11]. These efforts involved a combination of experimental and numerical modelling efforts whereby a multi-piece mining wheel was similarly loaded under conditions as observed during rim base testing. Different levels of mesh discretization were invoked for the FE model of the multi-piece wheel assembly and a suitable mesh size was determined which illustrated convergence to predicted strain values at critical locations within an acceptable level of error of less

than 15%. Results of this previous work were used within the context of the present virtual modelling efforts which are discussed in the following sections.

6.3.1 ISO 7141 Impact Test

Since no standard testing procedures exist for the purposes of validating the design of multi-piece wheels, the ISO 7141 wheel impact test standard was applied. The testing procedure, as discussed in Section 2.4.1, was performed virtually using the validated five-piece 29.5-29 wheel assembly as well as with the shield installed for comparison purposes. Per the test standard, the wheel is mounted on a 13 degree angle from the horizontal plane and the striker is restrained to free-fall motion in the vertical direction. The test stand was omitted from the virtual model as were the natural rubber mounts; whose overall effects on the result of the test are believed to be negligible and since comparison between the safety shield-equipped wheel assembly and the standard assembly is all that is under consideration. The mounting flange of the wheel assembly was treated as a rigid material, restrained from motion or rotation in all directions.

Following the test standard, a steel striker with an impacting face of 375 mm (width) by 125 mm (length) was dropped from a height of 230 mm above the rim flange under free-fall conditions, with an attached mass proportional to the maximum static wheel loading. For the purposes of the simulation, a rigid striker with consistent dimensions was used; however, at a reduced height and with a modified density to be representative of the correct test mass. To determine the test mass, vehicle manufacturer specifications [50] provided by Musselwhite Mine were referenced, since specific wheel information was unavailable. Though the wheel is used on a variety of applications, specifications for a Caterpillar R2900G LHD (Load-Haul-Dump) vehicle were referenced as it was the

vehicle used to collect experimental observations and subsequently aided in the development of the tire model. Additionally, it has the highest gross axle weight rating (GAWR) of the vehicles tested. Given a GAWR of 50,220 kg, equation (4) was used to determine the mass of the striker per the ISO standard; where W is the maximum static wheel loading weight and presumed to be half of the GAWR:

$$\begin{aligned}\text{Mass of Striker} &= 0.6 * W + 180kg \\ &= 0.6 * (25,110) + 180 \\ &= 15248 kg\end{aligned}\tag{4}$$

Furthermore, during the simulation the tire inflation process was carried out to ensure realistic seating of the bead and engagement/pre-loading of wheel components. This was achieved by gradually increasing the internal surface pressure of the tire to the cold inflation pressure used on the test vehicle; 591 kPa, its standard operating pressure. Additionally, gravitational load was applied to the model.

To save computational time, the height of the striker from the wheel assembly was reduced and an initial velocity of 1421.6 mm/s and 1534.4 mm/s was prescribed for a standard wheel assembly and one equipped with the safety shield, respectively. Though both strikers were at approximately the same height at the start of the simulations and the first point of contact between the striker and wheel assembly is the tire sidewall region, the reason for the difference in initial velocities is due to how the initial 230 mm drop height is measured, that is, from the highest point of the rim flange. Since the shield effectively adds height to the flange, this increased the starting height from which the striker was dropped. As a result, the impact force on the shield is anticipated to be greater than that on the wheel flange due to the higher amount absorbed by the tire prior

to the striker contacting the flange. The initial height and velocity allows the tire to fully inflate prior to contact occurring.

Limitations inherent to the simulation are related to boundaries and constraints. A half-model was used given the symmetry indicative of the testing scenario to reduce computational requirements, so appropriate boundary constraints were applied on the plane of symmetry. A time step scaling factor of 0.9 was implemented and the total simulation time was 38 hours and 22 minutes for a standard wheel assembly and 46 hours and 45 minutes for the shield-equipped wheel assembly.

Lastly, the tubenut-wheel and tubenut-shield threaded connections were prescribed using fully constrained conditions applied at the corresponding nodes. Thus, they are assumed to remain engaged throughout loading and not be a mechanism of failure. This was consistent practice for all virtual testing configurations where the shield was installed, and the same assumption was made.

6.3.2 Simulated Tire Blowout Test

A critical aspect of the shield is to aid or completely prevent wheel components from becoming dangerous projectiles should failure occur. Since the mode of failure can vary greatly as discussed in the literature review of Section 2.3, the shield is also meant to retain wheel and tire components by creating a physical barrier to the outside environment.

The virtual blowout test was designed to be similar to an over-pressurization of the tire, though it could also apply to a failure of a component that maintains engagement of locking components and results in the outward motion of the bead, flange, and BS band. This allows for quantitative analysis of the amount of force and plastic deformation

experienced by the wheel components prior to their complete disengagement and before they become freed projectiles. The end point of the simulation was assumed to be when the lock ring became sufficiently disengaged and resulted in complete depressurization of the tire. Furthermore, qualitative observations were made to study how the wheel and safety shield deform, and to identify the location of high stress and plastic deformation. Scenarios with both the standard wheel assembly and one with the shield installed were simulated for comparison.

Since the area of interest is limited to the locking components of the wheel, the safety shield and the tube nuts, the majority of the tire was removed to reduce computational requirements. Given the geometry and design of the wheel and shield, the FE model was reduced to half of a wheel assembly based on symmetry, with appropriate constraints applied to the nodes located on the plane of symmetry. This includes restricting nodal displacement perpendicular to the plane of symmetry and restricting all nodal rotation other than perpendicular to the plane of symmetry.

To ensure the realistic application and transfer of force, the bead of the tire that was typically in contact with the rim base, bead seat band, and outer flange remained in the model. An added layer of solid elements were created on the inner part of the tire and modelled as a rigid material with a prescribed motion applied to simulate the blowing out of the tire. The main interest of the blowout simulation was the behaviour of the outer wheel components as this is generally the side exposed to the outside working environment and most associated with injuries. As such, only this side of the wheel was modelled. The virtual test apparatus is seen in Figure 6.3.1.

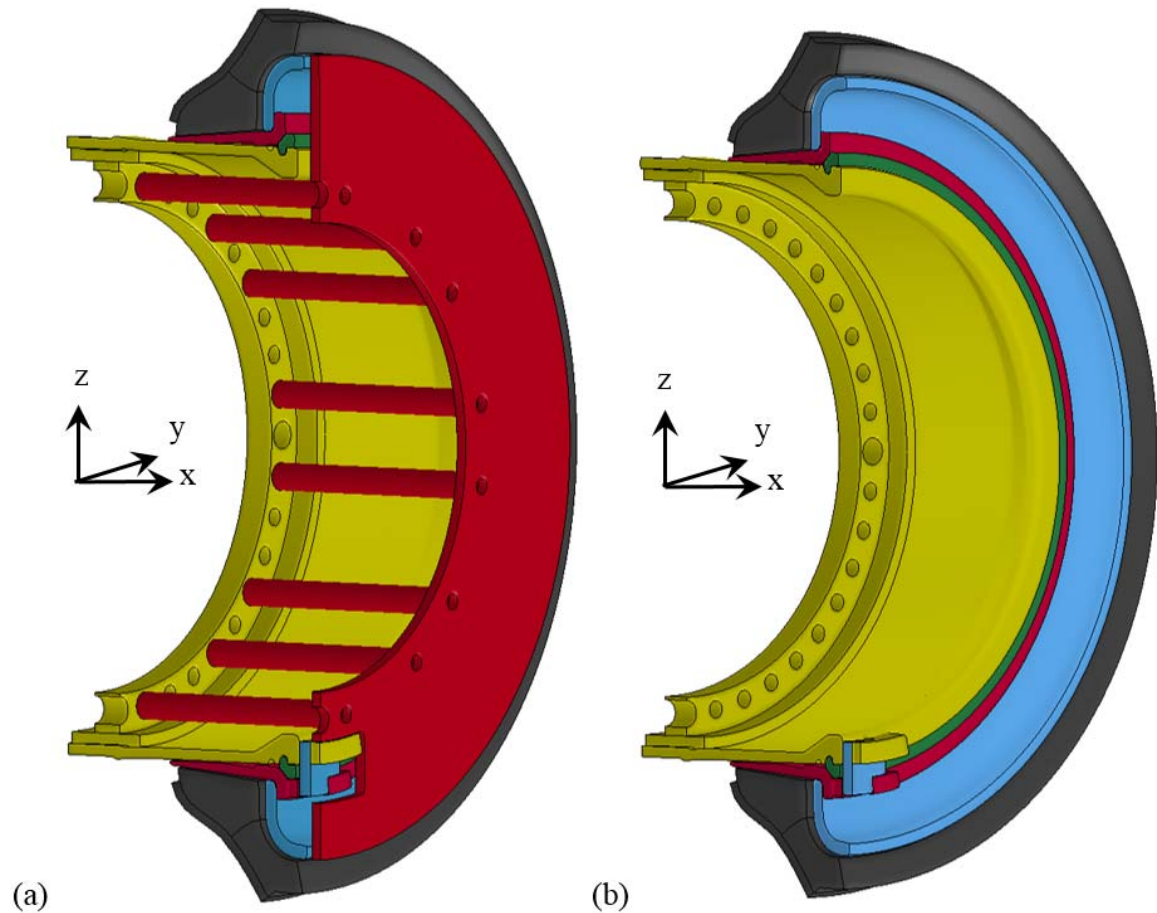


Figure 6.3.1- Virtual test apparatus for tire blowout simulations on a) shield-equipped and b) standard wheel assemblies.

A limitation of the simulation is that all component geometry and material properties were based on a new, unused wheel and did not take into account fatigue, degradation and/or deformation due to corrosion, impact and other wear. As such, it is acceptable to presume the resultant loads in the virtual blowout to be extreme and that a fatigued or damaged wheel would require less force to blowout.

Lastly, an important characteristic of the safety shield system that should also be considered, if the blowout is caused due to an over-pressurization, is the proposed over-pressurization blow-off valve, regardless if it is due to an external heat source, brake heat, tire overloading, or some other cause. Though its effect is not accounted for and as such

is considered another limitation of the virtual simulation, the blow-off valve is integrated within the safety shield system and would reduce the stored energy in the tire by releasing the inflation pressure in a controlled manner if the pressure exceeds a predetermined, overly high level. This in turn would result in some degree of a less severe blowout, if not preventing it entirely. An increase in pressure due to overloading or brake heat may result in a gradual increase that can be mitigated by the blow-off valve, whereas exposure to an external high heat source such as a fire may yield in a rapid increase and still result in a blowout.

6.3.3 Rotational Side Impact Virtual Test

Similar to the tire blowout simulation efforts, no standards exist that are indicative of the typical loading and impact situations experienced by multi-piece wheels in practice. Thus, based on experience gained from mine site surveys and experimental testing, a severe side-impact simulation that involved both rotation of the wheel and overall translation was created. This is meant to be representative of a mining vehicle rubbing and impacting the wall of a mine during in-field operation.

The virtual model included the validated full wheel assembly with elastic/plastic material properties consistent with those presented in Section 6.2.2. Virtual testing considered both a standard wheel assembly and one equipped with the safety shield system. Similar to both the ISO7141 and tire blowout virtual tests, the wheel mounting flange is modelled as a rigid material - which is a reasonable approximation since it would be mounted to a highly stiff vehicle axle in practice - and a rigid wall was created under the wheel assembly as a driving surface. The simulation progressed through subsequent steps depicting realistic loading conditions. Initially, a gravitational load was

applied followed by the wheel being inflated to 591 kPa, by gradually increasing the internal surface pressure of the tire. The wheel assembly was then vertically loaded with the equivalent of the static corner weight of the vehicle. This was accomplished in the model by creating a set of solid elements representative of the vehicle axle and constraining them the wheel's mounting flange, then applying the static load to the center node of these elements. Overall, this was done to have a consistent load path representative of the vehicle loading the wheel assembly and also provides a visual aid that acts as a reference point in simulations showing loading, translation, and rotation of the assembly.

A solid element, rigid object consisting with approximate dimensions of 155 mm by 125 mm by 40 mm was modelled to represent a rock face that makes contact with the wheel assembly. The profile of the striker is presented in Figure 6.3.2 (a) through (c).

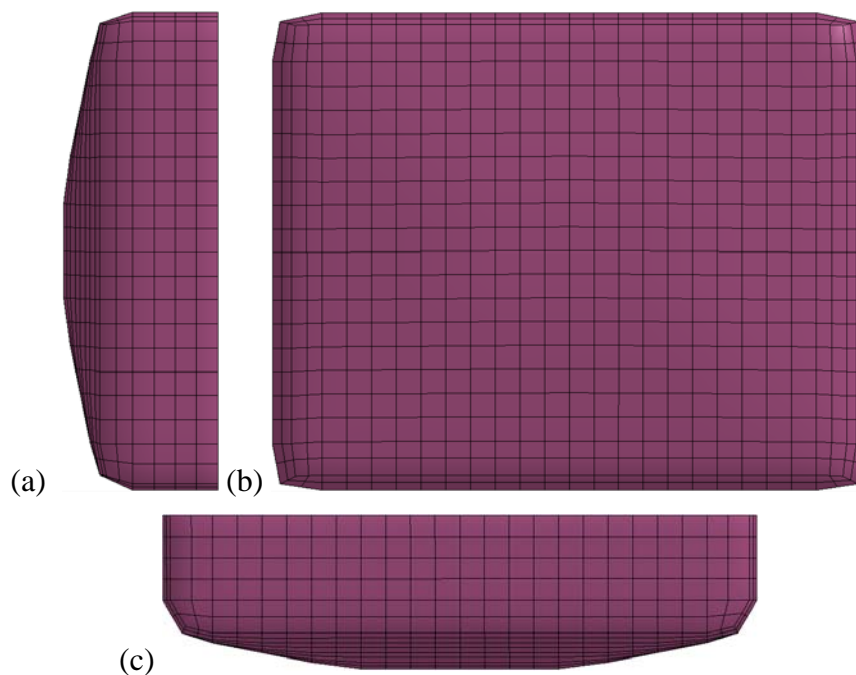


Figure 6.3.2 - (a) Side, (b) front and (c) top profile of rotational side impact virtual test striker.

In practice, the vehicle would traverse an underground mine and occasionally turn into and rub the wall of the mine. For simplification purposes, the model simulated the striker impeding the wheel assembly at its outermost radius by 20 mm. Similar to the ISO 7141 simulations, where the drop height of the striker was a set distance from the edge of the wheel and adjusted higher when the shield is installed, the global position of the striker was adjusted to maintain the 20 mm impact distance; though the contact point varied depending on whether or not the shield system is installed. The wheel assembly then rotated along its own centre axis while constrained to the virtual, horizontally translating axle and the simulation ends once the striker is no longer in contact with any wheel components and only the tire. This was achieved in the model by constraining the virtual axle to the mounting flange as a cylindrical joint, then prescribing translational and rotational motion to the virtual axle. Overall, this represents the vehicle being driven forward at an equivalent velocity of 10 kph. A cross-section of the virtual testing apparatus is shown in Figure 6.3.3.

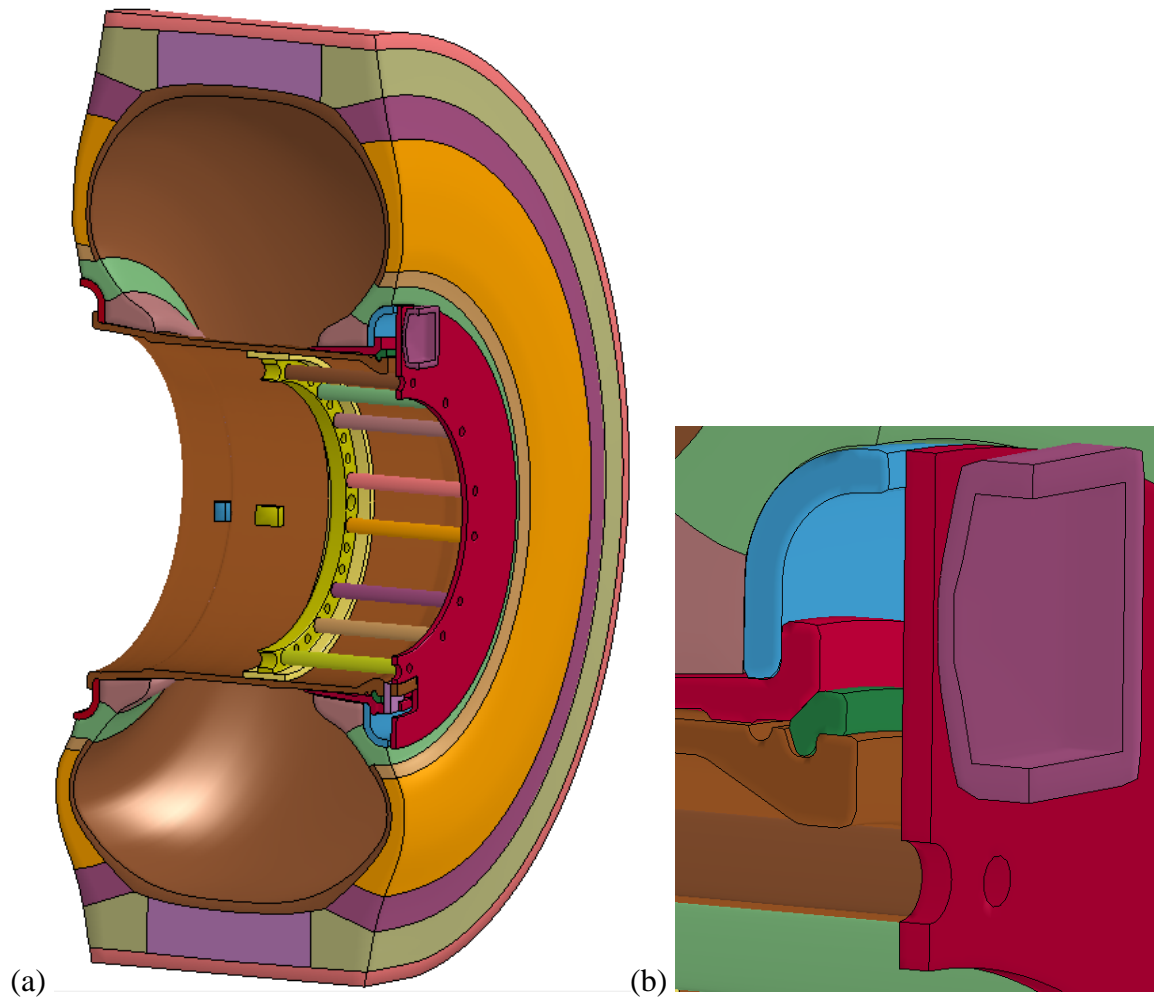


Figure 6.3.3 – a) Cross-section of rotational side impact virtual testing apparatus and b) an enlarged view of the striker to wheel contact area.

6.4 NUMERICAL RESULTS AND QUALITATIVE OBSERVATIONS

6.4.1 ISO 7141 Impact Testing Observations

The ISO 7141 virtual simulations performed were the only testing condition directly based on an industrial standard, though this standard is meant to be applied to passenger vehicle wheels. Overall both testing configurations, with and without the shield installed, pass the failure criteria of the standard such that none of the following are predicted to occur: visible fracture(s) penetrating through a section of the centre member of the wheel

assembly, separation of the centre member from the rim, nor a total loss of air pressure within 1 minute. However, quantitative and qualitative observations demonstrate the advantage of having the safety shield system installed. The figures below illustrate a cross-sectional view of the final resting place of the striker against the wheel assembly post-impact.

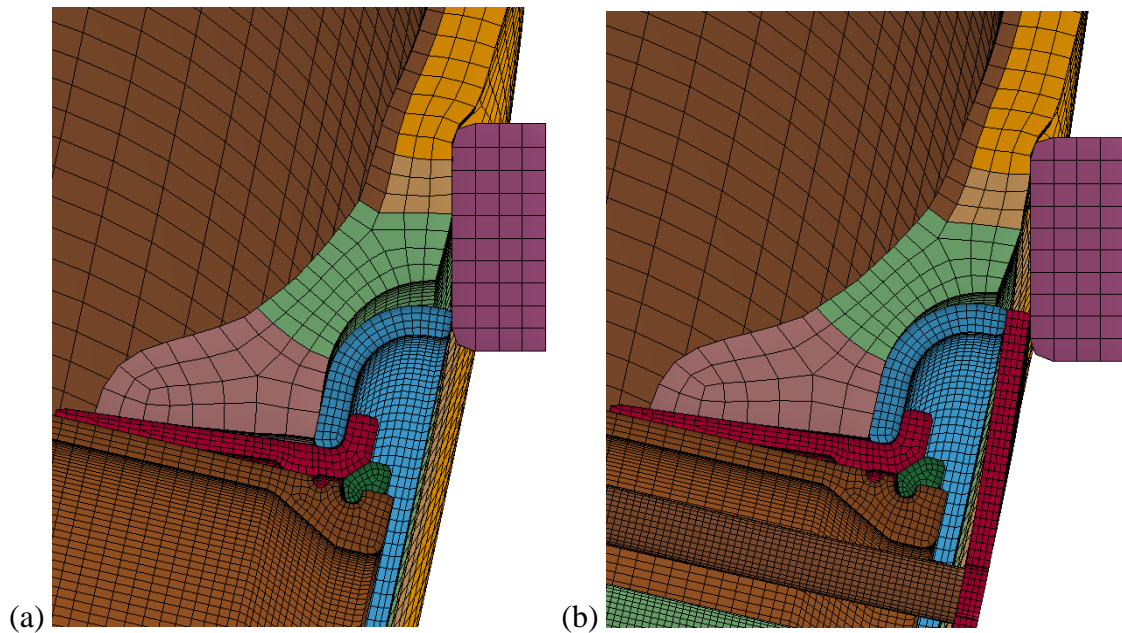


Figure 6.4.1 - ISO7141 virtual test observations for a) standard wheel assembly and b) assembly equipped with safety shield system.

Qualitative examination of the simulation results suggests the impact of the striker is not overly severe, nor would excessive deflection of the wheel assembly or its components be predicted. All locking components of the wheel remain engaged and since negligible movement of the bead seat band and lock ring was observed, there is no reason to believe the O-ring would be significantly disturbed; nor should any loss of air pressure be expected. However, the benefit of the safety shield is evident in that tire deflection and separation from the outer flange is reduced when the wheel is equipped

with a safety shield. With no shield installed, the tire bead is pulled away from the outer flange at its outside edge by approximately 14.15 mm compared to only 6.12 mm when the shield is used. This is despite the higher level of impact force due to the nature of the ISO 7141 test requiring a higher starting height of the striker when the shield is in place, which is represented by a higher initial velocity in the simulation (1534.4 mm/s versus 1421.6 mm/s) and resulted in a peak load approximately 11 kN higher transmitted by the striker. This is seen in Figure 6.4.2 showing the resultant contact force of the striker to the wheel assembly.

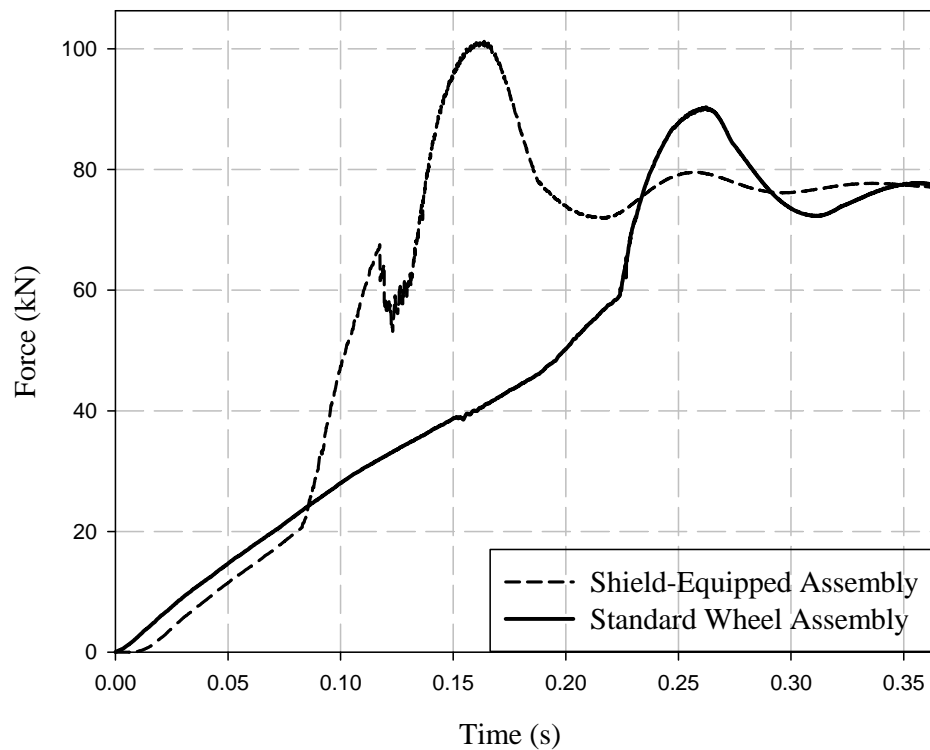


Figure 6.4.2 - Resultant contact force of striker during ISO 7141 impact simulation.

Though failure or loss of pressure does not occur under the testing parameters of the ISO 7141 standard, should a heavier test mass or different geometry striker be used the rationale exists to suggest air pressure would be lost and the subsequent inability of

locking wheel components to maintain engagement would follow earlier or under less severe conditions without the use of the safety shield. Additionally, though not called for by the test standard, through repeated similar style impacts the shield would deform and eventually fatigue as a result of the impact. The shield protects for this as it is considered a consumable resource that is easily replaceable, whereas degradation of the wheel components results in safety concerns.

An important parameter to consider is the ability of the wheel components to maintain proper engagement and, assuming structural integrity of locking components is upheld, the mechanism related to this is the contact force applied to the lock ring. For comparison purposes, the resultant contact force is examined for the contact property between the lock ring and bead seat band, which approximately equals that of the lock ring and rim base (the lock ring's other mating surface). Through study of simulation results, it is observed that the force transmitted to the outer flange most directly affects the contact force of the lock ring and thus its ability to maintain engagement. During the simulation, the striker initially hits the tire resulting in its deformation, then either makes contact with the outer flange or the shield, if so equipped, then springs back due to the absorption of energy through the tire, and finally comes to rest. With the shield installed, the striker first hits the shield which then deflects at its outer edge until it contacts the outer flange, which occurs at an earlier time than if it was not present. However, as seen in Figure 6.4.3, the test condition with the shield installed consistently maintains a higher contact force by approximately 4.5% (178 kN vs. 170 kN).

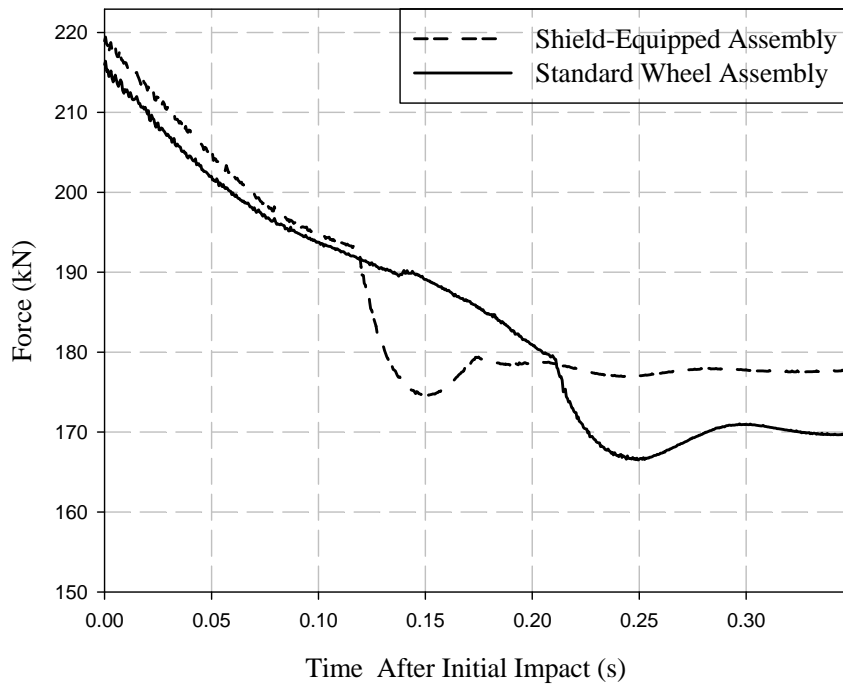


Figure 6.4.3 - Lock ring resultant contact force during ISO 7141 impact simulation.

Quantitative analysis of the simulations show that for a traditional wheel assembly the highest level of effective plastic strain is found in the centre of the outer flange, where the striker makes contact, with a value of approximately 1.54×10^{-3} (mm/mm). As one would expect, the advantage of equipping the wheel with the shield is a reduction in the effective plastic strain in the outer flange by more than an order of magnitude (1.26×10^{-4} mm/mm) or approximately 92%. However, an overall maximum value was significantly higher and located in the same general region as a standard wheel assembly, but on the shield versus the outer flange. A maximum value of 1.8×10^{-1} (mm/mm) was observed as well as visible deformation, as seen in the figures below.

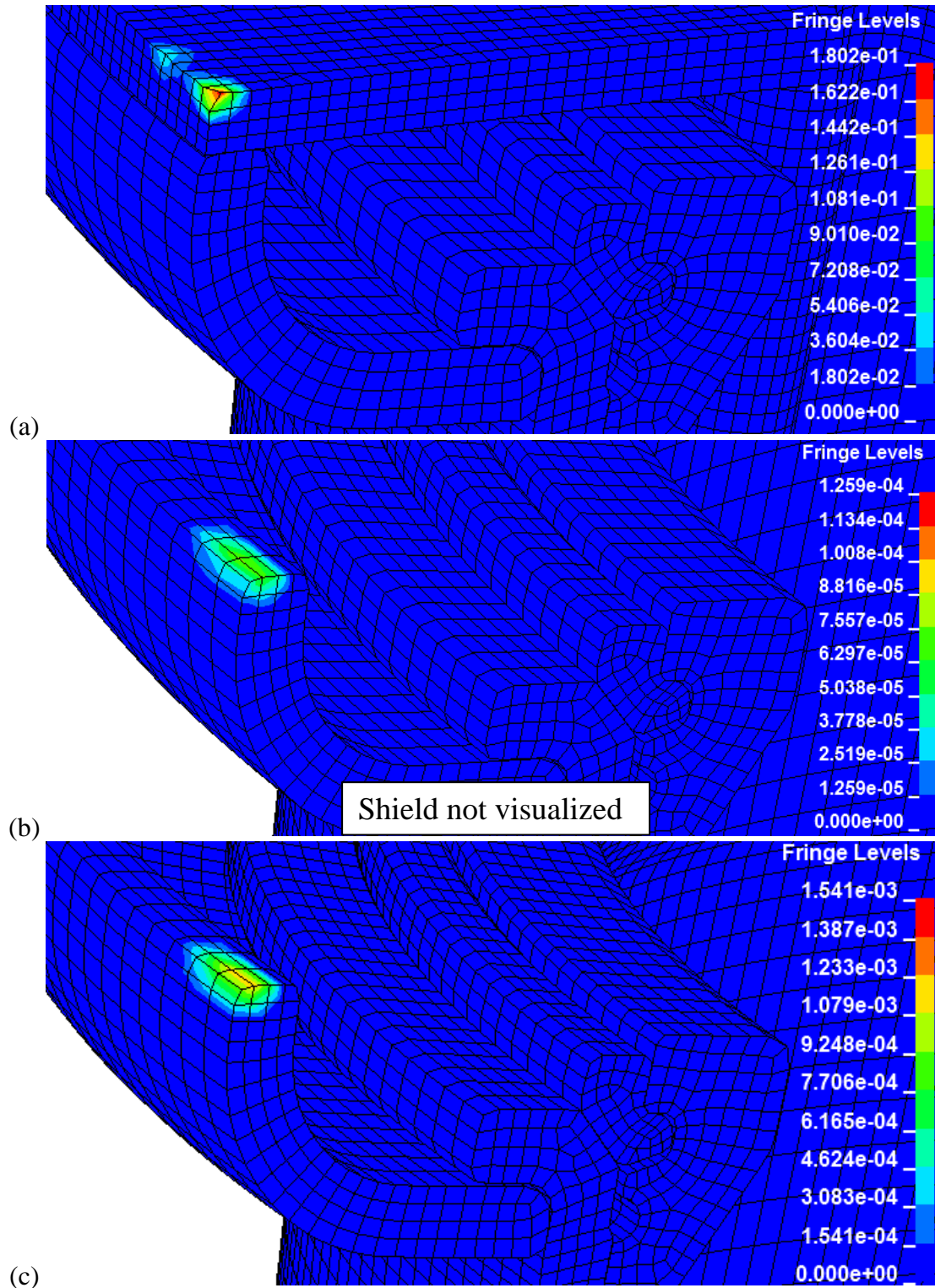


Figure 6.4.4 - Resultant effective plastic strain (mm/mm) for ISO 7141 test for the a) shield-equipped wheel and its b) outer flange with the shield not visualized, as well as c) the outer flange of the standard wheel.

A similar relationship is observed when considering von Mises stress as seen in Figure 6.4.5 (a) through (d).

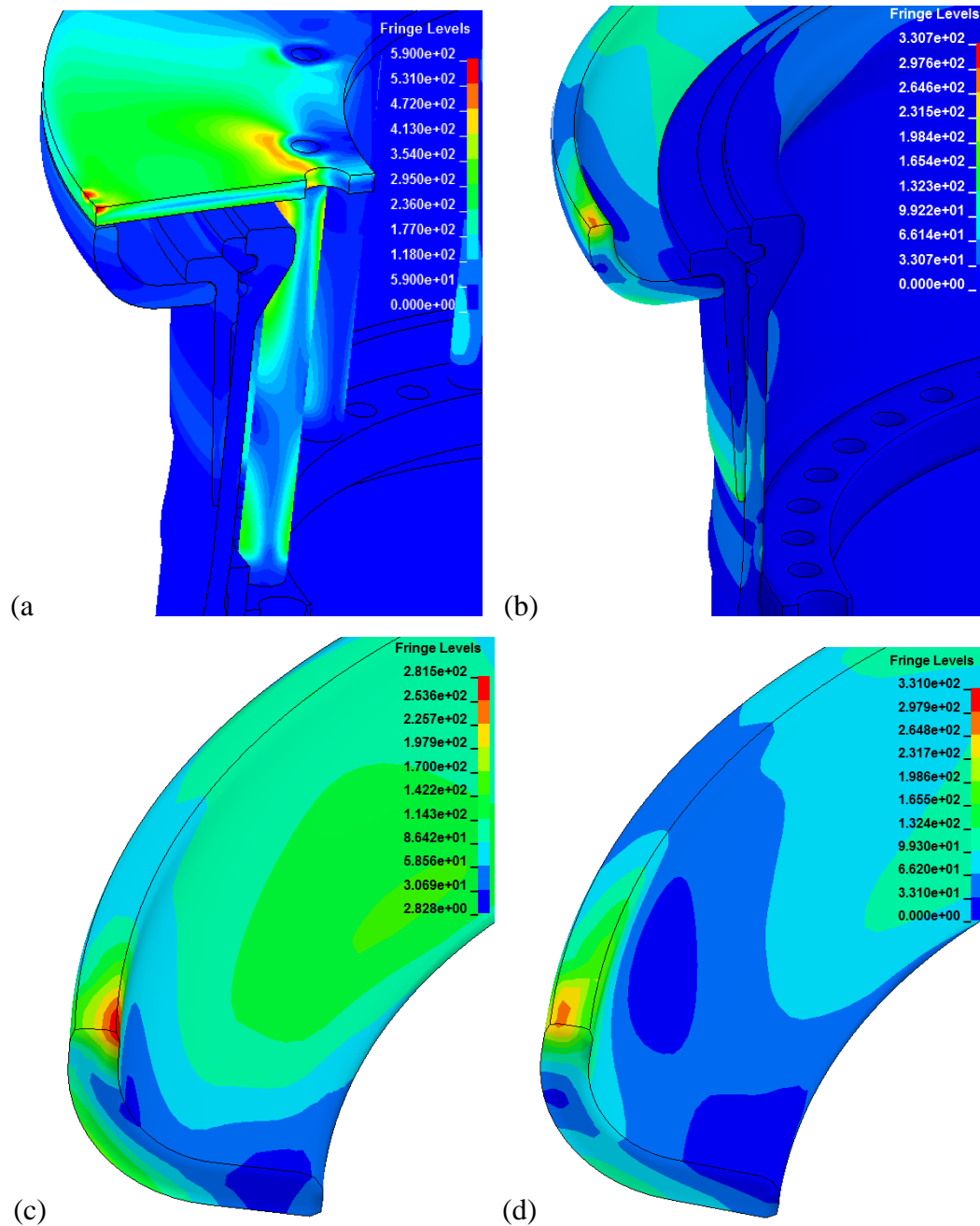


Figure 6.4.5 - Various views showing contours of effective von Mises stress for both the safety shield equipped (a, c) and standard (b, d) wheel assemblies when maximum values were observed during ISO 7141 test (in MPa).

Maximum von Mises stress levels were located in the same region as maximum effective plastic strain and similarly when equipped with the safety shield a reduction of stress levels in the outer flange by approximately 15% was observed, though overall impact force is higher. With no shield installed, a von Mises stress of 330 MPa maximum was observed in the outer flange compared to a von Mises stress of 281 MPa in the same region when equipped with the shield, while an overall peak in excess of 600 MPa is observed in the shield itself.

Energy balance analysis of simulation results show negligible hourglass energy and positive sliding interface energy throughout, as well as appropriate levels of external work and kinetic, internal, and total energies as would be expected. For the purposes of brevity, the following plots illustrate energy responses of a shield-equipped wheel assembly; however, similar verification and analysis was completed for each configuration (shield-equipped and standard wheel) and for each virtual testing method (ISO 7141, tire blowout, and rotational side impact).

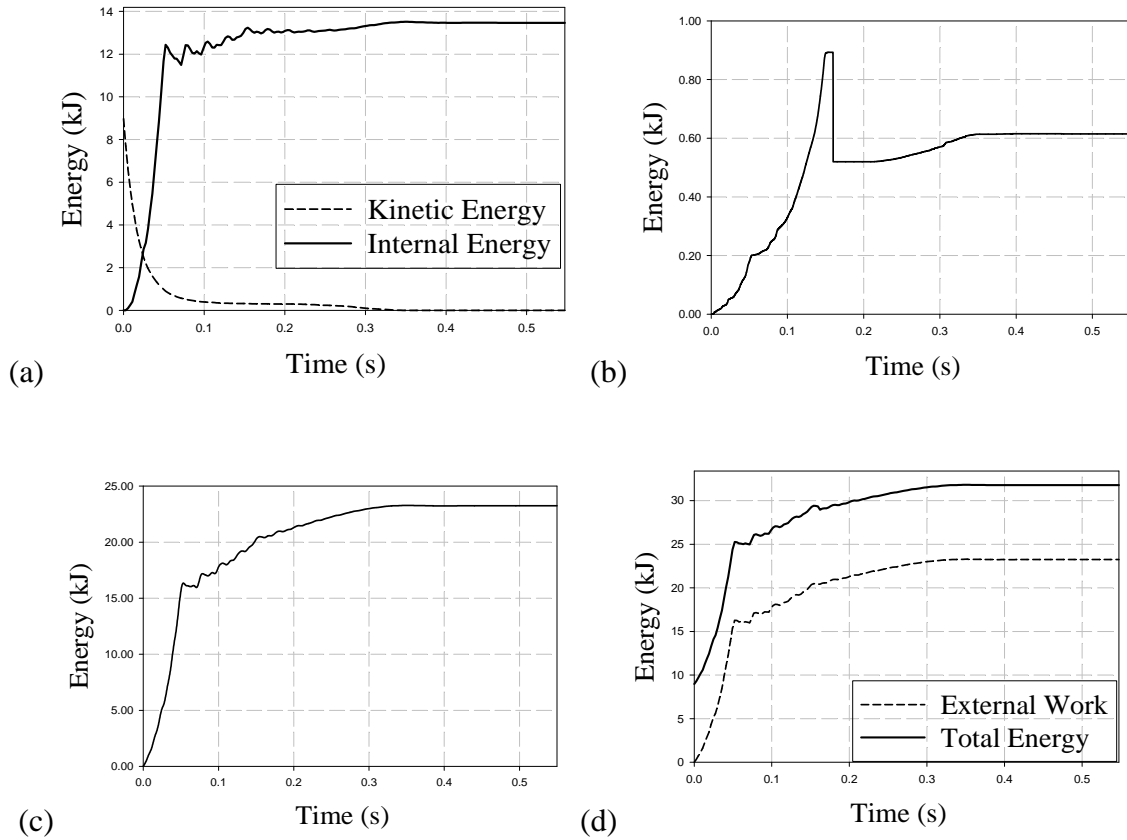


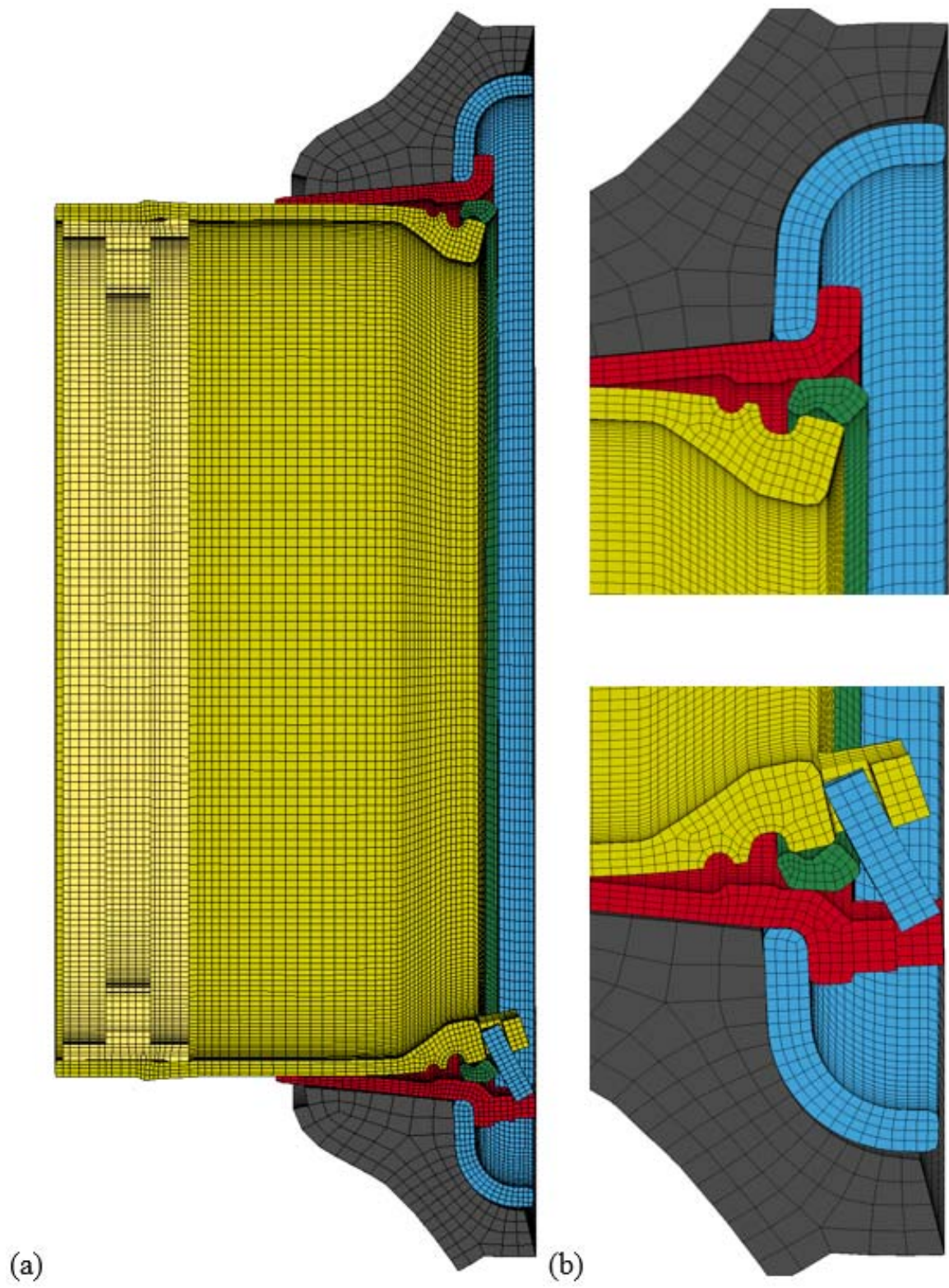
Figure 6.4.6 - Shield-equipped ISO 7141 test energy responses showing a) kinetic and internal energy, b) sliding interface energy, c) hourglass energy, and d) external work and total energy.

Note that at 0.15 seconds, the time-scaled inflation process of the tire is complete and a contact property between the tire and a dummy flange is terminated resulting in the sudden drop in sliding interface energy. Furthermore, the total energy is non-zero due to the inflation of the tire which is simulated by an applied surface pressure to the inside of the tire as previously described.

6.4.2 Simulated Tire Blowout Observations

To fairly evaluate the effectiveness of the safety shield system when undergoing the simulated tire blowout, a common failure criterion is set for both wheel configurations such that the point of failure is prescribed to occur when the lock ring becomes fully dislodged from the gutter section. This determination is based on the notion that once such dislodgement occurs, outer wheel components have no mechanism to remain affixed to the wheel and can become free projectiles that pose a hazard to the surrounding environment. From review of incident reports, such a failure mode is both very common and highly dangerous. Furthermore, once this point is reached there is essentially no mechanism to maintain inflation pressure and a rapid release of air would be expected as well as the elimination of the tires' load carrying capacity, thus resulting in major, unpredictable deformation.

Through comparison between observations of the standard and shield-equipped wheel assemblies undergoing the virtual blowout test, an obvious and significant advantage inherent to the design of the safety shield is presented immediately; though tire blowout occurs and wheel components become dislodged, they remain fully contained by the shield. Figures 6.4.7 (a) through (d) illustrate the deformation of wheel components at the prescribed point of failure.



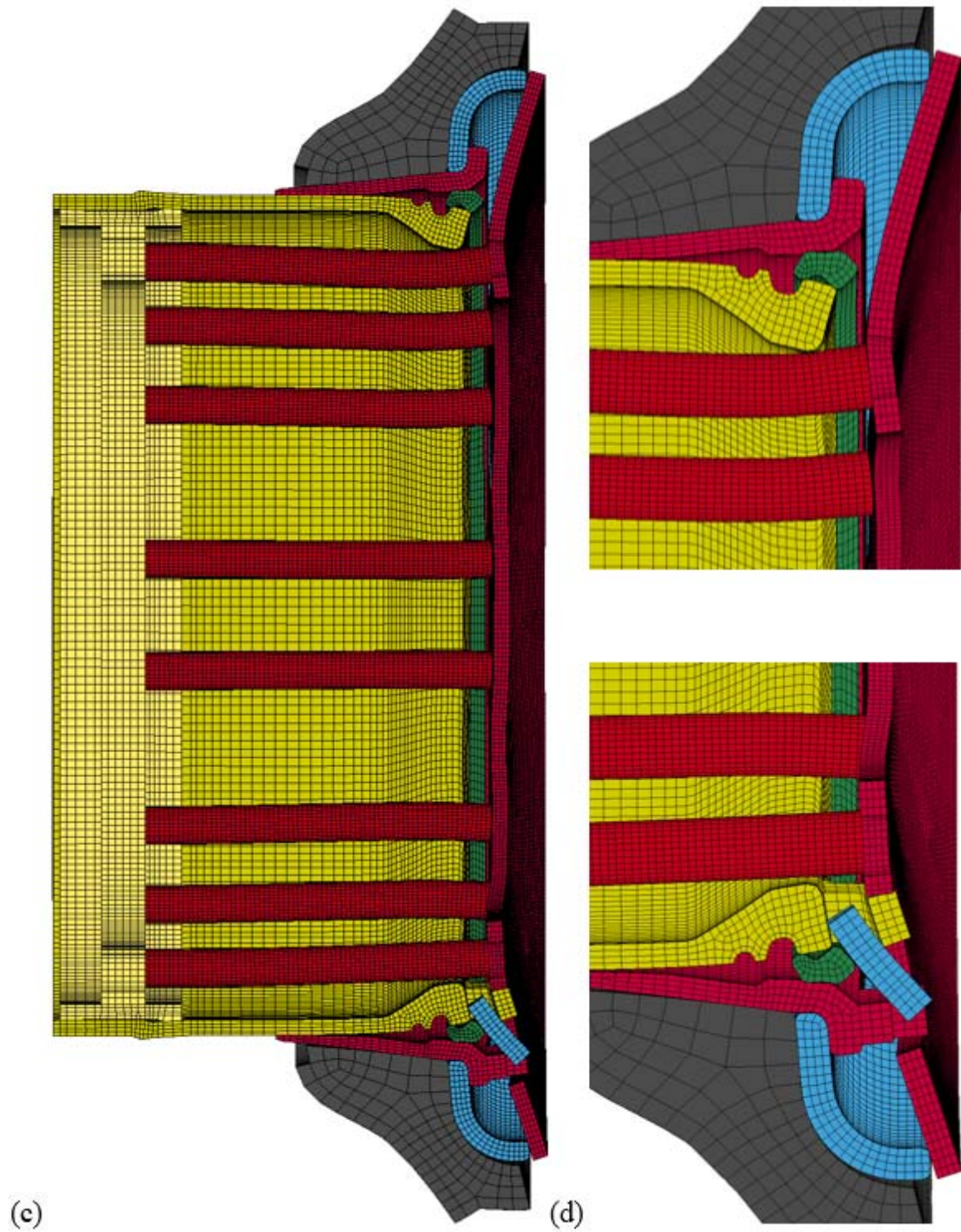


Figure 6.4.7 – Cross-sectional view of tire blowout simulation deformed geometry for a a) standard wheel assembly and b) a close up of its flange and lock ring areas, as well as c) a shield-equipped wheel assembly and d) a close up of its flange and lock ring areas.

Qualitative analysis of the wheel deformation reveals interesting observations and advantages when equipping the wheel assembly with the safety shield. On the standard wheel, the lock ring first slipped out of the gutter region on the non-lock key side (shown at the top in the preceding figures) and then dislodgement propagates around the circumference of the wheel. This is expected as the lock key is an added mechanism to retain components and aid in preventing failure. However, in the shield-equipped simulation, at least partial engagement is maintained longer and dislodgement occurs first in the lock key region. To reach the prescribed point of failure, the tire bead moves outward approximately an additional 9 mm prior to full dislodgement of the lock ring when equipped with the safety shield. Furthermore, analysis of the contact force between the bead and wheel components - which is all cumulative force input into the wheel during a blowout - shows the shield-equipped wheel experiences approximately 38% higher maximum contact force; approximately 5520 kN compared to 3440 kN for a shield-equipped wheel versus a standard wheel assembly, respectively. This demonstrates a significant increase in engagement capability under extreme loading conditions.

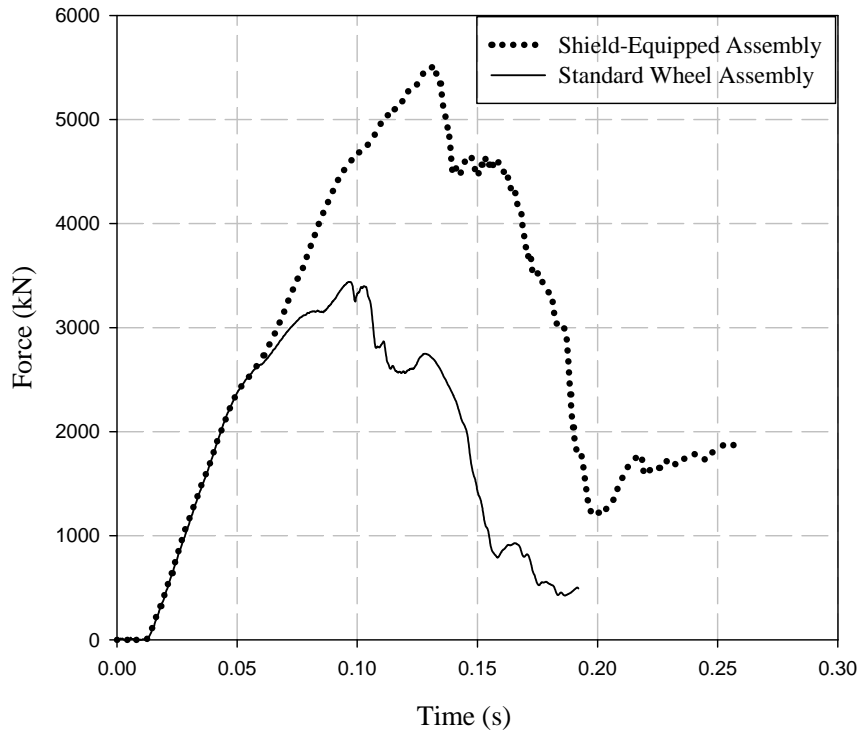


Figure 6.4.8 - Tire to wheel resultant contact force during tire blowout test prior to failure occurring.

Similarly, the resultant contact force of the lock ring is examined and presented in Figure 6.4.9. In the ISO 7141 simulations, a higher contact force indicates that engagement force is better maintained, and thus a greater degree of performance resulted under realistic impact conditions. On the contrary, the nature of the blowout test ensures failure will occur given extreme applied forces that result in plastic deformation. In this case, study of the lock ring contact force is of interest as it provides insight into the load path during a blowout.

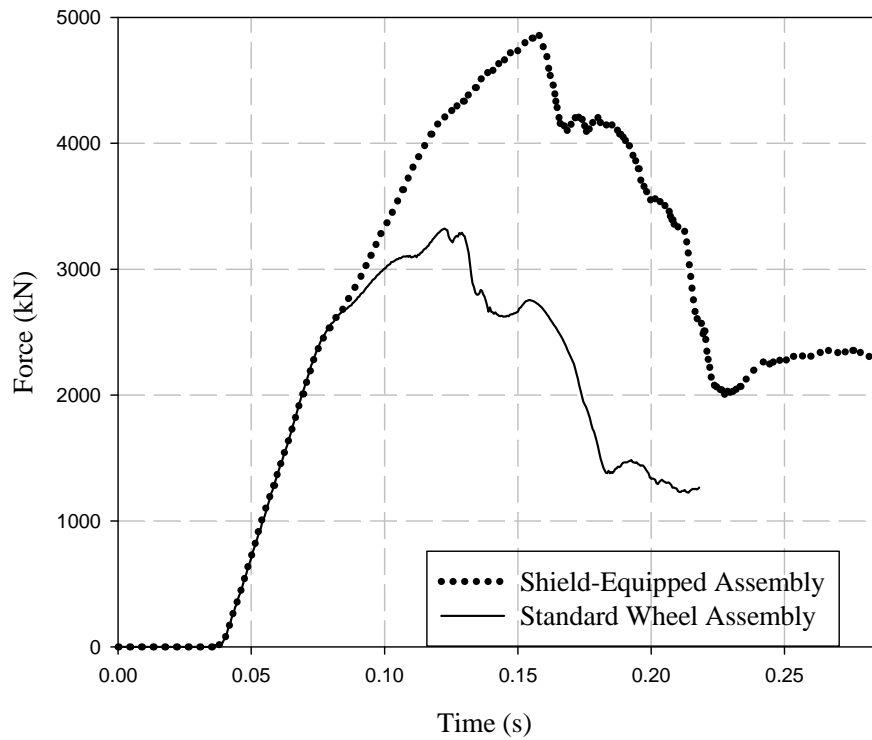


Figure 6.4.9 - Lock ring resultant contact force during tire blowout simulation.

For example, when comparing maximum tire input force to lock ring contact force in a standard wheel assembly, it is observed that a maximum value of 3440 kN yields 3330 kN of contact force in the lock ring, or a transfer of force at a ratio of approximately 97% through the lock ring. Similarly, if considering a shield-equipped wheel, an input contact force of 5520 kN yields only 4860 kN of force through the lock ring, or approximately 88%. Not only is a higher force observed prior to failure as mentioned previously, but the 9% reduction of force being transferred at peak loads through the lock ring suggests a measure of the shield's ability to aid in maintaining wheel component engagement.

When considering wheel components specifically, maximum levels of effective plastic strain are found in the lock ring for both test scenarios, as seen in Figure 6.4.10 below, with smaller regions of localized plastic strain in other areas.

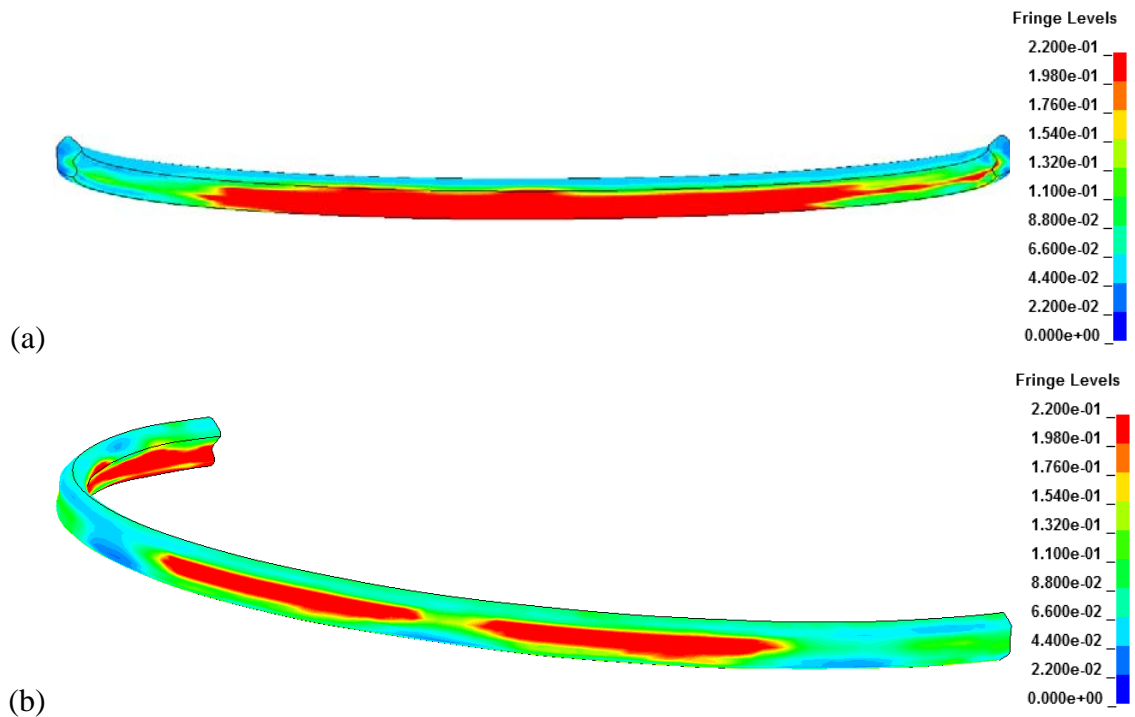


Figure 6.4.10 - Contours of effective plastic strain (mm/mm) in lock rings at failure during tire blowout simulation for a) a standard wheel and b) a shield-equipped wheel assembly.

For a traditional wheel assembly, maximum effective plastic strain is observed to be near the mid-span of the wheel and on the interior surface of the lock ring, with a peak predicted value of 1.70 mm/mm at the point the simulation reaches wheel engagement failure, indicating material rupture will most likely occur. The shield-equipped wheel experiences a predicted maximum effective plastic strain of 1.36 mm/mm on the outer surface of the lock ring and closer to the top of the wheel, once again predicting material failure will most likely occur. Despite the overall higher input force for a shield-equipped wheel, maximum effective plastic strain is 20.3% lower in the lock ring. When

examining effective plastic strain in the shield itself, regions near each of the tube nut fastened connections are observed; however, a maximum value is found near the underside of the lock key region, as illustrated in Figures 6.4.11 (a) and (b). A similar comparison of von Mises stress can be seen in the Figure 6.4.12.

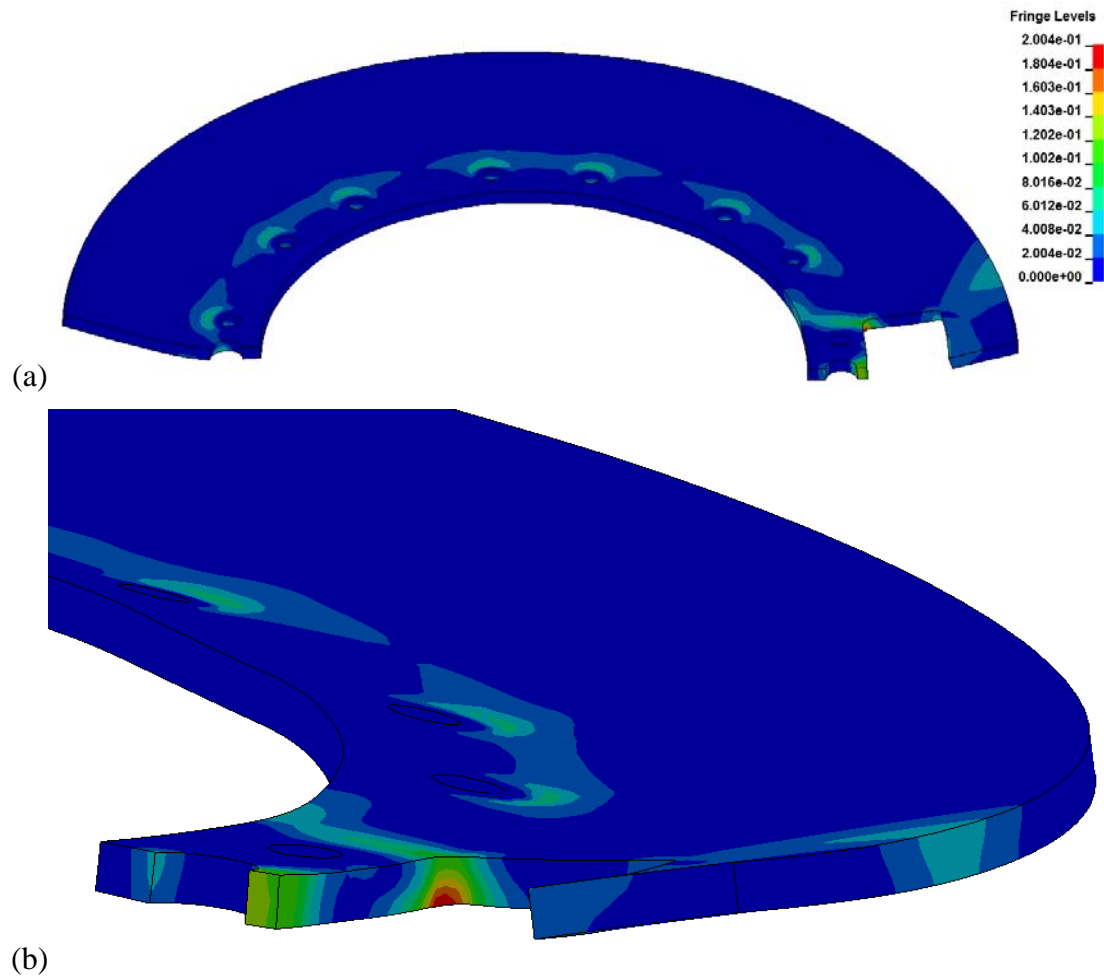


Figure 6.4.11 – Effective plastic strain contours as observed during the blowout simulation for the overall a) shield and b) near the lock key region of the wheel where the maximum value observed.

6.4.3 Rotational Side Impact Virtual Testing Observations

Though overall the testing condition is not identical to real-world impacts, it is designed to be representative and more importantly, provide a basis for fair comparison between wheel configurations to examine their performance and deformation characteristics. Through qualitative and quantitative analyses of simulation results, performance of the standard and shield-equipped wheel assemblies are compared to measure the effectiveness of the safety shield system at two points in the simulation: 1) when the striker initially reaches full impact depth, and 2) during rotation and forward translation of the wheel assemblies.

Figure 6.4.12 illustrates a cross-sectional view of the deformed geometry at full striker impact for both wheel configurations.

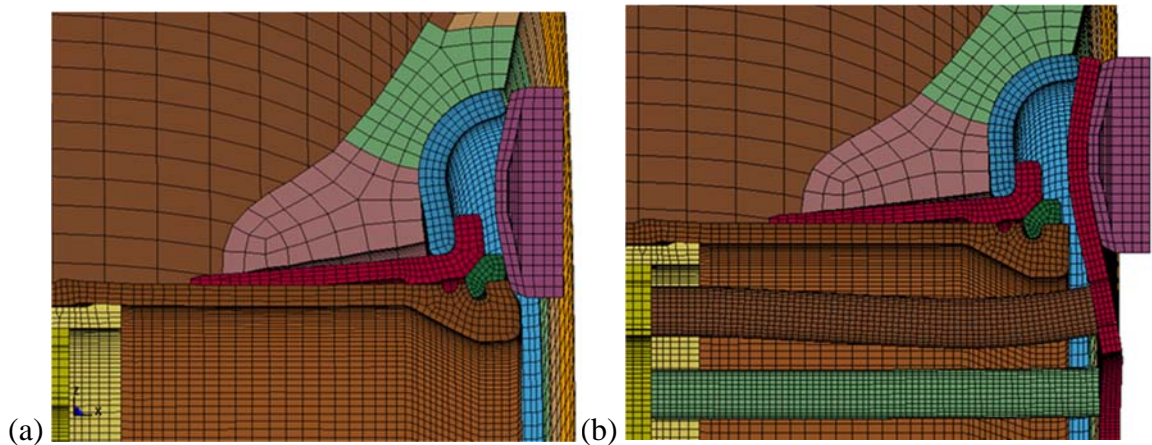


Figure 6.4.12 – Cross-sectional view of deformed geometry at full striker impact during rotational side impact virtual test for a) standard and b) shield-equipped wheel assembly.

Qualitative review of the simulation results show the outer flange's edge is displaced inward by 6 mm for the shield-equipped wheel and 22 mm for the standard wheel at maximum striker impact depth. Furthermore, with the shield installed, no contact or deflection in the lock ring or rim base with the striker or shield is observed though the

tube nuts contact the interior surface of the rim base. Additionally, overall deformation of the outer flange is significantly less at the end of the simulation for the shield-equipped wheel, which can be compared quantitatively through stress and strain analyses as follows. Figures 6.4.13 (a) through (c) illustrate the cross-sectional view of von Mises stress contours for both wheel configurations at full striker impact depth.

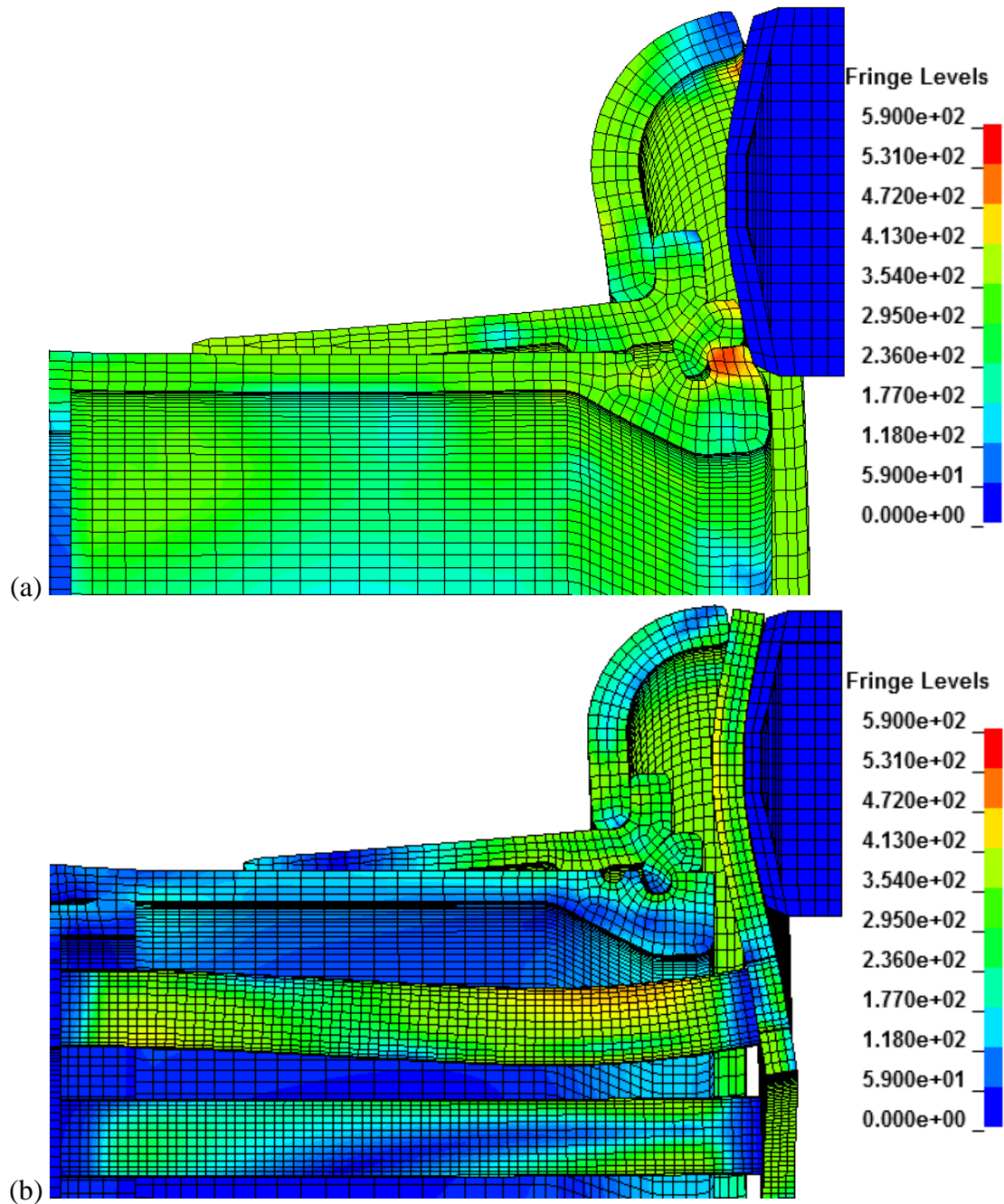


Figure 6.4.13 – Contours of von Mises stress (in units of MPa) at full striker impact depth for a) standard and b) shield-equipped wheel assembly.

In the shield-equipped assembly and at full striker impact depth, maximum von Mises stress was located in the top two tube nuts with values of approximately 490 MPa. When considering only the main wheel components, maximum von Mises stress levels are

located in the rim base (598 MPa) and bead seat band (381 MPa) for the standard and shield-equipped wheels, respectively; representing a difference of 36.2% in main wheel components and 18.1% for overall maximum values. Similar relationships exist when comparing maximum effective plastic strain for the same point in time, as shown in Figures 6.4.14 (a) through (d).

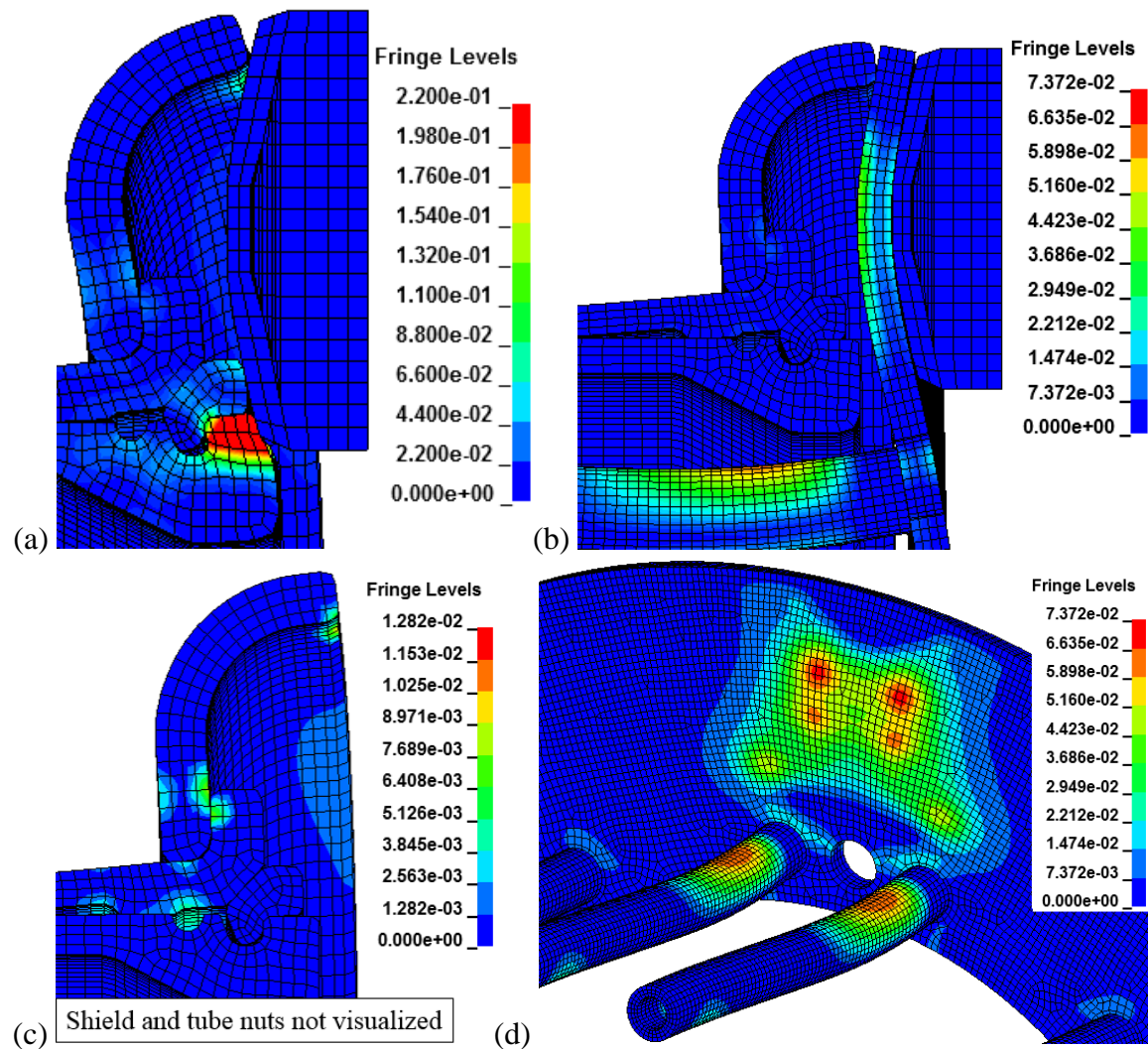


Figure 6.4.14 - Contours of effective plastic strain at full striker impact depth for a) standard and b) shield-equipped wheel assembly, as well as the c) shield-equipped assembly with no shield or tube nuts visualized and d) only the shield and tube nuts.

At full striker impact depth, maximum effective plastic strain in the shield-equipped assembly was located in the shield with a value of 7.37×10^{-2} mm/mm; though high values in the same region of the tube nut where maximum von Mises stress was previously observed were found (6.67×10^{-2} mm/mm). Considering only the main wheel components, maximum effective plastic strain levels are located in the bead seat band (1.28×10^{-2} mm/mm) for a shield-equipped wheel; however, the maximum for a standard wheel is found in the rim base and at levels in excess of 0.3 mm/mm. Overall, this represents a difference of 75.8% when comparing overall maximum values, and 95.8% if considering only main wheel components.

Examining von Mises stresses, effective plastic strains, and general deformation at the initial point of maximum striker impact are pertinent as they reflect a sudden dynamic load to the wheel assembly. However, overall maximum von Mises stresses and effective plastic strain values were observed in the outer flanges of both the standard and shield-equipped wheel assemblies once they begin forward rotational motion, representing vehicle operation as it traverses its environment. A similar comparison as previously performed was repeated for the point in time when these maximum values were observed, considering only the outer flanges. Figure 6.4.15 (a) and (b) and Figure 6.4.16 (a) and (b) illustrate contours of von Mises stress and effective plastic strain, respectively, for this point in the simulation.

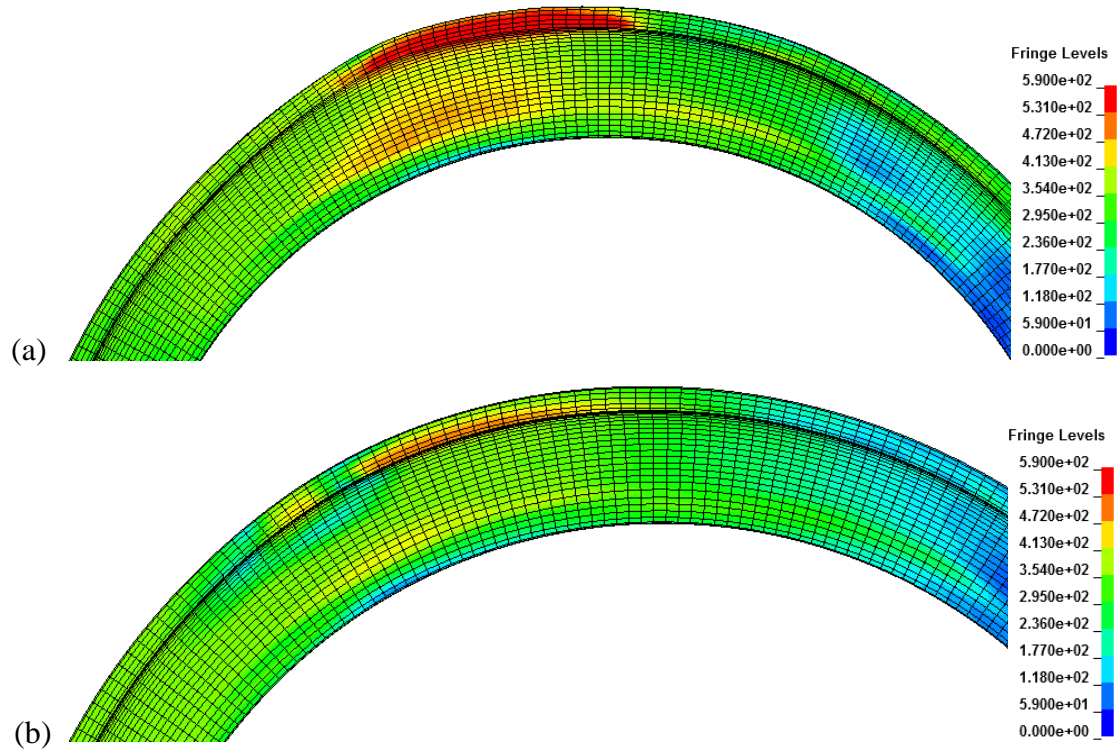


Figure 6.4.15 - Contours of von Mises stress in the outer flanges when overall maximum values were observed for both a) standard and b) shield-equipped wheel assemblies.

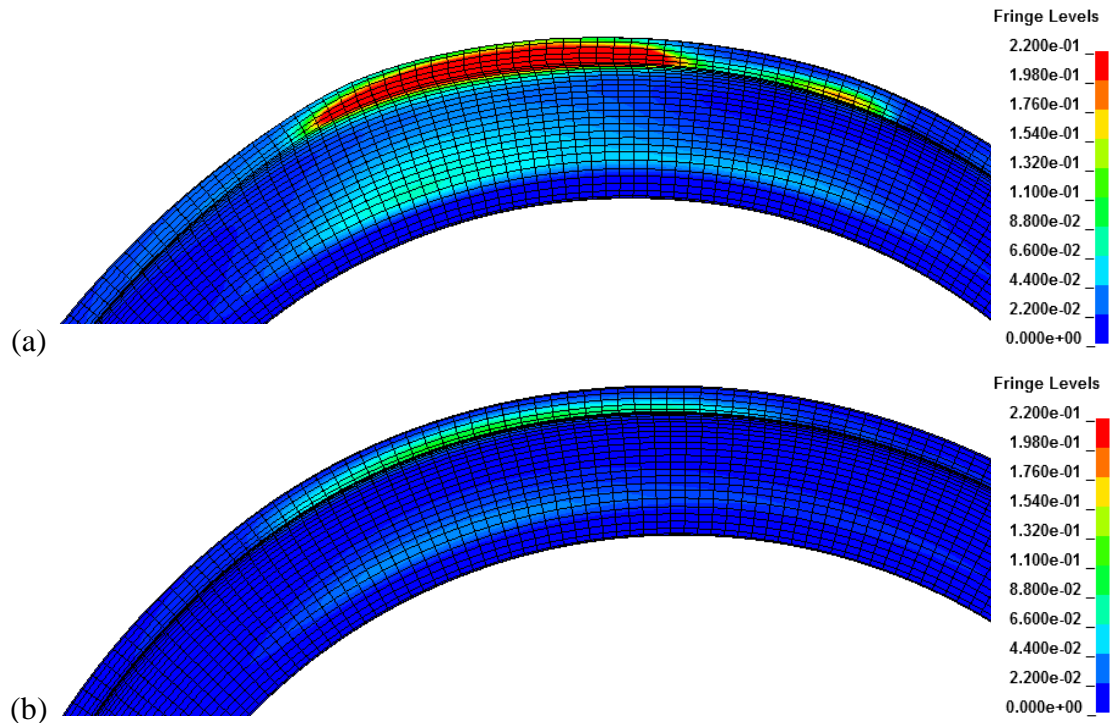


Figure 6.4.16 - Contours of effective plastic strain in the outer flanges when overall maximum values were observed for both a) standard and b) shield-equipped wheel assemblies.

Overall maximum values of von Mises stress and effective plastic strain were significantly higher in a standard wheel compared to a shield-equipped wheel. Values approximately 55% higher were observed for von Mises stress and effective plastic strains were an order of magnitude higher. Based on these observed values, significant permanent deformation, crack propagation and failure would be expected in a standard wheel assembly. These effects are significantly minimized in a shield-equipped wheel.

In previous simulation analyses, lock ring contact force was examined as a measure of engagement force for wheel components (ISO 7141) or to study the load transfer path (tire blowout). However, in the rotational side impact simulations, challenges arose as the striker made contact with the lock ring and altered engagement behaviour and contact forces in the standard wheel assembly; whereas no such contact occurred when equipped

with the shield. Similarly, resultant striker contact force is not a fair comparison between simulations as the striker is controlled by overall impact displacement and not dependent on force applied. Nevertheless, the resultant contact force of the striker to wheel components is presented in the figure below for reference purposes.

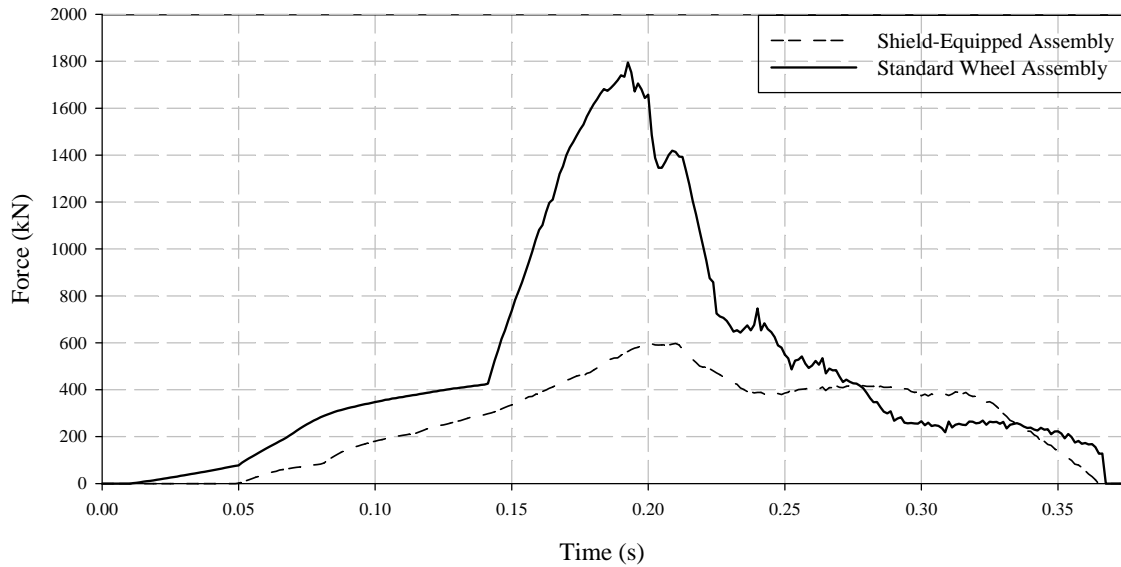


Figure 6.4.17 - Striker to wheel contact force for rotational side impact simulations.

7 CONCLUSIONS

7.1 EXPERIMENTAL TESTING SUMMARY

The experimental testing study investigated the mechanical response of three, five-piece wheel and tire assemblies that were used on heavy mining vehicles. The Goodyear 29.5R29, 29.5-29, and 26.5-25 sized tires, were experimentally tested to determine their mechanical performance and planar deformation characteristics to aid in the development of numerical models. Based upon the work completed within this study the following conclusions can be made:

- a) For the most aggressive loading conditions considered within this study, maximum vertical and sidewall lateral deflections of the wheel and tire assemblies were observed to be approximately equal to 72.2 mm and 23.3 mm, 74.9 mm and 27.1 mm, and 78.9 mm and 25.6 mm for the 29.5R29, 29.5-29, and 26.5-25 tires, respectively.
- b) For each tire, linear relationships were experimentally observed for vertical versus lateral deflections. Proportionality constants between the two deflection measurements of 0.310 mm/mm, 0.346 mm/mm, and 0.331 mm/mm for the 29.5R29, 29.5-29, and 26.5-25 tires, respectively, were determined.
- c) For each tire, linear relationships were observed during static load testing for tire load versus vertical and lateral deflection. For vertical deflection, approximate values of 2.41 kN/mm, 2.59 kN/mm, and 2.68 kN/mm were observed for stiffness of the 29.5R29, 29.5-29, and 26.5-25 tires, respectively. In the lateral direction, approximate values of 5.57 kN/mm, 6.29 kN/mm, and 5.38 kN/mm were observed for the 29.5R29, 29.5-29, and 26.5-25 tires, respectively.
- d) Good correlation between published engineering data and the experimental findings was found with respect to load versus vertical and lateral deflections with an average error of 21.3%, 5.6%, and 1.8% for the 29.5R29, 29.5-29, and 26.5-25

tires, respectively, based on static loading data to predict engineering load data points.

Based on an exhaustive literature review, it is believed the in-field testing conducted through the course of this research effort is the most comprehensive of its kind available in open literature.

7.2 HISTORICAL WHEEL TRACKING DATA ANALYSIS EFFECTIVENESS AND FINAL SUMMARY

The ultimate purpose of the historical wheel tracking database is to act as a simple, effective tool that aids in identifying common issues and proactively improving wheel safety. It provides insight into the frequency and trends of wheel repairs and maintenance, as well as provides the ability to determine average wheel life and estimate an expected wheel maintenance cycle based on this. The database contains data on a wide range of wheels, though the most valid data available are for 26.50 x 25, 29.5 x 25, and 29.5 x 29 wheels. A sample of quantitative data provided by the database includes:

- a) An overall average wheel life for 26.50 x 25, 29.5 x 25, and 29.5 x 29 wheels was determined to be 1805, 890, and 1465 days, respectively.
- b) Using a 26.50 x 25 as an example, the total number of wheels scrapped was organized by scrap description. The most common causes of scrapping include the rim base being bent or otherwise damaged, failing a magnetic particle inspection indicating the presence of a crack, and excessive wear in one or more critical areas of the wheel. These causes represent approximately 31%, 21%, and 19% of the total reasons for scrapping a wheel, respectively.

Overall, the database is a proof of concept stressing the effectiveness and importance of proper wheel tracking. Through continued wheel tracking and historical analysis

database usage, it can be used as a metric for the success of new wheel designs or other wheel assembly related safety improvements, or bring awareness to common failure mechanisms. Based on reviewed literature available in the public forum, it is believed the efforts presented and accomplishments of the database were novel and will provide substantial benefits to the users of multi-piece wheels.

7.3 SAFETY SHIELD SYSTEM

To enhance safety of current multi-piece wheel designs, an innovative safety shield system was developed as a cost-effective, consumable resource that aids in protecting the wheel from damage and prolonging the useful life of the wheel, as well as personnel and equipment should failure occur. To ensure common mishandling practices are avoided, a valve removal device that guarantees zero-pressure in the wheel assembly prior to removal from its vehicle is incorporated into the design. Furthermore, an integrated tire pressure monitoring system, an over-pressurization blow-off valve, and a visual pressure “go/no-go” gauge is similarly part of the design to aid in proper handling and enhanced safety during vehicle operation.

To examine the mechanical performance of the shield system and compare its effectiveness to a standard wheel design, finite element analysis techniques are used and virtual simulation of the ISO 7141 wheel impact test, a tire blowout, and a rotational side impact is conducted. Based upon this work the following conclusions can be made for each testing scenario.

7.3.1 ISO 7141 Virtual Test:

- a) Both the standard and shield-equipped wheel assemblies pass the virtual ISO 7141 test based on the failure criteria of the standard. The shield-equipped wheel maintains a higher lock ring engagement force at the point peak load is observed by approximately 4.5%; despite an overall higher impact force resulting from the parameters set forth in the standard regarding striker drop heights.
- b) A reduction in peak values of effective plastic strain and von Mises stress by approximately 92% and 15%, respectively, is observed in the outer flange when the safety shield is installed.

7.3.2 Simulated Tire Blowout Test:

Failure was prescribed as the point at which the lock ring becomes fully dislodged from its gutter region and thus the wheel's ability to maintain tire pressure would be negated. To reach this state of failure:

- a) The shield-equipped wheel experiences approximately 38% higher maximum contact force input from the tire's bead;
- b) The bead moves outward 9 mm further prior to failure than on a standard wheel;
- c) Magnitudes of effective plastic strains and von Mises stress were reduced by 20.3% and 18.6% in the lock ring, respectively, for a shield-equipped wheel.

Based on these observations, the effectiveness shield under tire blowout conditions shows clear advantages and additional qualitative review of wheel and shield deformation at failure shows all wheel components remain contained by the shield at the point of prescribed failure. In the case of a standard wheel assembly, these components would be free projectiles to which the surrounding environment would be exposed.

7.3.3 Rotational Side Impact Test:

To be representative of operating a vehicle that strikes a surrounding object with its wheel assembly, a rotational side impact test was simulated. A striker was impaled against each wheel assembly configuration by 20 mm and then the wheel assembly rotates and translates forward at 10 kph. When equipped with the safety shield system:

- a) Neither the striker nor shield contact the lock ring or rim base directly;
- b) At the initial point full striker impact depth is reached, a shield-equipped wheel experiences 36.2% and 18.1% lower peak values of von Mises stress, and 95.8% and 75.8% lower maximum values of effective plastic strain when comparing main wheel components and overall maximum values observed in the assembly, respectively;
- c) Overall maximum values of von Mises stress and effective plastic strain were observed during wheel rotation and forward movement, and were found in regions of the outer flanges of each wheel configuration. Observed peak values of von Mises stress were reduced by 55% and effective plastic strain values were approximately an order of magnitude.

Overall, through energy and contact force analysis and studying the deformation behaviour of the wheel, shield and tube nuts, it is evident the shield significantly aids in maintaining locking component engagement and protecting components from damage. The design was presented to wheel manufacturer NSIW Mfg. and the WSN Technical Advisory Committee (TAC). It received positive feedback from NSIW as no such device has previously been implemented by a wheel manufacturer, to their knowledge, and they feel the shield design and its safety features show significant promise. Despite initial apprehension from the TAC regarding the feasibility of the shield system to be readily implemented in the field, primarily due to mounting and maintenance concerns,

committee members gave overall positive feedback, commenting that the safety features are unique and ultimately very beneficial to multi-piece wheel users. Overall, industry experts agreed that safety of multi-piece wheels can and should be enhanced, and that the safety shield system holds promise to accomplish this.

8 REFERENCES

- [1] Natural Resources Canada, "Canada is a Global Mineral Exploration and Mining Giant," 4 March 2013. [Online]. Available: <http://www.nrcan.gc.ca/media-room/news-releases/2013/6907>. [Accessed 12 August 2013].
- [2] Mining Industry Human Resources Council, "Mining Industry," [Online]. Available: <http://www.acareerinmining.ca/>. [Accessed 25 August 2013].
- [3] The Mining Association of Canada, "Facts and Figures of the Canadian Mining Industry," 2011. [Online]. Available: http://miningnorth.com/_rsc/site-content/library/MAC-FactsFigures-2011-English-small.pdf. [Accessed 20 August 2013].
- [4] CBC News, "CBC News Online," 29 April 2006. [Online]. Available: <http://www.cbc.ca/news/background/workplace-safety/dyingforajob.html>. [Accessed 22 August 2011].
- [5] J. Gilks and R. Logan, "Occupational Injuries and Diseases in Canada, 1996-2008," Human Resources and Skills Development Canada, Ottawa, 2010.
- [6] L. Parsons, "Workplace deaths soar in Canada," 29 December 2006. [Online]. Available: <http://www.wsws.org/articles/2006/dec2006/cana-d29.shtml>. [Accessed 12 October 2011].
- [7] R. Banting, "Injury and Occupational Disease Trends in the Mining Industry," in *WSN Mining Health and Safety Conference*, Sudbury, Ontario, Canada, 2013.
- [8] Mines and Aggregates Safety & Health Association, "Take TEN for Safety," MASHA, Ontario, Canada, 2000.
- [9] Workplace Safety North, "Fatality Reports," [Online]. Available: http://www.masha.on.ca/fatality_details.aspx?fatality_id=9. [Accessed 7 September 2012].
- [10] Ministry of The Solicitor General, "Verdict of Coroner's Jury: Jerome Burns," Thunder Bay, Ontario, 2003.
- [11] V. Vijayan, W. Altenhof and R. Banting, "A Finite Element approach for prediction of fatigue life for a three-piece mining vehicle wheel," *Int. J. of Heavy Vehicle Systems*, vol. 17, no. 2, pp. 159-178, 2010.
- [12] V. Vijayan, *Numerical model development of a heavy mining vehicle multi-piece wheel assembly for structural analysis*, M.A.Sc. Thesis, Windsor, Ontario: Dept. of Mech. Eng., University of Windsor, 2008.

- [13] J. DeCastro, "ABC's of OTR," Goodyear Canada Inc., 2010.
- [14] Goodyear Off-The-Road Tires, "Off-The-Road Tire Engineering Data," 2010. [Online]. Available: <http://www.goodyearotr.com/cfm/web/otr/info/>. [Accessed 18 May 2010].
- [15] Australian Standard, "AS 4457-1997: Earth-moving machinery - Off-highway rims and wheels - Maintenance and repair," Standards Association of Australia, Homebush, Australia, 1997.
- [16] M. Cooney, "Is the CAT 797F Too Expensive? \$5 Million, Options Extra.," 2 February 2013. [Online]. Available: <http://www.industrytap.com/is-the-cat-797f-too-expensive-5-million-options-extra/1035>. [Accessed 20 August 2013].
- [17] R. Johnson, "This Is What A \$42,500 Tire Looks Like," 31 May 2012. [Online]. Available: <http://www.businessinsider.com/this-is-what-a-42500-tire-looks-like-the-5980r63-xdr-2012-5>. [Accessed 12 August 2013].
- [18] Work Safe Alberta, "Workplace Health and Safety Bulletin - Servicing Tires Safely," in *GS6003 - General Safety*, Canada, Alberta Human Resources and Employment, 2004, p. 7.
- [19] J. M. Torlach, "Haul Truck Tyre Explosion," *Significant Incident Report No. 15*, p. 2, 1990.
- [20] V. Vijayan, *Numerical model development of a heavy mining vehicle multipiece rim and wheel assembly for structural analysis*, A Literature Review, Windsor, Ontario: University of Windsor, 2006.
- [21] T. Rasche and T. Klinge, "Review and Analysis of Tyre Related Accidents and Incidents - an ACARP Study to Improve Tyre & Rim Maintenance and Operational Safety of Rubber Tyred Earthmover Equipment (ACARP C15046)," Klinge & Co. Pty Ltd. and ACARP, Queensland, Australia, 2007.
- [22] Edmonton Sun, "Exploding tire kills worker," EdmontonSun.Com, Edmonton, Alberta, 2013.
- [23] C. Skelding, "Safety Alert: Tyre air-blast catches three maintenance personnel," *Queensland Government: Department of Employment, Economic Development and Innovation*, vol. No. 275, 27 September 2011.
- [24] Occupational Safety and Health Administration, "Mechanic Dies After Wheel Failure During Tire Inflation, Report ID: 0729300," 2011. [Online]. Available: http://www.osha.gov/pls/imis/accidentsearch.accident_detail?id=200012912. [Accessed June 2013].

- [25] Occupational Safety and Health Administration, U.S. Department of Labor, "Exploding Multi-piece Wheel Rim Kills Auto Dealer Worker," 23 November 2010. [Online]. Available: <http://www.osha.gov/pls/imis/accidentsearch.id=202089462>. [Accessed 15 July 2013].
- [26] Occupational Safety and Health Administration, U.S. Department of Labor, "Employee Is Killed From Head Injury While Inflating Tire, Report ID: 0950633," 18 January 2010. [Online]. Available: https://www.osha.gov/pls/imis/accidentsearch.accident_detail?id=202609129. [Accessed 3 August 2013].
- [27] Occupational Safety and Health Administration, U.S. Department of Labor, "Worker Is Killed When Multi-Piece Rim Explodes, Report ID: 0521700," 28 August 2009. [Online]. Available: https://www.osha.gov/pls/imis/accidentsearch.accident_detail?id=200033496. [Accessed 5 August 2013].
- [28] Occupational Health and Safety, "Worker Fatally Injured When Tire Components Separate, Report File #: F-256084," 28 August 2009. [Online]. Available: http://www.osha.gov/pls/imis/accidentsearch.accident_detail?id=200012912. [Accessed 25 July 2013].
- [29] Occupational Safety and Health Administration, U.S. Department of Labor, "Tire Service Worker Is Killed In Rim Wheel Explosion, Report ID: 0452110," 23 January 2009. [Online]. Available: https://www.osha.gov/pls/imis/accidentsearch.accident_detail?id=201859931. [Accessed 5 August 2013].
- [30] Fatality Assessment and Control Evaluation (FACE) Program, U.S. Department of Health and Human Services, "Equipment Operator Killed by a Lock Ring Propelled from a Multi piece Rim Wheel, New York State Case Report: 07NY137," 2007. [Online]. Available: <http://www.health.ny.gov/environmental/investigations/face/07ny137.htm>. [Accessed 5 August 2013].
- [31] Fatality Assessment and Control Evaluation (FACE) Program, U.S. Department of Health and Human Services, "Mechanic Dies while Changing a Tire Mounted on a Multi-piece Split Rim Wheel, Massachusetts Case Report: 07-MA-058," 20 October 2009. [Online]. Available: <http://www.cdc.gov/niosh/face/stateface/ma/07ma058.html>. [Accessed 7 August 2013].

- [32] P. Fisher, "Zipper failures not only embarrassing," Crain Publication, 13 October 2003. [Online]. Available: <http://www.tirebusiness.com/article/20031013/NEWS/310139972/zipper-failures-not-only-embarrassing>. [Accessed 8 August 2013].
- [33] MASHA, "Health and Safety Guidelines: Working with Tires & Wheel Assemblies," 2011. [Online]. Available: <http://www.workplacesafetynorth.ca/resources/multi-piece-rims-controlling-hazards>. [Accessed 8 August 2013].
- [34] The Tire and Rim Association, Inc., TRA 2010 Standards Publication, Copley, Ohio, 2010.
- [35] Technical Committee ISO/TC 22, "Road vehicles - Light alloy wheels - Impact Test," in *ISO/FDIS 7141*, Geneva, The International Organization of Standards, 2005.
- [36] SAE Wheel Committee, "Road Hazard Impact Test for Wheel and Tire Assemblies," in *SAE J1981*, Warrendale, Pennsylvania: SAE International, 2005.
- [37] C. L. Chang and S. Yang, "Finite element simulation of wheel impact test," *Journal of AMME*, vol. 28, no. 2, pp. 167-170, 2008.
- [38] M. Cerit, "Numerical simulation of dynamic side impact test for an aluminum alloy wheel," *Scientific Research and Essays - AcademicJournals.org*, vol. 5, no. 18, pp. 2694-2701, 2010.
- [39] J. Y. Wong, *Theory of Ground Vehicles*, 4th ed., Wiley, 2008.
- [40] J. D. Reid, D. A. Boesch and R. W. Bielenberg, "Detailed tire modeling for crash applications," *International Journal of Crashworthiness*, vol. 12, no. 5, pp. 521-529, 2007.
- [41] F. Orengo, M. H. Ray and C. A. Plaxico, "Modeling tire blow-out in roadside hardware simulations using LS-DYNA," *American Society of Mechanical Engineers*, vol. Transportation, pp. 71-80, 2003.
- [42] A. M. Burke and O. A. Olatunbosun, "Static Tyre/Road Interaction Modelling," *Meccanica*, vol. 32, no. 5, pp. 473-479, 1997.
- [43] R. V. Neves, G. B. Micheli and M. Alves, "An experimental and numerical investigation on tyre impact," *International Journal of Impact Engineering*, vol. 37, no. 6, pp. 685-693, 2010.

- [44] S. Nguyen, E. Greenhalgh, L. Iannucci, S. Longstaff, R. Olsson and P. Curtis, "Experimental Characterisation of Tyre Indentation by Simulated Runway Debris," *Strain: An International Journal for Experimental Mechanics*, vol. 47, pp. 343-350, 2011.
- [45] W. Oberkampf and T. Trucano, "Verification and validation in computational fluid dynamics," *Progress in Aerospace Science*, vol. 38, pp. 209-272, 2002.
- [46] National Highway Traffic Safety Administration, "Tire Pressure Monitoring Systems: Controls and Displays," *Federal Motor Vehicle Safety Standards*, p. 571, 15 November 2004.
- [47] Coyote Enterprises, L.L.C., "How Staun II Internal Pneumatic Beadlocks Work," 2013. [Online]. Available: <http://www.coyoteents.com/beadlocks-how-they-work.html>. [Accessed 12 September 2013].
- [48] Z. Li, A. Tonkovich, S. DiCecco, W. Altenhof, R. Banting and H. Hu, "Development and validation of a finite element model of a mining vehicle tyre," *International Journal of Vehicle Design*, vol. 65, no. 2/3, pp. 176-201, 2014.
- [49] The Engineering ToolBox, "Metals and Alloys - Densities," [Online]. Available: http://www.engineeringtoolbox.com/metal-allows-densities-d_50.html. [Accessed 22 June 2012].
- [50] Caterpillar Inc., *R2900G Underground Mining Loader Specifications*, CAT.
- [51] H. Krahn, K. D. Hughes and G. Lowe, *Work, Industry, and Canadian Society*, Ithaca: Nelson, 2002.
- [52] V. Vijayan, *Numerical model development of a heavy mining vehicle multi-piece wheel assembly for structural analysis*, Windsor, Ontario: Dept. of Mech. Eng., University of Windsor, 2008.
- [53] A. Tonkovich, Z. Li, S. DiCecco, W. Altenhof and R. Banting, "Redesigning the Wheel: Enhancing Safety and Reducing the Cost of Heavy Mining Vehicle Wheel Assemblies," in *Partners in Prevention 2012*, Mississauga, Ontario, Canada, 2012.

9 APPENDICES

9.1 OBSERVATIONS OF ADDITIONAL WHEEL ASSEMBLIES DURING MUSSELWHITE TESTING

9.1.1 Vertical and Lateral Displacement for 29.5R29 Wheel Assembly

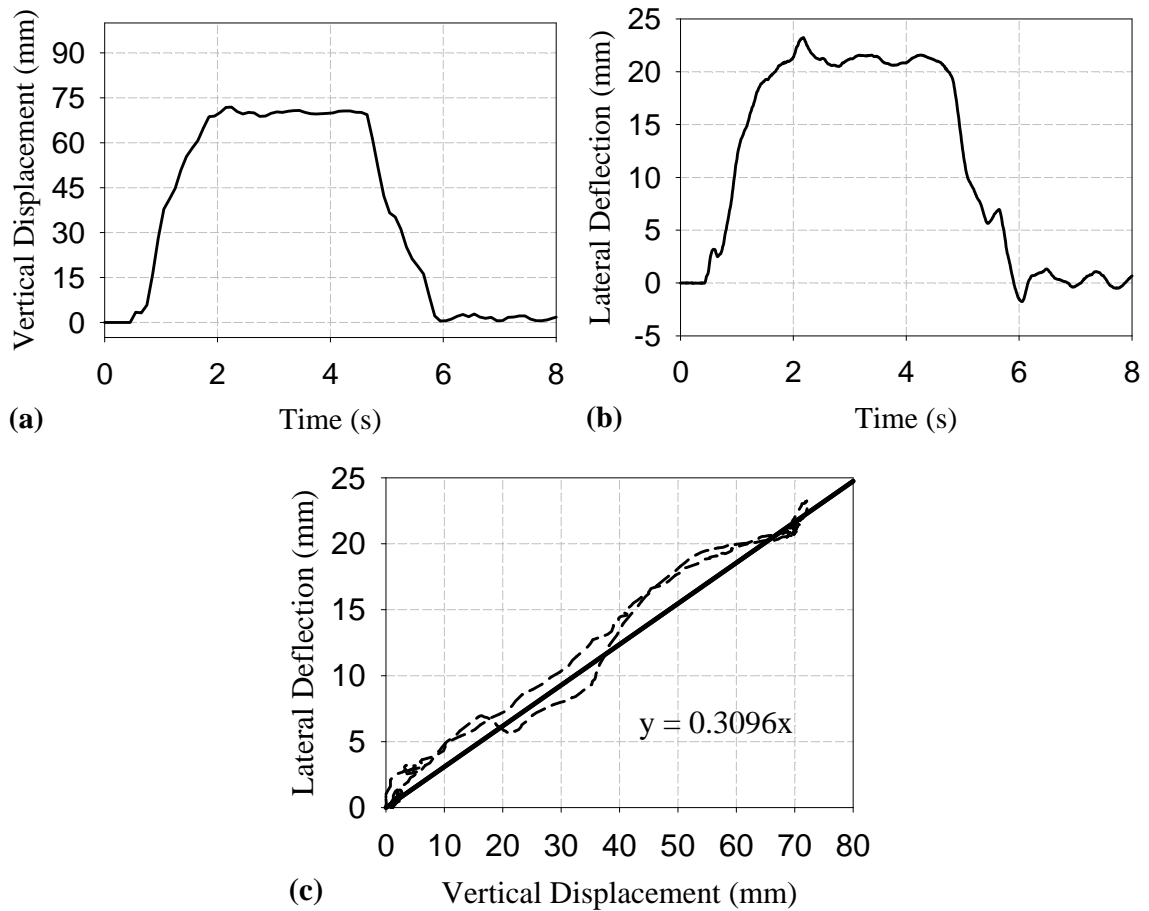


Figure 9.1.1 - Response for 29.5R29 tire test event exhibiting maximum deflection in the a) vertical and b) lateral directions as well as a c) cross-plot showing lateral deflection versus vertical deflection is provided.

9.1.2 Vertical and Lateral Displacement for 26.5-25 Wheel Assembly

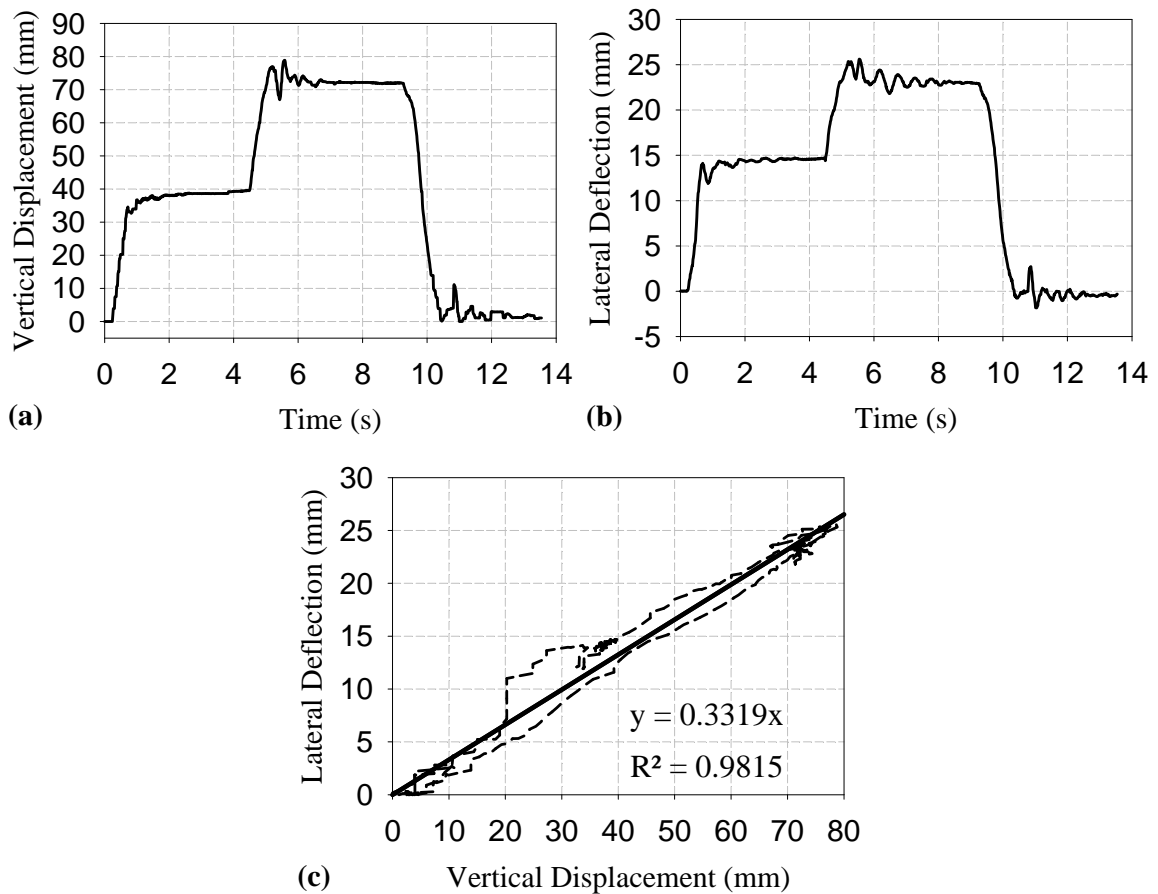


Figure 9.1.2 - Response for 26.5-25 tire test event exhibiting maximum deflection in the a) vertical and b) lateral directions as well as a c) cross-plot showing lateral deflection versus vertical deflection is provided.

9.1.3 Additional Wheel Assembly Vertical Displacement Comparisons

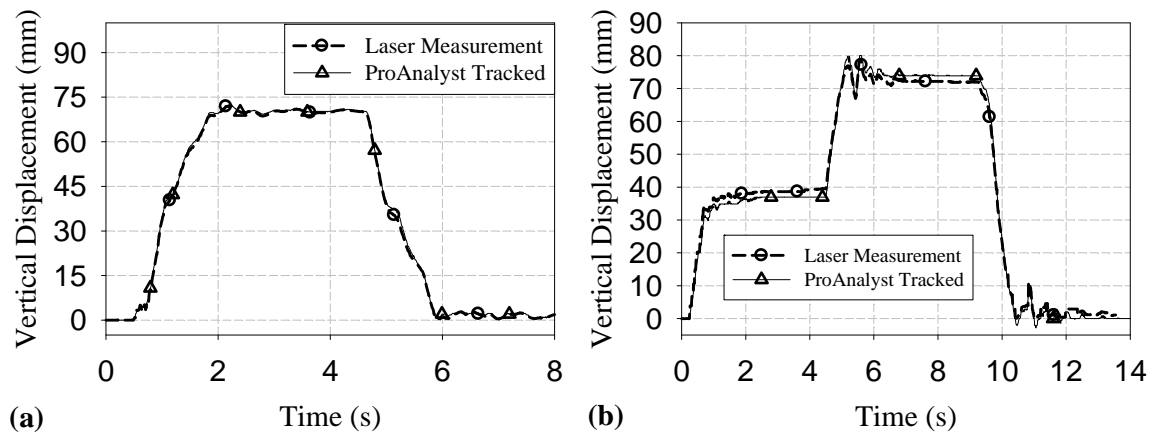


Figure 9.1.3 - Vertical displacement comparison for the a) 29.5R29 and b) 26.5-25 tires between laser displacement transducer measurements and high-speed camera image tracking using ProAnalyst for correlation purposes.

9.1.4 Tracked Node Deflection Responses for 29.5R29 Tire

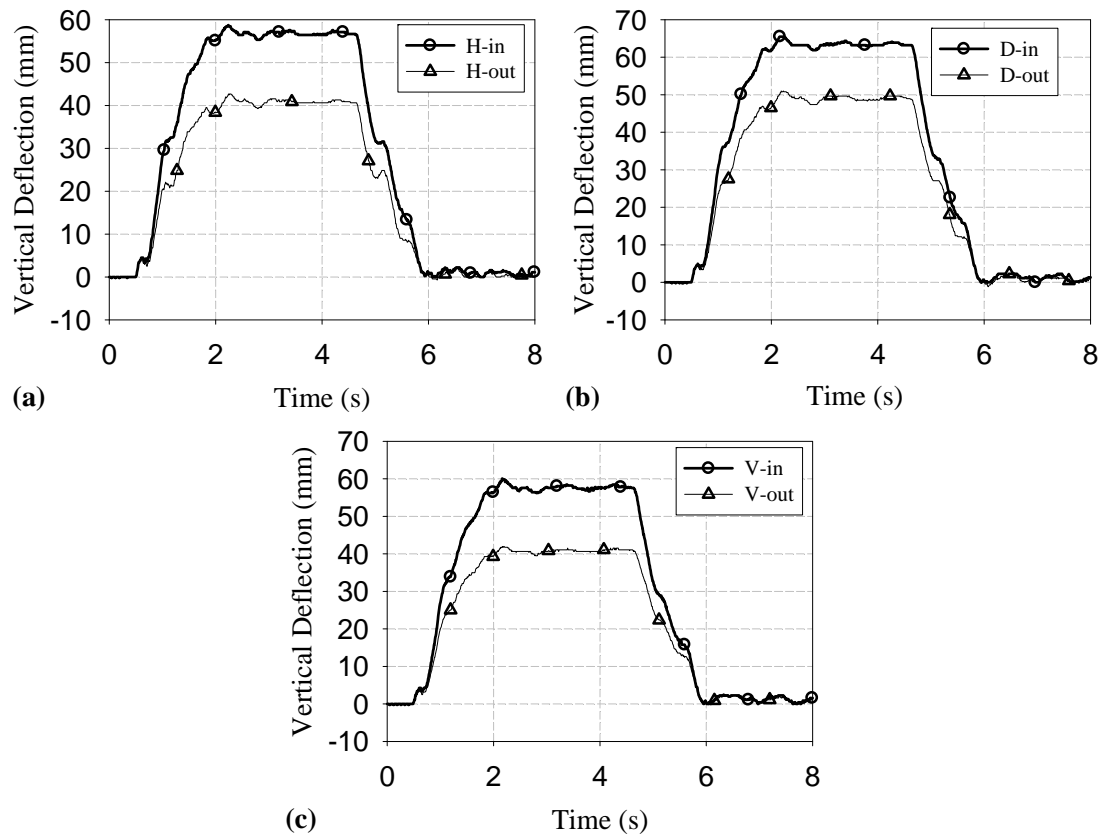


Figure 9.1.4- Vertical deflection responses for tracked nodes during 29.5R29 tire test event where maximum deflections were observed for the a) H-in and H-out points, b) D-in and D-out points, and c) V-in and V-out points.

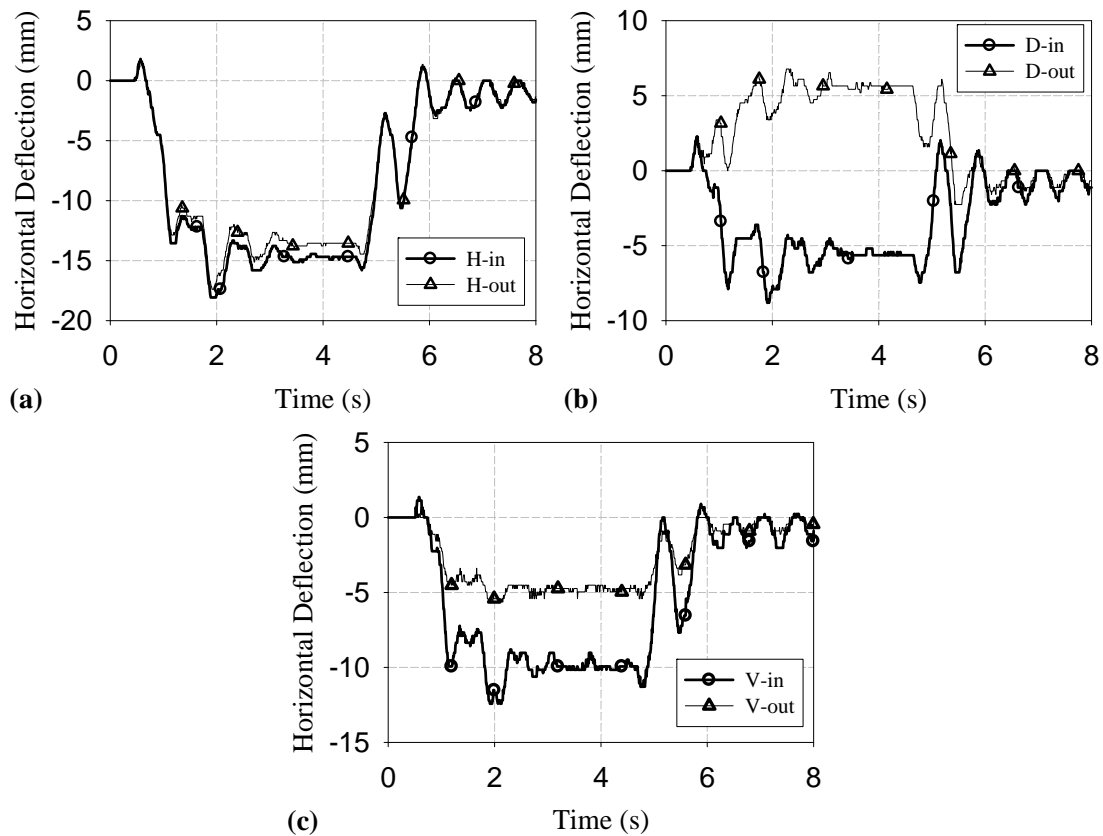


Figure 9.1.5– Horizontal deflection responses for tracked nodes during 29.5R29 tire test event where maximum deflections were observed for the a) H-in and H-out points, b) D-in and D-out points, and c) V-in and V-out points.

9.1.5 Tracked Node Deflection Responses for 26.5-25 Tire

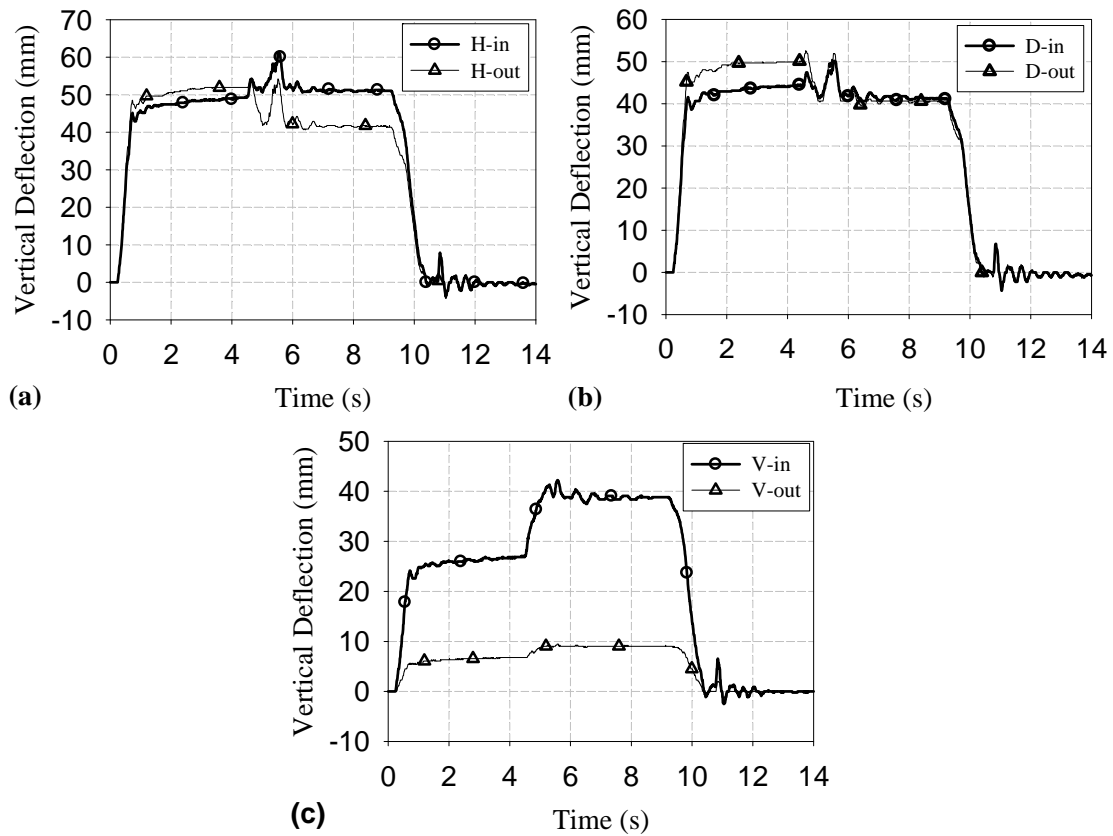


Figure 9.1.6- Vertical deflection responses for tracked nodes during 26.5-25 tire test event where maximum deflections were observed for the a) H-in and H-out points, b) D-in and D-out points, and c) V-in and V-out points.

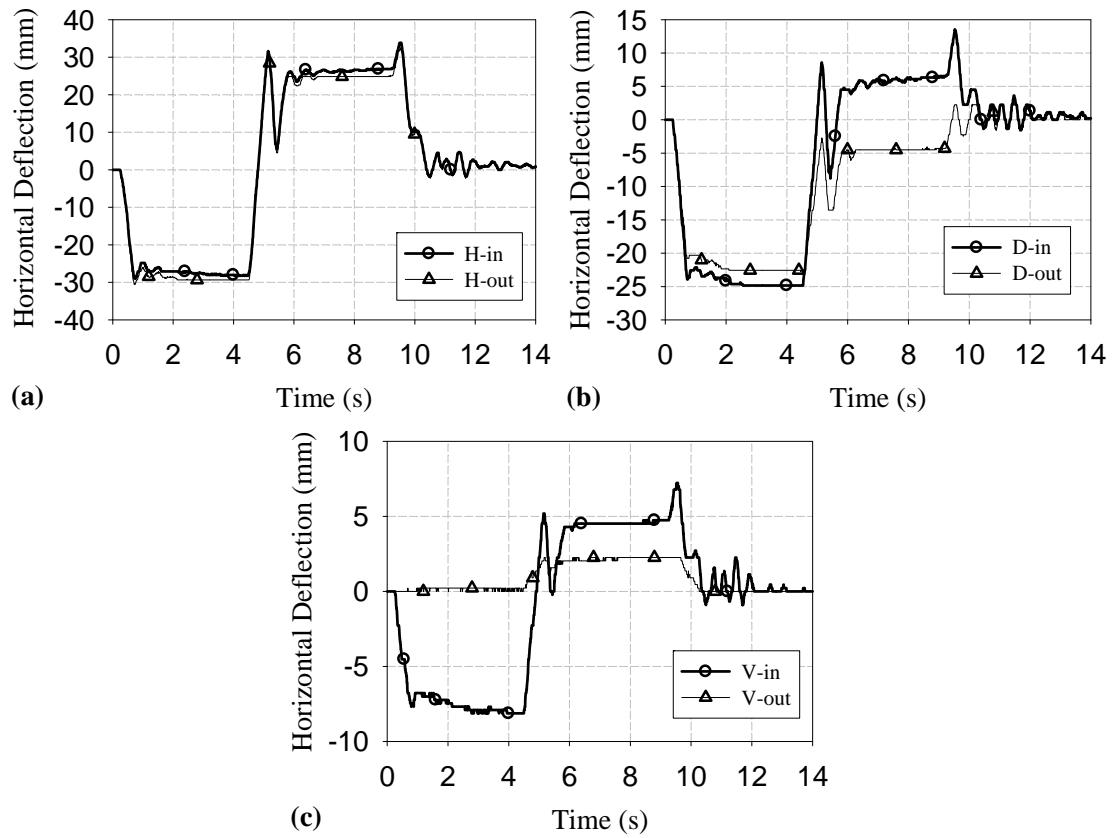


Figure 9.1.7– Horizontal/Longitudinal deflection responses for tracked nodes during 29.5R29 tire test event where maximum deflections were observed for the a) H-in and H-out points, b) D-in and D-out points, and c) V-in and V-out points.

9.1.6 Load versus Deflection Data for Additional Wheel Assemblies

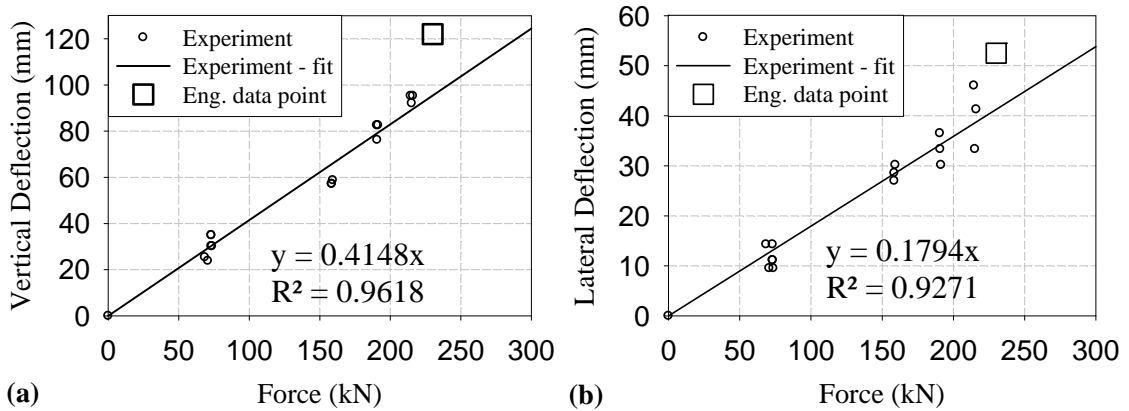


Figure 9.1.8– Deflection data for the 29.5R29 tire showing a) vertical deflection versus load force and b) lateral deflection versus load force compared to the corresponding Goodyear engineering data point.

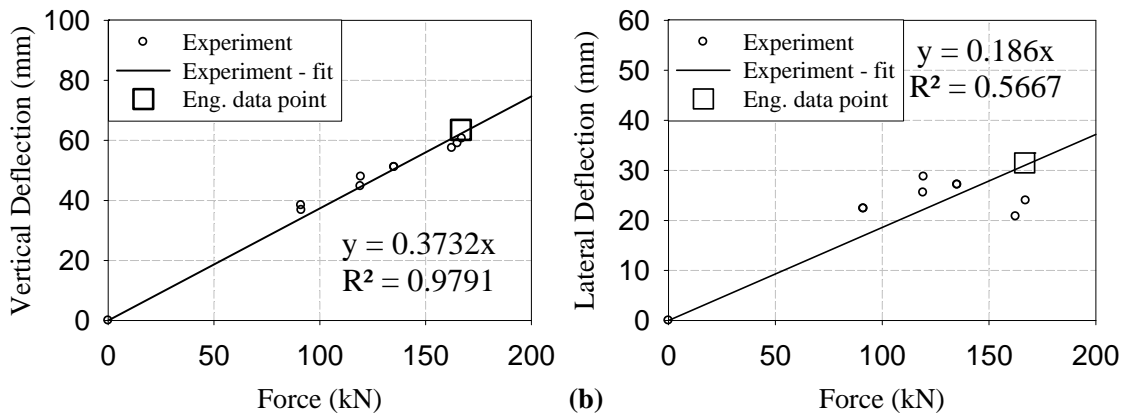


Figure 9.1.9– Deflection data for the 26.5-25 tire showing a) vertical deflection versus load force and b) lateral deflection versus load force compared to the corresponding Goodyear engineering data point.

9.2 HISTORICAL WHEEL TRACKING DATABASE MACRO CODE

9.2.1 Statistical Analysis Data Assembly Macro Code

```
Sub Calculate()  
,  
' Trial1 Macro  
,  
  
Dim i As Integer  
Dim j As Integer  
Dim k As Integer  
Dim h As Integer  
Dim TotalTireLife As Long  
Dim AvgTireLife As Long  
Dim Counter As Long  
  
j = 3      'j will be my sheet number variable I'll start at 2 since Fraiser is the 2nd sheet  
i = 4      'i will be my row count variable for the various sheets. Starts at 4 because that's  
           where the first line of data is  
k = 4      'k will be the value of the row that the data will be put into  
h = 4      'h will be the value of the row for the second set of data being input, for valid  
           scrap code  
m = 4      'm will be the value of the row for the compilation of tire sizes  
g = 4      'g will be the counter of the row for the valid scrap/concise valid scrap code  
d = 4      'd will be counter for assembling scrap code descriptions  
w = 4      'w will be counter for assembling tire sizes for scrap code stats  
  
Sheets("Assembled Data").Activate  
Range("A4:BD1000000").ClearContents  
Range("A4:AW4").ClearContents  
Range("BN4:BP46").ClearContents  
  
Do While j <= Sheets.Count  
  
    Sheets(j).Activate  
  
    Do While Cells(i, 1).Value <> ""  
  
        If Cells(i, 3).Value <> "" And Cells(i, 10).Value <> "" Then  
            mine_name = Cells(1, 1).Value  
            install_date = Cells(i, 3).Value  
            scrap_date = Cells(i, 10).Value  
            rim_life = scrap_date - install_date 'calculated rim life  
            rim_number = Cells(i, 1).Value  
            tire_size = Cells(i, 5).Value  
            scrap_code = Cells(i, 11).Value
```

```

Worksheets("Assembled Data").Cells(k, 1).Value = mine_name
Worksheets("Assembled Data").Cells(k, 2).Value = rim_number
Worksheets("Assembled Data").Cells(k, 3).Value = rim_life
Worksheets("Assembled Data").Cells(k, 4).Value = install_date
Worksheets("Assembled Data").Cells(k, 5).Value = scrap_date
Worksheets("Assembled Data").Cells(k, 6).Value = tire_size
Worksheets("Assembled Data").Cells(k, 7).Value = scrap_code
k = k + 1
End If

i = i + 1
Loop
i = 4
j = j + 1
Loop
'
' Creates new assembled data set based on modified scrap codes based on different
naming convention
' for MusselWhite and ValeInco. (If ValeInco 52 and 54 count as 50, if MusselWhite 25,
26, 27,28 are 21)
j = 3
i = 4

Do While j <= Sheets.Count

Sheets(j).Activate

Do While Cells(i, 1).Value <> ""

If Cells(i, 3).Value <> "" And Cells(i, 10).Value <> "" Then
mine_name = Cells(1, 1).Value
install_date = Cells(i, 3).Value
scrap_date = Cells(i, 10).Value
rim_life = scrap_date - install_date 'calculated rim life
rim_number = Cells(i, 1).Value
tire_size = Cells(i, 5).Value
If Cells(i, 11).Value = "25" And Cells(1, 1).Value = "MusselWhite" Then
mod_scrap_code = "21"
ElseIf Cells(i, 11).Value = "26" And Cells(1, 1).Value = "MusselWhite" Then
mod_scrap_code = "21"
ElseIf Cells(i, 11).Value = "27" And Cells(1, 1).Value = "MusselWhite" Then
mod_scrap_code = "21"
ElseIf Cells(i, 11).Value = "28" And Cells(1, 1).Value = "MusselWhite" Then
mod_scrap_code = "21"
ElseIf Cells(i, 11).Value = "52" And Cells(1, 1).Value = "ValeInco" Then
mod_scrap_code = "50"

```



```

ElseIf Cells(i, 11).Value = "54" And Cells(1, 1).Value = "ValeInco" Then
    mod_scrap_code = "50"
Else
    mod_scrap_code = Cells(i, 11).Value
End If

Select Case mod_scrap_code
Case 3 To 9, 12 To 20, 22, 23, 28, 30, 34, 36, 38, 40, 42, 44, 45
    mod_valid_scrap_code = mod_scrap_code
Case Else
    mod_valid_scrap_code = ""
End Select

Select Case mod_valid_scrap_code
Case 4, 8, 9, 36
    mod_combined_valid_scrap_code = 3
Case 6, 7
    mod_combined_valid_scrap_code = 5
Case 16, 17, 18
    mod_combined_valid_scrap_code = 15
Case 42, 44
    mod_combined_valid_scrap_code = 40
Case Else
    mod_combined_valid_scrap_code = mod_valid_scrap_code
End Select

Worksheets("Assembled Data").Cells(h, 10).Value = mine_name
Worksheets("Assembled Data").Cells(h, 11).Value = rim_number
Worksheets("Assembled Data").Cells(h, 12).Value = rim_life
Worksheets("Assembled Data").Cells(h, 13).Value = install_date
Worksheets("Assembled Data").Cells(h, 14).Value = scrap_date
Worksheets("Assembled Data").Cells(h, 15).Value = tire_size
Worksheets("Assembled Data").Cells(h, 16).Value = mod_scrap_code
Worksheets("Assembled Data").Cells(h, 17).Value = mod_valid_scrap_code
Worksheets("Assembled Data").Cells(h, 18).Value =
mod_combined_valid_scrap_code
    h = h + 1
End If

    i = i + 1
Loop
i = 4
j = j + 1
Loop

```

'Create list of tire sizes in new column with duplicates removed

```
Sheets("Assembled Data").Activate
```

```
Range("O3:O100000").AdvancedFilter Action:=xlFilterCopy, CopyToRange:=Range _  
("S3"), Unique:=True
```

```
Dim x As Long
```

```
Dim LastRow As Long
```

```
LastRow = Range("S100000").End(xlUp).Row
```

```
For x = LastRow To 4 Step -1
```

```
    If Application.WorksheetFunction.CountIf(Range("S1:S" & x), Range("S" & x).Text)  
> 1 Then
```

```
        Range("S" & x).Delete Shift:=xlUp
```

```
    End If
```

```
Next x
```

```
'loop to count scrap codes by tire size
```

```
Sheets("Assembled Data").Activate
```

```
i = 4
```

```
u = 4
```

```
Do While Cells(u, 19).Value <> ""
```

```
    Cells(u, 20).Value = 0
```

```
    Do While Cells(i, 15).Value <> ""
```

```
        If Cells(i, 15).Value = Cells(u, 19).Value Then
```

```
            Cells(u, 20).Value = Cells(u, 20).Value + 1
```

```
        End If
```

```
        i = i + 1
```

```
    Loop
```

```
    i = 4
```

```
    u = u + 1
```

```
Loop
```

```
'loop to count valid scrap codes by tire size
```

```
Sheets("Assembled Data").Activate
```

```
i = 4
```

```
u = 4
```

```
Do While Cells(u, 19).Value <> ""
```

```
    Cells(u, 21).Value = 0
```

```
    Do While Cells(i, 15).Value <> ""
```

```
        If Cells(i, 15).Value = Cells(u, 19).Value And Cells(i, 17).Value <> "" Then
```

```
            Cells(u, 21).Value = Cells(u, 21).Value + 1
```

```
        End If
```

```
        i = i + 1
```

```
    Loop
```

```
    i = 4
```

```
    u = u + 1
```

Loop

'Loop to count valid and reduced/combined scrap codes by tire size

Sheets("Assembled Data").Activate

i = 4

u = 4

Do While Cells(u, 19).Value <> ""

Cells(u, 22).Value = 0

Do While Cells(i, 15).Value <> ""

If Cells(i, 15).Value = Cells(u, 19).Value And Cells(i, 18).Value <> "" Then

Cells(u, 22).Value = Cells(u, 22).Value + 1

End If

i = i + 1

Loop

i = 4

u = u + 1

Loop

'Create list of Applicable Scrap Codes

Range("R4:R100000").Select

Selection.Copy

Range("Y4").Select

ActiveSheet.Paste

Application.CutCopyMode = False

ActiveSheet.Range("\$Y\$3:\$Y\$100000").removeduplicates Columns:=1,

Header:=xlYes

ActiveWorkbook.Worksheets("Assembled Data").Sort.SortFields.Clear

ActiveWorkbook.Worksheets("Assembled Data").Sort.SortFields.Add Key:=Range(_

"Y4"), SortOn:=xlSortOnValues, Order:=xlAscending, DataOption:= _

xlSortNormal

With ActiveWorkbook.Worksheets("Assembled Data").Sort

.SetRange Range("Y4:Y100000")

.Header = xlNo

.MatchCase = False

.Orientation = xlTopToBottom

.SortMethod = xlPinYin

.Apply

End With

Sheets("Assembled Data").Activate

d = 4

i = 27

Do While Cells(d, 25).Value <> ""

Sheets("Assembled Data").Cells(d, 26) = WorksheetFunction.VLookup(Cells(d, 25).Value, Worksheets("MasterScrapCodes").Range("M2:N29"), 2, False)

d = d + 1

'USE CAUTION: d is referenced below for total tire count.

Loop

Cells(6, 24).Value = d

Cells(d, 26).Value = "Total Number by Tire Size"

'Create list of tire sizes in new row to setup scrap codes by tire size stats

Sheets("Assembled Data").Activate

i = 4

w = 27

Do While Cells(i, 19).Value <> ""

 If Cells(i, 22) > 0 Then

 Cells(3, w) = Cells(i, 19)

 w = w + 1

 End If

 i = i + 1

Loop

'create title for 'total' column used in summation of # of wheels by scrap code.

Cells(3, w).Value = "Total # of Wheels Scrapped by Scrap Code"

counter_scrapcodetable_col = w

'create counter to be used after table is assembled for summing # of wheels by scrap code

'Assemble Count for Scrap Codes by Tire Size

Sheets("Assembled Data").Activate

i = 4

w = 27

k = 4

Do While Cells(3, w).Value <> ""

 Do While Cells(k, 25).Value <> ""

 Do While Cells(i, 15).Value <> ""

 If Cells(k, 25).Value = Cells(i, 18).Value And Cells(3, w).Value = Cells(i, 15).Value

Then

 Cells(k, w).Value = Cells(k, w).Value + 1

 End If

 i = i + 1

 Loop

 k = k + 1

 i = 4

Loop

 counter_rows = k 'creates variable for usage later to yield row and columns for average calculation purposes

 counter_cols = w

'Adds a total to the tire size count of valid scrap codes

'references 'd' counter from above scrap name vlookup.

For colsumming = 4 To d - 1

 Cells(d, w) = Cells(colsumming, w) + Cells(d, w)

```

Next colsumming

w = w + 1
k = 4
Loop
d = 4
Do While Cells(d, 25).Value <> ""
    For rowsumming = 27 To counter_scrapcodetable_col - 1
        Cells(d, counter_scrapcodetable_col) = Cells(d, counter_scrapcodetable_col) +
Cells(d, rowsumming)
    Next rowsumming
    d = d + 1
Loop
'Create list of tire sizes if valid scrap codes exist as well, used in tire life calculations
Sheets("Assembled Data").Activate
i = 4
w = 4
Do While Cells(i, 19).Value <> ""
    If Cells(i, 22) > 0 Then
        Cells(w, 52) = Cells(i, 19)
        w = w + 1
    End If
    i = i + 1
Loop

'Assemble average tire life
Sheets("Assembled Data").Activate
i = 4
k = 4
TotalTireLife = 0
AvgTireLife = 0
Counter = 0
Do While Cells(k, 52).Value <> ""
    Do While Cells(i, 15).Value <> ""
        If Cells(k, 52).Value = Cells(i, 15).Value And Cells(i, 17) <> "" Then
            TotalTireLife = TotalTireLife + Cells(i, 12).Value
            Counter = Counter + 1
        End If
        i = i + 1
    Loop
    If Counter > 0 Then
        AvgTireLife = CLng(TotalTireLife) / Counter
        Worksheets("Assembled Data").Cells(k, 53).Value = AvgTireLife
        TotalTireLife = 0
        AvgTireLife = 0
        Counter = 0
    End If
    k = k + 1
Loop

```

```

k = k + 1
i = 4
Else
Worksheets("Assembled Data").Cells(k, 53).Value = 0
TotalTireLife = 0
AvgTireLife = 0
Counter = 0
i = 4
End If
Loop

```

```

Format all cells
Range("J4").Select
Range(Selection, Selection.End(xlDown)).Select
Range(Selection, Selection.End(xlToRight)).Select
Selection.Borders(xlDiagonalDown).LineStyle = xlNone
Selection.Borders(xlDiagonalUp).LineStyle = xlNone
With Selection.Borders(xlEdgeLeft)
.LineStyle = xlContinuous
.ColorIndex = 0
.TintAndShade = 0
.Weight = xlThin
End With
With Selection.Borders(xlEdgeTop)
.LineStyle = xlContinuous
.ColorIndex = 0
.TintAndShade = 0
.Weight = xlThin
End With
With Selection.Borders(xlEdgeBottom)
.LineStyle = xlContinuous
.ColorIndex = 0
.TintAndShade = 0
.Weight = xlThin
End With
With Selection.Borders(xlEdgeRight)
.LineStyle = xlContinuous
.ColorIndex = 0
.TintAndShade = 0
.Weight = xlThin
End With
With Selection.Borders(xlInsideVertical)
.LineStyle = xlContinuous
.ColorIndex = 0
.TintAndShade = 0

```

```

        .Weight = xlThin
    End With
    With Selection.Borders(xlInsideHorizontal)
        .LineStyle = xlContinuous
        .ColorIndex = 0
        .TintAndShade = 0
        .Weight = xlThin
    End With
    Range("Y4:AW18").Select
    Range(Selection, Selection.End(xlDown)).Select
    Range(Selection, Selection.End(xlToRight)).Select
    Selection.Borders(xlDiagonalDown).LineStyle = xlNone
    Selection.Borders(xlDiagonalUp).LineStyle = xlNone
    With Selection.Borders(xlEdgeLeft)
        .LineStyle = xlContinuous
        .ColorIndex = 0
        .TintAndShade = 0
        .Weight = xlThin
    End With
    With Selection.Borders(xlEdgeTop)
        .LineStyle = xlContinuous
        .ColorIndex = 0
        .TintAndShade = 0
        .Weight = xlThin
    End With
    With Selection.Borders(xlEdgeBottom)
        .LineStyle = xlContinuous
        .ColorIndex = 0
        .TintAndShade = 0
        .Weight = xlThin
    End With
    With Selection.Borders(xlEdgeRight)
        .LineStyle = xlContinuous
        .ColorIndex = 0
        .TintAndShade = 0
        .Weight = xlThin
    End With
    With Selection.Borders(xlInsideVertical)
        .LineStyle = xlContinuous
        .ColorIndex = 0
        .TintAndShade = 0
        .Weight = xlThin
    End With
    With Selection.Borders(xlInsideHorizontal)
        .LineStyle = xlContinuous
        .ColorIndex = 0

```

```

        .TintAndShade = 0
        .Weight = xlThin
    End With
Range("AZ4").Select
Range(Selection, Selection.End(xlDown)).Select
Range(Selection, Selection.End(xlToRight)).Select
Selection.Borders(xlDiagonalDown).LineStyle = xlNone
Selection.Borders(xlDiagonalUp).LineStyle = xlNone
With Selection.Borders(xlEdgeLeft)
    .LineStyle = xlContinuous
    .ColorIndex = 0
    .TintAndShade = 0
    .Weight = xlThin
End With
With Selection.Borders(xlEdgeTop)
    .LineStyle = xlContinuous
    .ColorIndex = 0
    .TintAndShade = 0
    .Weight = xlThin
End With
With Selection.Borders(xlEdgeBottom)
    .LineStyle = xlContinuous
    .ColorIndex = 0
    .TintAndShade = 0
    .Weight = xlThin
End With
With Selection.Borders(xlEdgeRight)
    .LineStyle = xlContinuous
    .ColorIndex = 0
    .TintAndShade = 0
    .Weight = xlThin
End With
With Selection.Borders(xlInsideVertical)
    .LineStyle = xlContinuous
    .ColorIndex = 0
    .TintAndShade = 0
    .Weight = xlThin
End With
With Selection.Borders(xlInsideHorizontal)
    .LineStyle = xlContinuous
    .ColorIndex = 0
    .TintAndShade = 0
    .Weight = xlThin
End With
End Sub

```


9.2.2 Scrap Code Creation Macro Code

```
Sub ExtraSavedCode()  
' Macro1 Macro  
  With Selection.Validation  
    .Delete  
    .Add Type:=xlValidateList, AlertStyle:=xlValidAlertStop, Operator:= _  
    xlBetween, Formula1:="$AA$3:$AX$3"  
    .IgnoreBlank = True  
    .InCellDropdown = True  
    .InputTitle = ""  
    .ErrorTitle = ""  
    .InputMessage = ""  
    .ErrorMessage = ""  
    .ShowInput = False  
    .ShowError = True  
  End With  
  ActiveWindow.ScrollColumn = 42  
  ActiveWindow.ScrollColumn = 43  
  ActiveWindow.ScrollColumn = 45  
  ActiveWindow.ScrollColumn = 50  
  ActiveWindow.ScrollColumn = 51  
  ActiveWindow.ScrollColumn = 54  
  ActiveWindow.ScrollColumn = 55  
  ActiveWindow.ScrollColumn = 56  
  ActiveWindow.ScrollColumn = 57  
  
  Dim sumrng As Range  
  
  Sheets("Assembled Data").Activate  
  'Create row of totals of scrapped rims to determine top 3 to plot. Uses counters created  
  above to determine dimensions of chart  
  'counter_rows yields row max, counter_cols yields columns max  
  i = 27 'counter for summing starting at col 27 (beginning of table)  
  k = counter_rows - 1  
  w = counter_cols  
  
  Do While i <= counter_cols  
    With Application.WorksheetFunction  
      Cells(2, i).Formula = .Sum(Range(Cells(4, i), Cells(k, i)))  
    End With  
    i = i + 1  
  Loop  
  'START EDITING HERE  
  Dim WorkRange As Range  
  Dim MaxVal As Double
```

```

Set WorkRange = Worksheets(1).Range("AA18:AR18")
    MaxVal = Application.Max(WorkRange)
    Sheets("Assembled Data").Cells(23, 40) = MaxVal
With Application.WorksheetFunction
    MaxName = Application.HLookup(MaxVal, "AA3:AR18", 1, False)
    Sheets("Assembled Data").Cells(24, 40) = MaxName
End With
End Sub
Sub CreateScrapDataList()
Sheets("Assembled Data").Activate
i = 4
Do While Cells(i, 26).Value <> ""
    Cells(i, 66) = Cells(i, 26)
    i = i + 1
Loop
i = i - 1
'create variable based on selection from drop down list for plotting purposes.
'used to offset in size lookup chart
size_select = 26 + Cells(4, 68).Value
'uses "i" from above loop to determine how many rows values are looked up based on
'number of scrap reasons are found
w = 4
Do While w <= i
Cells(w, 67).Value = Cells(w, size_select).Value
w = w + 1
Loop

End Sub

```

9.3 MINING WHEEL MATERIAL DATA

9.3.1 Material Card For Numerical Model Steel

```

$-----1-----2-----3-----4-----5-----6-----7-----8
$ MATERIAL CARDS
$-----1-----2-----3-----4-----5-----6-----7-----8
*MAT_PIECEWISE_LINEAR_PLASTICITY_TITLE
Wheel and Shield Steel
$ This is a material data model developed by Aleksander Tonkovich for steel mining
$ vehicle multipiece wheels based on tensile testing performed by Sante DiCecco
$ Note the following set of units: tonne, mm, sec - all other units are derived
$ from this base set
$ MID RO E PR SIGY ETAN EPPF TDEL
$# mid ro e pr sigy etan fail tdel
57 7.8500E-9 2.1540E+5 0.303000 368.89999 0.000 0.000 0.000
$# c p lcss lcsr vp
0.000 0.000 9 0 1.000000
*DEFINE_CURVE_TITLE
ExperimentalStressStrainCurve
$ Note the following set of units: tonne, mm, sec - all other units are derived
$ LCID SIDR SCLA SCLO OFFA OFFO
$# lcid sidr sfa sfo offa offo dattyp
9 0 0.000 0.000 0.000 0.000 0
$# a1 o1
0.000 367.899902
0.001370 370.160370
0.005000 371.548065
0.008370 372.019684
0.012776 380.620270
0.018219 397.310638
0.024698 417.651520
0.032214 437.040100
0.040766 453.861694
0.050355 469.164978
0.060981 483.874268
0.072642 497.208099
0.085341 508.458832
0.099076 518.930908
0.113847 529.209961
0.129655 537.813416
0.146500 545.727478

```

9.3.2 Mining Wheel Material Tensile Test and Virtual Validation Simulation Observations

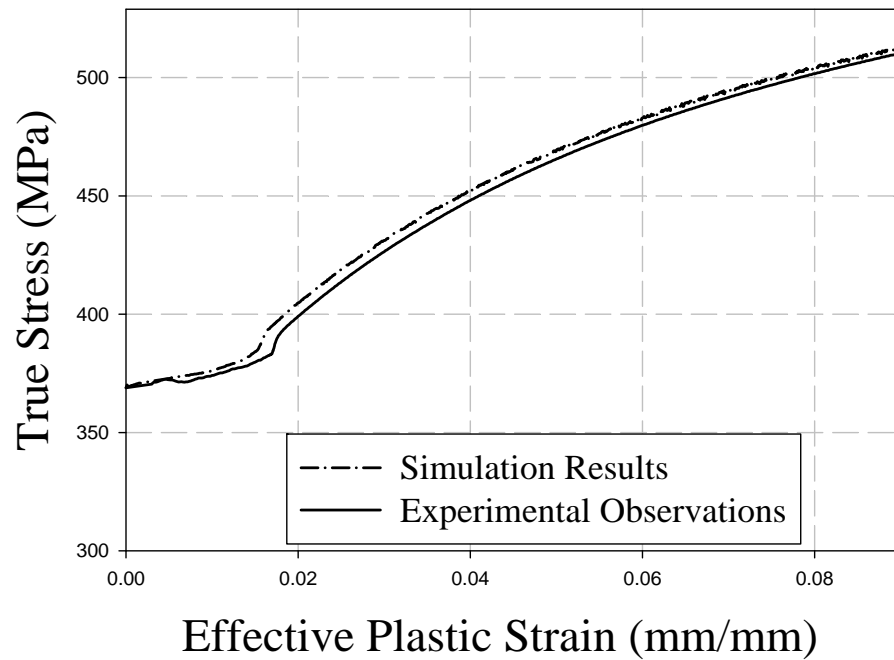


Figure 9.3.1 - Effective plastic strain versus true stress of mining wheel material sample tensile test showing virtual and experimental observations.

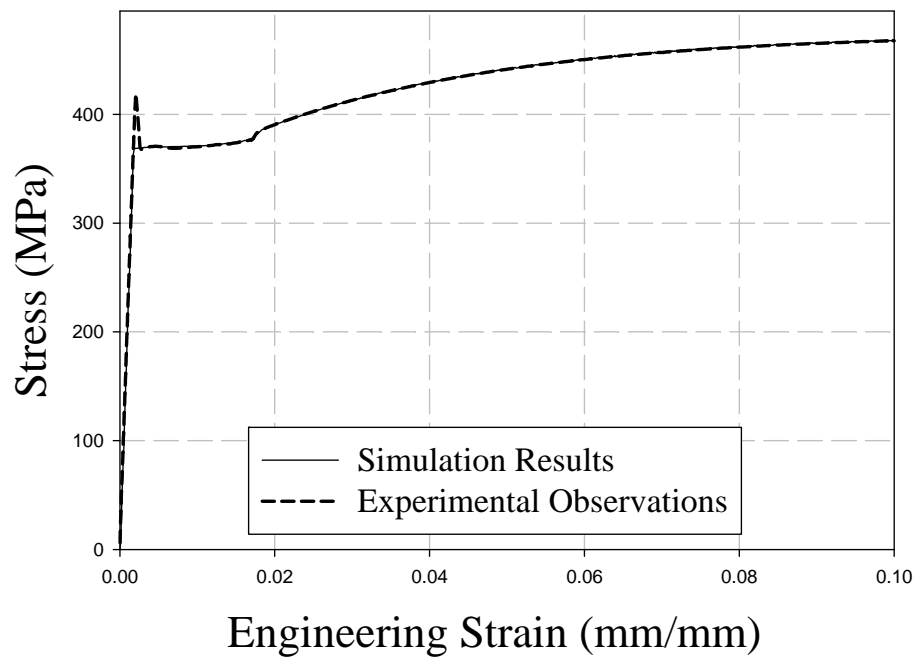


Figure 9.3.2 - Engineering strain versus engineering stress of mining wheel material sample tensile test showing virtual and experimental observations.

9.3.3 *Numerical Tensile Test Apparatus*

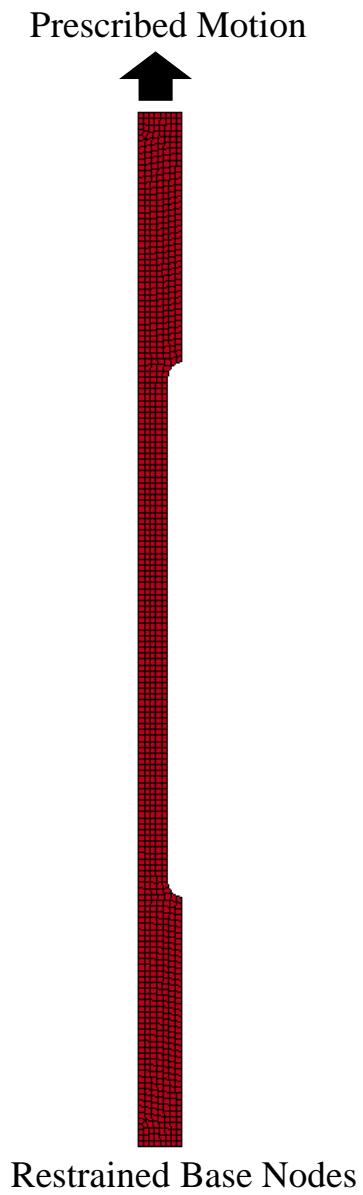


Figure 9.3.3 - Virtual tensile test model.

9.4 COPYRIGHT RELEASES

9.4.1 Copyright Release for Figures 2.1.1 and 2.1.2



University
of Windsor

Aleksander Tonkovich <tonkovi@uwindsor.ca>

Request for Permission to Use

Aleksander Tonkovich <tonkovi@uwindsor.ca>

Mon, Dec 2, 2013 at
6:41 AM

To: jude.decastro@goodyear.com

Hello Mr. DeCastro,

I hope you are keeping well. I am writing to request copyright release of images associated with the presentation you prepared "ABCs of OTR" as well as the Goodyear OTR Engineering Data Book. The requested images present common terminologies associated with OTR wheels and tires as well as basic engineering data such as overall dimensions. I wish to include these images in my M.A.Sc. thesis related to enhancing the safety of multi-piece wheels. All associated publication or reproduction of the image are for educational purposes with no financial gain. Your attention to this matter and prompt response is greatly appreciated.

Thank you in advance,
Aleksander Tonkovich

M.A.Sc. Candidate
University of Windsor
Department of Mechanical, Automotive, and Materials Engineering
tonkovi@uwindsor.ca, amtonkovich@gmail.com

jude.decastro@goodyear.com <jude.decastro@goodyear.com> Mon, Dec 2, 2013 at 8:19 PM

To: tonkovi@uwindsor.ca

Alek you are good to use this information
Good luck
Thanks

Goodyear Canada Inc.
Jude deCastro
Regional and Corporate Account Manager Off Road Tires
211 Edenwood Crescent
Orangeville, Ontario, Canada
L9W 4M8
Phone 519-938-5506
Fax 519-938-5507
Mobile 705-690-4156
JLTTGWD

"Contains Confidential and/or Proprietary Information. May not be copied or disseminated without the express written consent of The Goodyear Tire & Rubber Company"

9.4.2 Copyright Release for Figure 2.1.3

Janis Hardy <Janis.Hardy@saiglobal.com>

Wed, Dec 4, 2013 at
12:30 AM

To: "tonkovi@uwindsor.ca" <tonkovi@uwindsor.ca>

SAIG Ref: 1312-c017

Dear Aleksander

REPRODUCTION OF STANDARDS AUSTRALIA LTD. COPYRIGHT MATERIAL – PERMISSION GRANTED

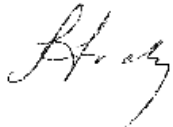
Purpose – AS 4457 Figure 1.5 within a Masters of Applied Science thesis related to enhancing the safety of multi-piece wheels for reference purposes.

Standards Australia Limited (“Standards Australia”) is the copyright owner of the Australian Standard ® brand and standards developed by Standards Australia (the *Works*). Pursuant to an agreement between Standards Australia and SAI Global Limited (“SAI Global”), SAI Global is exclusively authorised to permit third parties to reproduce the *Works* on certain terms.

SAI Global grants permission to Aleksander Tonkovich to reproduce the nominated content for the purpose stated above, subject to the following conditions

1. The electronic and printed extract must include a footnote, wherever the Standards Australia material appears, stating the extract is from the relevant standard, or based on it, and acknowledging permission to reprint has been given by SAI Global Ltd, with the following statement – **“Reproduced with permission from SAI Global Ltd under Licence 1312-c007”**.
2. The granting by SAI Global of a licence to reproduce is in no way represented as approval from SAI Global of any alterations, additions or deletions.
3. The licence granted to your organisation is a non-exclusive licence and cannot be assigned or transferred without the consent of SAI Global.
4. The permission last for the life of the current standard and commences from date of issue of this notification.

Regards



Janis Hardy
Manager, Copyright
Information Services (Asia Pacific)
SAI Global
Phone: +61 (0) 2 8206 6742
janis.hardy@saiglobal.com
www.saiglobal.com/information/

9.4.3 Copyright Release for Figure 2.1.4

Michael Cooney <mc@engnetglobal.com>

Mon, Dec 2, 2013 at 10:57 AM

To: Industry Tap <tonkovi@uwindsor.ca>

Hello Aleksander,

You are welcome to use the images as described in your email.
Your thesis sounds interesting, maybe you could do a short write up for industry tap when you are finished.

Kind Regards,

Michael Cooney

President - mc@engnetglobal.com

Engineering Network

Phone: + 1 704-541-3311

||

www.engnetglobal.com

Fax: + 1 704-943-0560

||

www.industrytap.com

Cell: +1 980-297-2221

||

www.enginesnetwork.com

From: industr1@server1.industrytap.com [mailto:industr1@server1.industrytap.com] **On**

Behalf Of Industry Tap

Sent: Monday, December 2, 2013 6:53 AM

To: mc@engnetglobal.com

Subject: Industry Tap - Contact

Your Name - Aleksander Tonkovich

Your Email - tonkovi@uwindsor.ca

Your Phone Number -

Your Comments/Suggestions - I am writing to request copyright release of images associated with the Caterpillar 797F in Michael Cooney's article "Is the CAT 797F Too Expensive? \$5 Million, Options Extra." I wish to include the images in my M.A.Sc. thesis related to enhancing the safety of multi-piece wheels. All associated publication or reproduction of the image are for educational purposes with no financial gain. Your attention to this matter and prompt response is greatly appreciated. Thank you in advance, Aleksander Tonkovich M.A.Sc. Candidate University of Windsor Department of Mechanical, Automotive, and Materials Engineering tonkovi@uwindsor.ca, amtonkovich@gmail.com

Form Displayed on Page: www.industrytap.com/contact

Sender IP: 129.9.104.10

9.4.4 Copyright Release for Figure 2.4.1



Standards Council of Canada
Conseil canadien des normes

2014-03-27

Attention: Aleksander Tonkovich
M.A.Sc. Candidate
Mechanical, Automotive, and Materials Engineering
University of Windsor
Windsor, Ontario, Canada

Dear Mr. Tonkovich:

Subject: Reproduction of Figure 1 from ISO 7141:2005

In response to your recent request and based on the information that you have provided to us, Standards Council of Canada is pleased to grant you permission to reproduce Figure 1 from ISO 7141:2005 for use in the preparation and publication of your Master Thesis, the “In-Field Observations of Heavy Mining Vehicle Wheels and Analyses of Proposed Solutions to Enhance Safety”.

This permission is based on the condition that recognition will be given by including the attached notation in your document.

Permission to reproduce Figure 1 from ISO 7141:2005 was provided by Standards Council of Canada. No further reproduction is permitted without prior written approval from Standards Council of Canada.

Please sign below and return a copy indicating your acceptance of the condition outlined above.

Sincerely

Julianna El-sabeh
National Copyrights Exploitation Agreements

9.4.5 Copyright Release for Figure 2.5.2

Used under an “Open Access” policy as described by the following statements from the journal’s website:

OPEN ACCESS

Open Access is a publication model that enables the dissemination of research articles to the global community without restriction usually through the internet. Thus, all articles published under open access can be accessed by anyone with internet connection. Academic Journals strongly supports the Open Access initiative. Abstracts and full texts (usually in PDF format) of all articles published by Academic Journals are freely accessible to everyone immediately after publication.

CREATIVE COMMONS ATTRIBUTION LICENSE

All articles published by Academic Journals are under the terms of the Creative Commons Attribution License. This permits anyone to copy, distribute, transmit and adapt the work provided the original work and source is appropriately cited.

10 VITA AUCTORIS

NAME	Aleksander Tonkovich
PLACE OF BIRTH	Etobicoke, Ontario, Canada
YEAR OF BIRTH	1987
EDUCATION	University of Windsor, Windsor, Ontario, Canada 2009 – 2013 Master of Applied Science 2005 – 2009 Bachelor of Applied Science